METEOROLOGICAL OFFICE

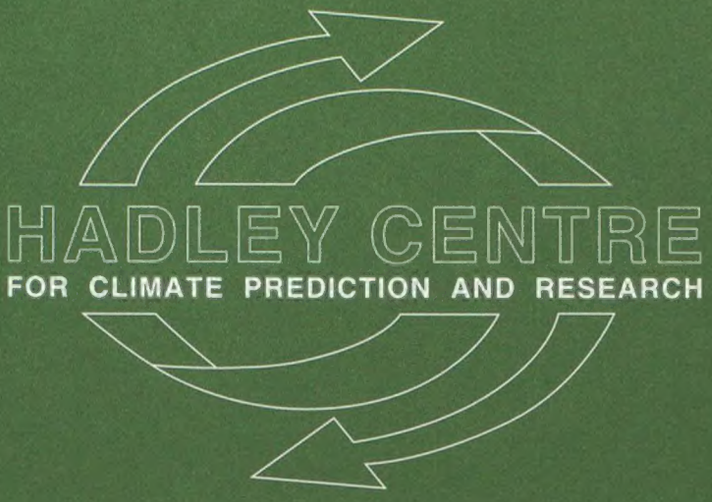

A high resolution AMIP run using the Hadley Centre model HadAM2b

by

R A Stratton

CRTN 77

December 1996

CLIMATE
RESEARCH
TECHNICAL
NOTE

Hadley Centre
Meteorological Office
London Road
Bracknell
Berkshire RG12 2SY

CLIMATE RESEARCH TECHNICAL NOTE NO. 77

A HIGH RESOLUTION AMIP RUN USING THE HADLEY CENTRE MODEL HadAM2b

by

R A Stratton

Hadley Centre for Climate Prediction and Research
Meteorological Office
London Road
Bracknell
Berkshire RG12 2SY

NOTE: This paper has not been published. Permission to quote from it should be obtained from the Director of the Hadley Centre.

© Crown Copyright 1996

A high resolution AMIP run using the Hadley Centre model HadAM2b.

December 1996

by R A Stratton

Summary

A high resolution (0.833° latitude by 1.25° longitude) AMIP run is compared with a standard resolution (2.5° by 3.75°) AMIP run. Both runs use HadAM2b, a recent version of the Hadley Centre GCM. ECMWF reanalysis data for the AMIP period (1979-1988), together with other climatologies, are used to validate the model runs. Increasing resolution increases the vertical motion, intensifies the hydrological cycle, reduces slightly the model's cold bias in the troposphere, shifts the westerly jets polewards and tends to increase the eddy kinetic energy and variability of the model. The high resolution simulation has less mid-latitude cloud, so altering the radiation balance. The detail in the precipitation field is generally improved at high resolution.

1. Introduction

Most GCMs used for long climate integrations use resolutions close to or lower than that used at the Hadley Centre, ie 2.5° latitude by 3.75° longitude, giving a grid point spacing of about 300km at mid-latitudes, (approximately equivalent to a T42 spectral model). Models of this resolution cannot accurately resolve small scale systems. Global operational numerical weather prediction (NWP) models use higher resolution and are better able to resolve many of the synoptic weather systems. The high resolution used here is the same as that used for the UK Meteorological Office's operational forecast model, 0.833° latitude by 1.25° longitude (approximately 100km at mid-latitudes).

Recently there have been a number of studies using higher resolution climate models (T63 - Boville (1991); T106 - Kiehl and Williamson (1991) using the NCAR CCM1, Boyle (1993), Phillips et. al. (1995) using the ECMWF model cycle 33, Williamson et. al. (1995) using CCM2, Wild et. al (1995) using ECHAM3). All the studies mentioned used spectral models and most give results from runs of five years or less. The runs described here both use a grid point model and are AMIP runs (Gates (1992)) i.e. they are forced by analyzed sea surface temperatures (SSTs) for 1979 to 1988. There are two other AMIP high resolution runs, one with the ARPEGE model (Deque and Piedelievre (1995)) and one with ECHAM4 (no reference available) both using T106. These two AMIP runs together with the high resolution AMIP run described here form part of a European project to assess the impact of increasing model resolution on climate simulation. This paper will concentrate on assessing and understanding the impact of increased resolution on the simulation of the Hadley Centre model HadAM2b and not attempt to compare results from this model with the two other runs.

HadAM2b is an improved version of the atmospheric model HadCM2 used in the Hadley Centre coupled climate change integrations. A brief description of the model is given in section 2 as it is not documented elsewhere. Emphasis is given to describing the parts of the model formulation which may depend on resolution. The model simulation at both resolutions is assessed by studying a wide range of model fields and comparing these with climatologies.

2. Description of the model used

The model used for both AMIP runs is the UK Meteorological Office's Unified Model (Cullen (1993)). The Unified Model is a hydrostatic primitive-equation model with a hybrid vertical coordinate system. In the version of the model used here the main model variables are held on 19 levels in the vertical, the first four having sigma coordinates and the top three pressure coordinates. The lowest level is at about 25m, the top level is at 4.6 hPa with the top boundary of the model at 0.5 hPa.

The orographies at the bottom boundary of the model are derived from the U.S. Navy 10-minute resolution data set, area-averaged to the required horizontal resolutions. Near the poles the model has far more grid points per km east-west than near the equator so from 60° to the pole the orography is smoothed by applying a 1-2-1 filter. Many of the other land surface characteristics required by the model are derived from the 1° x 1° data of Wilson and Henderson-Sellers (1985).

The SST and sea ice data used were the standard AMIP values for 1979-88 which came from NMC analyses and were on a 2°x2° grid. The data were interpolated to the model grids used. In the case of the high resolution model some inland lakes were present in the model grid but no data were available in the SST analyses. In particular the high resolution

model resolves Lake Victoria in Africa. Values of surface temperatures for Lake Victoria were derived by interpolating from the surrounding oceans values at the same latitudes and adjusting these for the height of the Lake which is approximately 1160m above sea level. The resulting values were compared with any available nearby air temperature observations as a check.

Ozone profiles are specified by using a zonally averaged monthly ozone climatology based on that of Keating et. al. (1987) for the top 2 model levels (ie levels at pressures below 20 hPa) and McPeters et. al. (1984) for the other levels. The level of CO_2 in the model is set to 345ppm the value prescribed for AMIP experiments.

The basic model variables, surface pressure, p_*, wind components, u and v, total water, q_T and potential temperature adjusted for the latent heat of cloud water and cloud ice, θ_L, are held on the Arakawa B grid. The integration scheme (Cullen and Davies (1991)) acts on the basic model variables, conserving the mass weighted mean of these quantities and the atmospheric angular momentum. At standard resolution the advection scheme is fourth order accurate in space but this is reduced to a second order scheme at high resolution to reduce the computational cost. This difference is thought unlikely to have much impact on the simulation at high resolution. The basic timestep of the model is determined by a stability criterion, and is chosen to be as long as possible to reduce computing costs. The basic timestep is used for the advection scheme and for all the physics schemes apart from radiation. At standard resolution a 30 minutes timestep is used but this has to be reduced to 10 minutes at high resolution. This difference in timestep has an impact on the behaviour of some of the physics schemes and will be discussed later.

Horizontal diffusion is applied to the model variables after advection. At standard resolution the horizontal diffusion applied is ∇^6 and at high resolution the diffusion is ∇^4. At both resolutions the diffusion applied to winds and potential temperature at the top model level is ∇^2. At standard resolution the coefficient used for the diffusion implies an e-folding time for the damping of two-grid length waves of 12 hours. At levels above 150 hPa the diffusion applied to q_T is altered to ∇^4 and the coefficient increased giving an e-folding time of about 4 hours. At high resolution the coefficient used for winds and potential temperature has an e-folding time of 13 hours for the damping of 6 grid length waves (1 standard grid length = 3 high resolution grid lengths). The damping applied to q_T is reduced to an e-folding time of 50 hours for 6 grid length waves. Horizontal diffusion is switched off where the pressure gradient between adjacent grid points at a given model level is steep. The switching off of diffusion occurs mainly in the bottom 5 model levels over mountains and is done to help retain the physically realistic steep gradients in model variables over orography.

Fourier filtering is applied near the poles to mass weighted horizontal wind fields, and to mass weighted advection increments of q_T and θ_L to remove short wave lengths. After advection, diffusion and filtering a check is made on the values of q_T to see that there are no negative values. It is possible for the integration scheme to lead to small negative values. This often occurs near the top of the model, in regions of steep moisture gradients and in regions of descending dry air. If any values of q_T are negative, moisture is removed from the neighbouring grid points at the same level and the negative values set to zero. If this fails for any grid points, may be because the neighbouring grid points are also negative or cannot contribute enough moisture to correct the negative values, the correction is done on a global basis. Global corrections are avoided if possible as they can result in large spurious moisture fluxes. At standard resolution over a period of 10 years the model tends to lose moisture in the stratosphere and therefore calls to correct for negative specific humidity on a global basis become more frequent with time. At high resolution the loss of specific humidity in the

stratosphere accelerated and the frequency of calls to correct for negative specific humidity on a global basis increased more rapidly.

The parametrization of sub-grid scale orographic gravity wave drag is a modified form of the Palmer et. al.(1986) scheme (Gregory et. al. (1996)) which includes the effects of trapped lee waves, the anisotropy of the orography and a better representation of high drag states where the flow can be blocked or hydraulic jumps occur. As the high resolution model is able to resolve more detail in the orography there is an implied difference in the coefficients required in the gravity wave drag scheme. These were chosen so that roughly the same amount of stress due to gravity wave drag was produced at 45°N in DJF (December, January, February).

When the Unified Model is run in climate mode it usually uses a 360 day year. The seasonal variation of incoming solar radiation is modified to take account of this. The radiation scheme has 3 active gases, water vapour, ozone and carbon dioxide. The shortwave radiation scheme has 4 bands and is based on an extended version of Slingo (1985) with interactive cloud optical properties (Slingo (1989)) modified to take account of a land sea contrast observed in the effective radius of water drops (Han et al. (1994)). The shortwave scheme sees cloud combined into 3 layers - high, medium and low. The longwave scheme has 6 bands and is based on Slingo and Wilderspin (1986). In the longwave scheme cloud is treated using a maximum random overlap method similar to that of Geleyn and Hollingsworth (1979). The radiation scheme is called every 3 hours at both model resolutions.

The cloud scheme allows layer cloud to form at all levels except the top model level. Cloud variables, ie cloud water, cloud ice and cloud amount are diagnosed from the primary model variables q_T and θ_L using parametrizations described in Smith (1990). The temperature range for mixed phase clouds has been modified from -15° to 0°C to -9° to 0°C based on observations made by the UK Meteorological Research Flight (Gregory and Morris (1996)). Precipitation from layer cloud is calculated as in Senior and Mitchell (1993) with modifications to make the precipitation rate dependent on cloud water contents within the cloud part of the grid-box and to the treatment of ice fallout. The evaporation of precipitation is described in Gregory (1995).

Moist and dry convection are modelled using the mass-flux scheme of Gregory and Rowntree (1990) with the addition of convective downdraughts (Gregory and Allen (1991)). The scheme has been modified to make the initial mass flux dependent on the surface fluxes from the boundary layer scheme.

The model boundary layer is restricted to the bottom 5 model layers. Mixing in the boundary layer is calculated in terms of local turbulent fluxes, based on mixing length theory, and a rapidly-mixing term in which the increments from the surface fluxes are distributed evenly throughout the depth of the boundary layer(Smith (1990), (1993)). In this version of the model the rapid mixing is restricted to below the convective cloud base if convective cloud is present. Roughness lengths for momentum used in the boundary layer scheme have been revised to include the effect of orographic form drag (Mason (1985)).

The temperature of the soil is simulated using a 4 layer thermodynamic model (Warrilow et. el. (1986)). The surface hydrology is based on that of Warrilow et. al. with an alteration to include the effects of the inhomogeneity of rainfall (Dolman and Gregory (1992)) and a replacement of the one layer soil moisture scheme by a multi-layer soil moisture scheme with the same 4 layers as in the soil thermodynamic scheme.

Both model runs started from the beginning of December 1978 and continued for 10 years and one month. The first month of each run was treated as a spinup and not included

in the 10 year means. A second AMIP run was done at standard resolution using a 10 minute timestep to help determine whether any difference between the two different resolution runs was due to a model timestep dependence.

3. Climatologies used to validate the model simulations.

The only way of assessing how well a climate model is able to simulate the present day climate is to compare the model with observational climatologies. Observations do not usually cover all regions of the globe so a good way of obtaining a global climatology of the main model variables like winds and temperature is to form a climatology from NWP analyses. NWP analyses will provide the best fit to all the available observations and fill in areas where there is no data. In regions of no observations the NWP analysis will depend more on the characteristics of the model being used.

The mean climate and climate variability depend on the period considered. The mean climate of a short period eg 10 years will depend partly on the sea surface temperatures, partly on various natural and anthropogenic forcing eg CO_2 , volcanic aerosols, and partly on the chaotic variability. Over a long period ie at least 30 years if a climate model is good and is forced with observed forcing e.g. sea surface temperatures, aerosol etc it should reproduce the observed mean climate and variability but it is unlikely to reproduce individual years and seasons exactly. The AMIP period is relative short so the model runs are unlikely to reproduce exactly the observed climate for the same period. The AMIP period, 1979-88, contains two strong El Nino events in 1982/83 and 1986/87 which will have a strong influence on the observed mean climate particularly in the tropics. Some of the El Nino signal should be present in the model climate and for this reason where possible climatologies based on the period 1979-88 have been used.

3.1 ECMWF reanalysis for 1979-1988

The ECMWF reanalysis project (ECMWF reanalysis workshop, (1996)) involved reanalysis of the period 1979 to 1994 using all available observations for the period. The model used was the IFS 13r1 model with a horizontal resolution of T106 and 31 model levels in the vertical. The climatology formed from the reanalyses has the advantage of using the same model throughout the whole period unlike climatologies formed from operational NWP analyses where the model and the assimilation scheme evolve with time. The only differences in the quality of the analyses throughout the period are likely to be due to changes in the distribution and types of observations available for use in the assimilation scheme. This climatology has been used to provide values of temperature, winds, relative humidity, heights and eddy diagnostics on pressure levels. Climatologies of relative humidity derived from analyses are often regarded as suspect as they usually depend strongly on the treatment of moisture in the model and little on observations. In the case of the ECMWF reanalyses, satellite retrievals of moisture have been used in the assimilation scheme. The reanalysis climatology of relative humidity in the troposphere is thought to be good as it compares well with TOVS retrievals though it must be remembered that the same TOVS data will have been used in the assimilation.

3.2 ERBE radiation fluxes at the top of the atmosphere.

Short wave and long wave radiation fluxes at the top of the atmosphere have been accurately measured by satellites between 1985 and 1990 by the Earth Radiation Budget Experiment (Barkstrom et. al. (1989)). Measurements from 3 satellites were used to produce

a global climatology of total and clear sky fluxes (Harrison et. al. (1990)). Means formed from the five years of data have been used to validate the model.

3.3 Cloud climatologies.

Total cloud amounts from the International Satellite Cloud Climatology Project (ISCCP) are used to validate the model total cloud amounts. The cloud amounts are estimated from measurements of visible and infrared radiances made from the operational geostationary and US polar orbiting satellites (Rossow and Schiffer (1991)) for the period 1984-90. The satellite cloud climatology compares well with the surface based cloud climatology of Warren et. al. (1986 & 1988) in most regions. There are some regions particularly over the Indian Ocean where the ISCCP total cloud amounts look odd e.g. west of 60°E the cloud amounts are high in all seasons, east of this there is a sudden fall in cloud amounts suggesting a mismatch between some of the satellite data.

3.4 Legates & Willmott Precipitation and screen-level temperature climatology

The Legates and Willmott climatologies (1990a & b) provide mean monthly values of precipitation and screen-level air temperatures on a 0.5°x0.5° grid. The climatologies were created using observations over land for the period 1920-1980 and data over the oceans from the COADS (Comprehensive Ocean-Atmosphere Dataset , Woodruff et. al. (1987)). The precipitation climatology tends to lack observations over the oceans and so should be treated with caution. The climatology has a large maximum in precipitation in DJF over the Eastern Pacific ITCZ which is unrealistic when compared with satellite data. The screen level climatology lacks observations over Antarctica and over the ocean round the South Pole and tends to disagree with model values in these regions. Most land stations making observations tend to be located in valleys in mountainous regions so direct comparison of the climatologies against model output for mountainous regions is not useful. For this reason direct comparison of model and observations has been restricted to regions where the model orography is less than 500m.

3.5 University of East Anglia precipitation climatology.

This climatology of precipitation is on the same grid as the standard climate model and is based on land station data only (Hulme (1992)) . It provides no information over the oceans or over regions over land where there are no observations but has one advantage over the Legates and Willmott climatology; monthly mean data are available for years between 1951 to 1990. This means that climate means can be formed for any period of interest. In this study means for the AMIP period have been used for comparison against the model and not the climatology for the period 1951 to 1980.

3.6 Da Silva climatology of surface fluxes

The Da Silva climatology (Da Silva et. al. (1994)) is a climatology of surface fluxes over the oceans derived on a 1° x 1° grid from COADS data for 1945 to 1989. The fields from the climatology used in this study are net surface shortwave radiation, net surface longwave radiation, latent heat flux and sensible heat flux. All these fluxes are estimated from the COADS data making certain assumptions about exchange coefficients which are not the same as the assumptions used in the boundary layer scheme in the Unified Model. The version of the Da Silva surface fluxes used in this study do not have a global annual mean heat flux of zero.

4. Model comparison

Ten year monthly and seasonal means for the period 1979 to 1988 from the high resolution run and the standard resolution run were compared with climatologies where possible, to assess how well both models are able to simulate the climate. Results from the high resolution run were compared with those from the standard resolution run to see if changing horizontal resolution made a difference to the climate simulation. Results from a third run at standard resolution but with a 10 minute timestep were used to see whether the model has any timestep dependencies which could explain differences between the different resolution runs.

4.1 Mean sea level pressure

Figures 1(a) to 4(a) show the global mean sea level pressure for all four seasons from the high resolution run. Figures 1(b) to 4(b) show the difference between the high resolution and the climate resolution runs and figures 1(c) to 4(c) the differences between the high resolution run and the ECMWF climatology. In addition Table 1 gives objective verification figures for comparison of mean sea level pressure from both model runs with values from the ECMWF climatology for different latitude bands. The verification has been restricted to grid points where the orography is less than 500m to avoid comparing regions where the mean sea level pressure will depend strongly on the model's orography and on the method used to derive the mean sea level pressure from the surface pressure. The main result from table 1 and figures 1 to 4 is that increasing resolution does not seem to reduce the systematic errors in mean sea level pressure. In all seasons apart from MAM (March, April, May) the high resolution model has higher global root mean square errors.

Table 1 - Objective validation of mean sea level pressure.

Mean and root mean square differences from ECMWF climatology for 1979-88 for model grid points where the model surface height of the standard grid is less than 500m. The high resolution data are extracted on the standard grid for comparison. All values are in hPa.

	DJF				MAM			
Region	High resolution		Standard resolution		High resolution		Standard resolution	
	mean	rms	mean	rms	mean	rms	mean	rms
90°N - 20°N	1.36	4.41	1.81	4.38	0.77	2.02	1.46	2.86
20°N - 20°S	-0.90	1.23	-0.48	0.99	-0.60	0.95	-0.26	0.76
20°S - 90°S	0.30	3.56	0.04	2.07	0.12	3.11	-0.14	2.96
global	0.18	3.26	0.37	2.73	0.05	2.22	0.28	2.38

	JJA				SON			
Region	High resolution		Standard resolution		High resolution		Standard resolution	
	mean	rms	mean	rms	mean	rms	mean	rms
90°N - 20°N	0.22	2.17	1.28	2.18	1.25	2.13	2.21	3.04
20°N - 20°S	-0.31	0.95	-0.53	1.12	-0.89	1.15	-0.97	1.17
20°S - 90°S	-0.15	3.67	-0.19	3.19	0.15	4.08	-0.13	2.62
global	-0.10	2.53	0.12	2.32	0.10	2.77	0.25	2.36

In the northern hemisphere the pressure over the North Pole is decreased at high resolution in all seasons (figures 1-4(b)) giving better agreement with climatology (see Table 1). In DJF the pressure over the North Pole is much higher at standard resolution giving a very different simulation over Northern Siberia, the high resolution model being better in this region. There are two possible reasons for the differences over the pole, firstly the high resolution model may represent the effects of gravity wave drag in a better way contributing to a better northern hemisphere circulation. Recent experiments with a newer version of the Hadley Centre GCM at standard resolution suggest that the high pressure over the North Pole is sensitive to the coefficient used in the gravity wave drag scheme and can be reduced by using a lower coefficient which results in less drag tending to reduce the easterly wind bias over the northern hemisphere in the stratosphere. Secondly, the high resolution model is better able to model flow across the poles. It is known that the advection scheme used in the Unified Model is not very good at advecting systems across the poles. DJF is the season with the strongest mean cross polar flow and therefore mostly likely to be influenced by problems with the advection scheme. In the southern hemisphere most strong low level flow is around Antarctica and therefore inaccuracies in cross polar flow are not so important.

In both hemispheres between 30° and 50° the high resolution model has higher pressure than the standard resolution model particularly over the oceans. This tends to correspond to a poleward shift in the westerly jets (see later) and does not always improve agreement with the climatology. In the southern hemisphere in DJF and SON(September, October November) the pressure gradient is substantially increased (figures 1(b) and 4(b)), making the westerly bias even worse. Deque and Piedelievre, (1995), using the ARPEGE model, also find that increasing model resolution from T42 to T106 increases the model bias in the southern hemisphere. In the northern hemisphere, the ARPEGE model does not have a large high pressure bias over the North pole in DJF at T42 equivalent to the standard resolution.

In the tropics at both model resolutions the model pressure tends to be too low. Increasing resolution lowers the pressure in DJF and MAM slightly increasing the systematic bias. In JJA (June, July August) and SON the pressure lowers over land and the western Tropical Pacific but rises over the rest of the tropical oceans giving an overall improvement.

4.2 Upper air winds

Figures 5 and 6 show the zonal mean winds for DJF and JJA. The main difference (figures 5(b) and 6(b)) is the poleward shift of the westerly jets at high resolution. This occurs in all seasons and is in agreement with the findings of Boville(1991) and Williamson et. al. (1995). The other difference at high resolution is an increase in the westerly bias over the equator in the middle stratosphere. Over the equator both models have a westerly bias near the surface with an easterly bias above. Recent experiments including convective momentum transfer in the model have almost eliminated the westerly bias over the equator and reduced the easterly bias above it. In all seasons in both models the westerly jet in the southern hemisphere is too strong compared with climatology.

In DJF the main difference between the two models occurs in the Northern hemisphere where the high resolution model makes a much better attempt at simulating the westerlies in the stratosphere. The magnitude of the subtropical upper troposphere jet maximum in the northern hemisphere at high resolution is closer to climatology. In JJA, like DJF, the biggest difference occurs in the winter hemisphere and again improves the westerlies in the stratosphere. An easterly bias seen at standard resolution in the southern hemisphere between 60°S and 90°S is reduced at high resolution. In both JJA and DJF the

easterly bias in the troposphere at 30°N and 30°S is increased at high resolution due to the polewards shift of the westerly jets.

Figures 7 and 8 show the zonal mean v component of velocity for DJF and JJA. In both seasons the Hadley circulation at high resolution is slightly stronger than that at standard resolution. This may be linked to the increase in convection over the tropics at high resolution, see section 4.5.

At higher resolution the frequency of occurrence of strong vertical motion increases. This difference is important and is referred to again later to help explain the differences in temperature and humidity. Figure 9 shows the probability distribution of 0 UTC values of vertical velocity at 850 and 500 hPa calculated using all July values for the ten year period. The analysis of the model vertical velocities was done on the standard resolution grid with the high resolution model data being area averaged to the new grid before calculating the frequency distribution. Over land at both 850 and 500 hPa the spread of the vertical velocity is far larger at high resolution. At 40° - 60°N and in the tropics the high resolution values over land are close to the ECMWF climatology. Between 40° and 60°S there is very little land in the model i.e. mainly South America which contains the Andes which may explain the increase in the distribution at high resolution. Over the sea the differences between the two resolutions are reduced but the high resolution model still has a greater range of values. Over the sea between 40° and 60°N both models have less intense vertical motions than the analyses.

4.3 Upper air temperature and humidity

In all seasons both models have a cold bias in the troposphere. In the two seasons shown, DJF, figure 10 and JJA, figure 11, and in the other seasons, the high resolution model is warmer in the troposphere reducing the cold bias. This agrees with the findings of Williams et al. (1995) who find a decrease in the cold bias of the CCM2 model when increasing resolution from T42 to T106. The largest increases in temperature occur in mid-latitudes and correspond to the regions where the westerly jets have shifted polewards in the high resolution model. The warming at mid-latitudes in the high resolution model extends throughout most of the troposphere to the surface over land but only as far as model level 4 (eta=0.870) over the sea (not shown). The magnitude of the warming is slightly larger over the sea at mid-latitudes as is the shift in the westerly jets. Over the sea both models are constrained by the same SSTs at the surface whereas over the land the high resolution model is able to have higher surface temperatures; this may explain the land sea differences near the surface.

The warming of the troposphere at high resolution may be due to the more intense vertical motion in the model. More frequent occurrences of rapidly ascending moist air will lead to a more active hydrological cycle and a greater release of heat due to condensation.

In the stratosphere increasing resolution increases the temperature everywhere except over the winter pole. This increases the warm bias in most of the stratosphere. Both models have a large cold bias near 200 hPa over the summer pole which is a common feature of many climate models. This cold bias is reduced at high resolution in DJF, figures 10(b) and 10(c).

Zonal means of the humidity (figures 12 & 13) show that the high resolution model has a lower humidity (up to 5% less) at mid-latitudes which is generally in better agreement with radiosonde observations. The reduction in relative humidity at mid-latitude found in this study differs from the findings of Phillips et al. (1995). In the ECMWF cycle 33 model the

relative humidity increases with resolution from T42 to T106 at mid-latitudes but their cold bias also increases in the same region with resolution. The lower humidities at mid-latitudes are linked with the warmer troposphere in the high resolution model. If water vapour (specific humidity in the model) remains constant a 1 degree rise in temperature will tend to give a 8-10% decrease in relative humidity. At high resolution in parts of the warmer troposphere the specific humidity of the atmosphere tends to increase by a small amount so the reduction in relative humidity is not as large as might be expected. The relative humidity at both resolutions is too high in the models compared with the ECMWF analyses. In the tropics in all seasons the relative humidity is higher in mid-troposphere at high resolution due to an increase in convection (see later). This does not improve agreement with the analysis climatology except around 300hPa. Figures 10 and 11 show that in both models the location of the tropopause differs from the climatology, the model tropopause being higher than observed at mid-latitudes, accounting for the large differences in relative humidity around 200hPa.

4.4 Clouds

The model has two different types of cloud, convective cloud and layer cloud. Figure 14 shows the zonal mean convective cloud amount against model level over land and over sea. The main difference between the two models is an increase in convection over the tropics and a reduction over mid-latitudes with increasing resolution. Over land most of the convective cloud occurs in the tropics or the summer hemisphere. At high resolution the convective cloud over tropical land is increased particularly near the surface. At mid-latitudes the amount of convective cloud over land is decreased. Over the sea, like the land, the largest and highest convective cloud amounts occur over the tropics but unlike the land the highest amount at mid-latitudes occur in the winter hemisphere. The tropical convective cloud over the sea is increased at high resolution at all levels and by a larger amount than over the tropical land. The mid-latitude convective cloud over the sea is reduced at high resolution. The convection scheme used in the model is known to have a timestep dependence. When the convection scheme is run with a 10 minute timestep (ie as in the high resolution model) the convection at a gridbox tends to be more continuous in time whereas when the scheme is run with a 30 minute timestep (ie standard resolution), convection tends to switch on for one timestep and off for the next giving lower mean convective cloud amounts. The convective cloud in the model is related to the log of convective precipitation. This timestep dependence accounts for the increases in mean convective cloud amount seen in the tropics at high resolution but is unable to explain the decrease in convective cloud at mid-latitudes.

A possible explanation of the reduction in convection at mid-latitudes at high resolution is that the presence of more subsidence at lower levels e.g. 850 hPa in the high resolution model at 40° - 60°S (figure 9) leads to a more stable atmosphere and therefore less convection. Over land and sea at mid-latitudes the upper troposphere is warmer in the high resolution run, figures 10(b) and 11(b), consistent with this.

Figure 15 shows the zonal mean layer cloud amounts for DJF and JJA over land and sea. Overall the amount of layer cloud in the model is reduced at high resolution particularly at mid-latitudes. Over the winter pole, 60° - 90°N or 60° - 90°S between model levels 8 and 13, the high resolution model has more layer cloud. Below level 6 there is less layer cloud over the poles in both seasons and both hemispheres. At mid-latitudes (30°-60°N or S) at high resolution there is less layer cloud over land at all levels and less over the sea at levels greater than 5. Over the tropical land in JJA there is more cloud between levels 6 and 10 at high resolution. Over the tropical and mid-latitude oceans there is more layer cloud at levels

3 and 4, i.e. more low level boundary layer cloud.

There are three possible explanations for the reduction in layer cloud;

1. Timestep dependence of the ice fallout scheme. Differences in layer cloud can partly be explained by a timestep dependence in the large-scale precipitation scheme which leads to a different distribution of cloud ice. The fall speeds of ice are high relative to the timestep of the model, therefore ice precipitation can fall through more than one model level in a timestep. The version of the model used in these runs includes changes to the original scheme to remove some of the timestep dependence but there is still some timestep dependence mainly due to the fact that at the end of a timestep any cloud ice present in a level is assumed to be distributed evenly throughout the model layer. This assumption means some ice may effectively fall further than or not so far as its fall speed may imply. The run at standard resolution with a 10 minute timestep suggests that this reason is unlikely to account completely for the difference.

2. Over mid-latitude land in July there is more subsidence at higher resolution leading to a drying of the atmosphere. Also the high resolution model tends to have more vigorous ascent and descent which will tend to reduce the relative humidity of the atmosphere. This explanation may account for a large part of the difference seen in layer cloud amounts between the two runs and agrees with the findings of Jones et al. (1995).

3. The amount of horizontal diffusion applied to moisture in a model can influence the amount of cloud. Decreasing diffusion tends to lead to more cloud. At high resolution on the scale of 6 grid-lengths there is less diffusion of specific humidity than at climate resolution but for 2 grid-lengths the diffusion is higher and may contribute to a reduction in cloud. Experiments changing the diffusion coefficient for moisture suggest that this alone is unlikely to account for the differences in cloud.

Investigation of the extra layer cloud at level 3 over the sea in the tropics suggests this is linked to the timestep dependence of convection. The extra layer cloud at level 3 is present at standard resolution if the model is run with a 10 minute timestep. The rapid mixing in the boundary layer is confined to below convective cloud base and will therefore respond to the timestep behaviour of the convection scheme. If this link is removed from the model the extra layer cloud at level 3 seen in runs with a 10 minute timestep disappears.

The distribution of cloud in the vertical is hard to validate but the total cloud cover can be compared with the ISCCP cloud climatology and the Warren et. al climatologies (1986, 1988). Figures 16 and 17 show the zonal mean total cloud over land and sea. Both resolutions of the model lack stratocumulus cloud over the sea e.g. to the west of South America, off California and to the west of Namibia. As seen in the zonal means of layer cloud and convective cloud, the high resolution model has less total cloud at mid-latitudes, particularly over land (Central USA, Europe and Asia) in JJA. The reduction in cloud over land at high resolution tends to make the agreement with the climatologies worse. Over high latitudes in both hemispheres the two climatologies differ significantly, figures 16(b) and 17(b). In the winter hemisphere the model cloud cover at high latitudes is too high relative to both climatologies. Over the summer hemisphere the model values fall between the two climatologies the Warren et al values being higher than the models and the ISCCP values.

Over the sea the model cloud amounts are in closer agreement, the high resolution values being slightly higher around 30°N and 30°S where the high resolution model has extra level 3 cloud and lower north of 60°N. Over the equator the high resolution values are higher due to the extra convective cloud and small increases in layer cloud but as the two climatologies differ it is difficult to say which model is better. From about 20° to 60° in both hemispheres both climatologies are at least 10% higher than the model values. The Warren

et al. climatology based on surface observations being lower than the ISCCP climatology based on satellite observations.

The reduction in cloud at mid-latitudes with increasing resolution agrees with Kiehl and Williams, 1991 but disagrees with Phillips et al. 1995. The more recent study using the CCM model (Williams et al, 1995) chooses to tune the model cloud for each resolution to give similar values. A similar approach is also used in the ARPEGE model (Deque and Piedelievre (1995)).

4.5 Top of the atmosphere radiation

Table 2
Global annual mean radiation budget at the top of the atmosphere, all values in Wm^{-2}.

	high	Standard	ERBE	uncorrected
Incoming shortwave	341.4	341.4	342	341.3
Outgoing shortwave	102.3	98.9	105	100.3
Clear-sky outgoing shortwave	46.3	47.0	55	53.0
Outgoing longwave	241.6	240.4	237	235.3
Clear-sky outgoing longwave	266.3	264.1	266	265.2
net downward radiation	-2.5	+2.2	0	+5.7
shortwave cloud forcing	-56.0	-51.9	-50.	-47.3
longwave cloud forcing	24.7	23.7	29.	29.9

Top of atmosphere (T.O.A.) radiation fields can be validated by comparison against ERBE data. Table 2 gives the annual mean values for both runs and estimates from ERBE derived from a mean of 1985-1990 data. In Table 2 there are two sets of ERBE values, the first set have been corrected to give zero net downward radiation at the top of the atmosphere and the other set are from the uncorrected data. The ERBE data used in Table 3 are uncorrected values. Shortwave and longwave cloud forcing are defined as the differences between the clear sky values and total outgoing values at the top of the atmosphere.

The two models have a different radiation balance, the high resolution model reflects and emits more radiation than the standard resolution model. The increased reflection is mainly due to the additional low level water cloud over the ocean in the tropics, figures 15(d) and (h). Both models absorb too much shortwave radiation and emit too much longwave radiation when compared with ERBE values. The excess absorption of shortwave radiation may be partly due to the lack of aerosols in this version of the model. Like many other climate models, giving a reasonable fit to ERBE values was an important factor in deciding on what changes were introduced into the climate model to form HadAM2b. This tuning was done at standard resolution; the high resolution model was not tuned to give a good fit to ERBE data.

Looking in more detail at the shortwave radiation, Table 3(c) supports the idea that the main increase in reflected solar radiation occurs over the sea. In contrast over the land there is less reflected shortwave radiation due to a reduction in bright low level layer cloud, figures 15(c) and (g). Similar differences show up in the values for shortwave cloud forcing. Over tropical land where there is less bright cloud, the high resolution values are in good

agreement with ERBE data but over the sea, the presence of the extra low level water cloud, leads to much larger errors in the cloud forcing.

Figures 20 & 21, model zonal mean albedo for DJF and JJA together with ERBE values, show a similar picture. Over land at mid-latitudes the high resolution model has a lower albedo than the standard resolution model run due the reduction in layer cloud. In both seasons at 40° - 60°N the standard resolution model is in better agreement with ERBE. Closer to the equator over land both models do well but over the sea the high resolution model with more convective cloud (see figures 14(d) and (h)), ie brighter cloud, agrees better with the ERBE data. At 10° to 30° over the sea either side of the equator the high resolution model is too bright due the presence of cloud liquid water in level 3.

The high resolution model emits more longwave radiation in worse agreement with ERBE data. If the effects of clouds are removed the annual mean outgoing radiation is in slightly better agreement with ERBE which may be partly due to the reduction in atmospheric relative humidity at high resolution. Table 3(a) shows that the increase in outgoing radiation at high resolution occurs over both land and sea at mid-latitudes. This increase at mid-latitudes gives worse agreement with ERBE. The largest differences from ERBE at mid-latitudes occur during JJA over the land, (figure 19). At high resolution in JJA there is less cloud over the northern hemisphere land, a lack of precipitation and as a result the land surface warms more.

Some of the largest biases in outgoing radiation and in longwave cloud forcing occur over the tropical land, Tables 3(a) and (b) and figures 18 and 19. At high resolution these biases are reduced i.e. there is less outgoing longwave radiation. The biases over the tropical oceans are also reduced with increased resolution. In both seasons the models have too much outgoing radiation over the warm pool around Indonesia where both models lack cloud and precipitation and too little over part of the Indian ocean where the models tend to have too much precipitation relative to climatology (figure 22).

Table 3 - Objective validation of radiation at the top of the atmosphere.
Mean and root mean square differences from ERBE data are calculated for each latitude band over land and sea using the land sea mask for the standard resolution grid. Values are given for the seasons DJF and JJA. All values are in Wm^{-2} and consist of the mean value followed by the rms value.

(a) Outgoing longwave radiation

Season DJF	High resolution			Standard resolution		
latitude	land	sea	all	land	sea	all
90°N - 20°N	7.0/10.3	5.0/ 8.1	5.9/ 9.2	1.8/ 9.1	3.0/8.2	2.5/8.6
20°N - 20°S	14.9/19.8	3.0/16.5	5.8/17.3	15.7/20.6	6.8/17.7	8.9/18.4
20°S - 90°S	4.5/ 8.8	6.3/ 8.6	6.0/ 8.6	1.6/9.3	3.4/6.5	3.1/7.1
global	8.6/13.4	4.9/12.2	6.0/12.5	5.7/13.4	4.5/12.1	4.9/12.5

Season JJA	High resolution			Standard resolution		
latitude	land	sea	all	land	sea	all
90°N - 20°N	14.5/18.6	6.6/10.7	10.3/14.9	8.8/14.5	3.7/7.3	6.1/11.3
20°N - 20°S	9.7/14.6	2.0/11.8	3.8/12.5	13.0/17.2	4.6/14.8	6.7/15.4
20°S - 90°S	5.6/ 9.5	5.8/ 7.7	5.7/ 8.0	0.4/7.9	2.4/6.2	2.1/6.5
global	11.3/16.0	4.6/10.1	6.6/12.1	8.3/14.3	3.5/10.4	4.9/11.7

(b) Longwave cloud forcing

Season DJF	High resolution			Standard resolution		
latitude	land	sea	all	land	sea	all
90°N - 20°N	-1.8/9.5	-4.2/7.8	-3.1/8.7	-3.3/10.1	-3.7/7.8	-3.5/9.0
20°N - 20°S	-10.1/15.2	-3.1/13.2	-4.8/13.7	-11.3/16.6	-7.2/15.3	-8.3/15.6
20°S - 90°S	-2.2/9.5	-5.8/7.6	-5.2/7.9	-1.5/10.	-5.7/7.4	-5.0/7.9
global	-4.2/11.5	-4.6/10.2	-4.5/10.6	-5.2/12.3	-5.8/11.0	-5.6/11.4

Season JJA	High resolution			Standard resolution		
latitude	land	sea	all	land	sea	all
90°N - 20°N	-7.3/10.3	-4.1/7.8	-5.6/9.0	-7.7/11.0	-4.7/6.8	-6.1/9.0
20°N - 20°S	-6.3/11.4	-2.1/9.5	-3.1/10.0	-9.8/14.7	-5.4/13.1	-6.4/13.5
20°S - 90°S	-2.3/8.9	-3.2/10.6	-3.1/10.4	-1.5/8.7	-2.5/10.4	-2.3/10.1
global	-6.2/10.4	-3.1/9.7	-4.0/9.9	-7.0/11.8	-4.1/10.8	-4.9/11.1

(c) Outgoing shortwave radiation

Season DJF	High resolution			Standard resolution		
latitude	land	sea	all	land	sea	all
90°N - 20°N	-3.8/12.2	0.2/ 9.8	-1.6/11.0	3.8/16.8	-3.1/8.1	0.1/12.9
20°N - 20°S	-8.3/18.8	5.2/19.6	2.0/19.4	-1.0/21.4	-7.9/20.3	-6.2/20.6
20°S - 90°S	11.3/17.9	2.9/24.0	4.3/23.1	17.2/26.3	-5.3/20.0	-1.5/21.2
global	-2.0/15.8	2.8/19.8	1.4/18.8	5.2/20.6	-5.8/18.2	-2.7/18.9

Season JJA	High resolution			Standard resolution		
latitude	land	sea	all	land	sea	all
90°N - 20°N	-11.7/22.8	5.8/19.5	-2.4/21.1	3.7/25.8	1.7/15.6	2.6/21.1
20°N - 20°S	-3.4/19.1	6.2/21.3	3.9/20.8	0.0/21.6	-8.3/21.9	-6.3/21.9
20°S - 90°S	1.1/ 8.1	2.5/7.9	2.3/7.9	6.9/14.6	-2.3/7.1	-1.1/8.5
global	-7.4/20.2	4.4/16.8	1.1/17.9	3.0/23.2	-3.6/16.2	-1.7/18.5

(d) Shortwave cloud forcing

Season DJF	High resolution			Standard resolution		
latitude	land	sea	all	land	sea	all
90°N - 20°N	0.4/9.2	-6.2/13.4	-3.2/11.7	-1.3/13.1	-3.0/9.1	-2.2/11.1
20°N - 20°S	-0.1/15.5	-16.1/25.7	-12.3/23.7	-6.0/20.3	-3.4/19.7	-4.1/19.9
20°S - 90°S	-11.0/25.2	-11.2/35.6	-11.1/34.1	-12.9/30.4	-3.3/29.9	-4.9/30.0
global	-2.0/15.8	-11.4/28.0	-8.8/25.2	-5.1/20.0	-3.3/23.0	-3.8/22.2

Season JJA	High resolution			Standard resolution		
latitude	land	sea	all	land	sea	all
90°N - 20°N	6.2/19.0	-15.2/30.9	-5.2/26.0	-6.5/24.1	-11.5/26.6	-9.1/25.4
20°N - 20°S	-5.8/17.6	-16.4/27.0	-13.9/25.1	-7.2/20.4	-2.5/21.5	-3.6/21.2
20°S - 90°S	-1.8/7.1	-8.1/12.5	-7.3/11.9	-7.2/13.5	-3.5/8.6	-4.0/9.4
global	1.6/17.4	-12.7/23.7	-8.6/22.1	-6.8/21.7	-5.0/19.4	-5.5/20

4.6 Hydrological cycle

Global precipitation fields at high resolution for DJF (figure 22(a)) and JJA (figure(23(a)) are very similar to those at standard resolution (figures(22(b) and 23(b). The high resolution data and that from the Legates and Willmott climatology have been area averaged to the standard resolution before plotting as contour plots of the full resolution data tend to have too much small scale detail to reproduce well. Objective validation against the University of East Anglia climatology for the AMIP period, Table 4, shows that the model has a slightly higher precipitation at high than at standard resolution in all seasons except JJA.

Table 4 - Objective validation of precipitation.

Mean and rms differences from University of East Anglia climatology of precipitation for 1979-88 over land points with model orography less than 500m on the standard grid and a climatological value (ie approximately 560 points, about a quarter of the models land points). All values are in mm/day.

	High resolution		Standard resolution	
	mean	rms	mean	rms
DJF	0.51	1.28	0.29	1.13
MAM	0.50	1.38	0.41	1.43
JJA	0.06	1.63	0.17	1.63
SON	0.13	1.25	0.05	1.22

In DJF both models have too much precipitation at about 30°N over Asia and too little precipitation over the warm pool around Indonesia in the tropics. Zonal means of precipitation and evaporation for DJF (figures 24(a) and (c)) show little difference between the two resolutions and a good agreement with the climatology over land. The zonal mean runoff figure 24(e), is higher at high resolution in the tropics. This implies that the rainfall at high resolution occurs as more intense high rainfall events where more of the rain runs away. In the northern hemisphere between 30°N and 60°N the soil moisture at high resolution is lower.

In JJA the high resolution model is able to reproduce the rain shadow over Eastern India, figure 23. Both models tend to overestimate the precipitation over land between 60° and 75° N in JJA. At high resolution the precipitation over Europe and the USA between about 30° and 50° N is lower than at standard resolution and lower than climatology. The reduction in precipitation with increase in resolution may be linked to the decrease in cloud amount over land in JJA. This lack of precipitation in JJA leads to a drying out of the soil moisture at high resolution over Europe (figure 24(h)) which will also act to reduce the precipitation as later in the summer there will be little soil moisture left to evaporate. Between 60°N and 80°N at high resolution the runoff is much greater than at standard resolution although the amount of mean precipitation and evaporation is the same. The runoff is also higher in the tropics. Like DJF this implies that the rainfall events at high resolution may be more intense allowing more rainfall to run off.

The precipitation was examined in more detail by looking at the daily precipitation for January and July over the ten years. To make the comparison fairer the high resolution daily mean precipitation was first area averaged to the standard resolution grid. At high resolution in mid-latitudes, and the tropics over land, there is more large scale rainfall (up to 0.5mm/day, figures 25a, b, e and f). There is less convective rainfall (of order 0.5mm/day,

figures 25c, d, g and h) giving approximately the same total rainfall in January and July, apart from mid-latitude northern hemisphere land. A comparison of mean precipitation from the 10 minute timestep standard resolution run with the normal 30 minute timestep run showed differences between the large scale and convective rainfall in the same sense as the differences between the high and standard resolution but the magnitude was only up to 0.1mm/day. This suggests that the differences are mainly due to resolution and not timestep. The more frequent rapidly ascending air at high resolution will lead to more large scale precipitation as the water vapour condenses and falls out. The changes in the relative amounts of large scale and convective rainfall at mid-latitudes with resolution agree with the findings of Jones et. al. (1995) comparing results from a standard resolution model with a high resolution limited area model over Europe and with the results of Williams et al. (1995). The study of Phillips et al. (1995) finds the opposite effect; the amount of convective rainfall in the ECMWF cycle 33 model increases with resolution and the dynamic rainfall decreases.

Over the land in July the standard deviation of daily precipitation is higher at high resolution, figure 26, both in the tropics and between 60°N and 80°N providing a reason for the increased runoff. The higher standard deviation in precipitation comes mainly from a greater day to day variability in the large scale rainfall. The variation in convective rainfall from day to day is little changed by resolution. In January the higher standard deviation in large scale rainfall between 0° and 45°S corresponds to the increased runoff.

4.7 Surface fluxes and near surface fields

4.7.1 Over Land

In DJF the zonal mean surface fluxes of latent heat, sensible heat and net radiation in the northern (winter) hemisphere, figures 27 (a), (c) and (e) are similar. In the southern hemisphere the net radiation at the surface increases at high resolution, where the model has less cloud, figure 16(b). Where the net radiation increases at the surface, the surface temperature and the sensible heat flux increase. In the tropics the latent heat flux is lower at high resolution figure 24(c), and the sensible heat flux has increased to give a similar net surface heating.

In JJA, the picture is similar: the net surface radiation is higher over the summer hemisphere giving higher sensible heat fluxes and high temperatures. The soil between 60°N and 30°N dries out reducing the latent heat flux. The increase in temperature near the surface at high resolution is confirmed by Table 5. Temperatures at high resolution are higher than those at standard resolution giving generally better agreement with the climatology. An exception is in JJA where the high resolution model values are too high. Figure 28(a) shows the annual cycle of the model's 1.5m temperature for a region over western Europe together with the values from the standard resolution model and the climatology. The values at high resolution are higher than those at standard resolution because there is less cloud cover at high resolution and, during the summer, not enough precipitation so the soil dries out. During June to August the high resolution model temperature, up to 4°C higher than at standard resolution, is in better agreement with climatology. Figure 28(b) shows the annual cycle for a region in South America. The higher temperatures of the high resolution model agree better with the climatology.

Table 5 - Objective validation of 1.5m temperatures.
Mean and rms differences from Legates and Willmott climatology for model grid points over land on the standard grid and where the model orography is less than 500m on the standard grid. All values are in Kelvin.

	High resolution		Standard resolution	
DJF	-0.35	3.20	-2.29	4.68
MAM	-0.03	2.32	-1.01	2.78
JJA	+0.63	3.06	-0.54	2.81
SON	-0.65	2.37	-1.71	3.34

4.7.2 Over the sea

Table 6 gives a comparison of the annual mean surface fluxes with the da Silva climatology. The largest differences occur in the latent heat fluxes but this could be due to the error in the annual mean of the da Silva climatology. The da Silva climatology used here, integrates to give a $28Wm^{-2}$ net annual mean heat flux into the ocean on the standard resolution model grid. The other main difference is in the net surface shortwave flux which is lower in the high resolution run. The difference seems to occur over the tropics, figures 29 (e) and (f) where the high resolution model has far more low level water cloud. At mid-latitudes the net surface radiation over the sea is very similar. Both the sensible heat flux, figures 29 (c) and (d), and the latent heat flux, figures 29(a) and (b), of the models are higher than the climatology over the sea.

In JJA the sensible heat flux over the sea is very similar in both models a part from 40°-80°N where the standard resolution values are higher. In DJF there is a difference at 40°N. The high resolution model has smaller sensible heat flux near the east coast of the USA and off the east coast of China and across the western part of the Pacific. The reduction in sensible heat near the east coast of the continents makes agreement with the climatology worse but further out from the coast the difference improves the agreement with climatology. Latent heat fluxes over the sea in DJF show similar differences to the sensible heat, the latent heat flux off the east coasts of the northern hemisphere continents is lower in worse agreement with climatology but agreement over the sea to the east is better. In JJA at high resolution the latent heat flux under the monsoon flow is lower in better agreement with climatology. Over the tropics the latent heat flux is too high compared with climatology at both resolutions.

Surface fluxes over the sea are important in coupled models. Increasing resolution does not seem to alter the basic systematic errors in the surface fluxes and tends to increase the westerlies round the southern hemisphere.

Table 6 Objective validation of surface fluxes
Mean and rms differences from the da Silva climatology annual means are calculated on the standard resolution model grid for sea points. All values are in Wm^{-2}.

surface flux	High resolution		standard resolution	
	mean	rms	mean	rms
Shortwave downwards	5.1	14.4	14.2	20.2
Longwave downwards	-2.4	7.1	-5.2	8.2
Sensible heat	4.2	9.3	4.7	8.6
Latent heat	31.1	37.8	29.4	36.2

4.8 Eddy Kinetic energy, Northward fluxes of momentum and heat

Low resolution climate models usually have problems simulating eddy fluxes as they are unable to resolve synoptic systems properly. The standard resolution climate model is able to do a reasonable job of simulating eddy fluxes but it might be expected that a higher resolution model would do a better job. The transient (denoted by $'$) and stationary (denoted by *) eddy components of a quantity, eg northward momentum flux, are defined in this study as

$$\overline{u'v'} = \overline{uv} - \overline{u}\,\overline{v} \qquad (1)$$

and

$$\overline{u^*v^*} = (\overline{u} - [\overline{u}])(\overline{v} - [\overline{v}]) \qquad (2)$$

where

$$\textit{Transient component of } u \textit{ is} \quad u' = u - \overline{u}$$
$$\textit{Stationary component of } u \textit{ is} \quad u^* = u - [\overline{u}]$$

The overbar indicates a mean over the whole ten years of a given season and the square brackets a zonal mean. In some studies (eg. Hoskins et. al. 1989) the transient and stationary components are calculated with respect to the mean for each season of each year separately. The method used here will also pick up transients and stationary components due to interannual variability eg. the quasi-biennial oscillation. In the case of the model fields the eddy components are derived from using values every model timestep whereas in the case of the climatology only 6 hourly fields are available. This could lead to the model having very slightly different values from those if just 6 hourly fields had been used.

Figures 30 & 31 show the zonal mean transient eddy kinetic energy for DJF and JJA. In both hemispheres and both seasons the transient eddy kinetic energy in the region of the strong westerly jets increases with resolution. This agrees with the finding of Boville, (1991). The study of Boyle, (1993) also finds an increase of kinetic energy with resolution when going from T42 to T106 but finds their model had a maximum value at T63, a resolution not considered here. The maxima in the eddy kinetic energy in both hemispheres at high resolution are close to the maxima in the climatological values but occur higher in the atmosphere; this may be connected with the model tropopause being higher than observed. At both model resolutions there is too much transient eddy kinetic energy at about 150 hPa over the tropics, but too little above this in the tropical stratosphere. The excess of eddy kinetic energy at 150hPa may be connected with the winds being too strong in the models at this level. Both models have a large easterly bias in the zonal mean wind and the Hadley circulation tends to be too strong. The lack of transient eddy kinetic energy in the stratosphere over the tropics is due to the models' inability to simulate the quasi-biennial oscillation. At high resolution the transient eddy kinetic energy in the stratosphere over the winter pole, particularly in DJF, is stronger giving better agreement with the climatology.

As with the eddy kinetic energy the transient momentum flux at high resolution, figures 32 and 33, tends to be slightly too strong in the winter hemisphere and agrees very well with the maximum in the summer hemisphere. In the models the momentum flux extends too high up due to the difference in tropopause height. The standard resolution model has southward flux of momentum at about 60°N which exceeds that at high resolution or in the climatology. This may be related to the difference in the DJF mean sea level pressure circulation seen in the standard resolution model. Both models have an unrealistic southward momentum flux at 150hPa over the tropics, the level at which there is too much transient eddy kinetic energy.

The stationary eddy momentum flux (not shown) over the equator in JJA and DJF at 200hPa is too strong at both resolutions. In DJF the high resolution model has too large a stationary momentum flux between 50° - 60°N centred on 200hPa.

The main difference between the transient eddy heat fluxes in DJF and JJA (figures 34 & 35) is the poleward confinement and strength of the stratospheric maximum in the winter hemisphere associated with the poleward shift and strengthening of the jets at high resolution. In the troposphere the transient heat flux increases with resolution and is stronger than the climatology in both hemispheres.

4.9 Variability

4.9.1 Filtered 500 hPa heights

Climate models can sometimes simulate the correct mean climatology well but are unable to capture the variability. The variability at both resolutions has been investigated by looking at 500 hPa heights using a Blackmon filter (Blackmon et. al. 1977). The band pass filter used selects variability on timescales of 2.5 to 6 days and provides a means of assessing storm tracks. In both DJF, figure 36 and JJA, figure 37, the high resolution model has higher values than the standard resolution model in both hemispheres. At high resolution, in DJF, the storm tracks over both the Pacific and Atlantic penetrate too far into the downstream continents. At standard resolution the DJF Atlantic storm track does not penetrate inland and is not as strong as the ECMWF analysis. The study of Deque and Piedelievre (1995) does not show the same increase in storm tracks with resolution but in their case increasing resolution improves the shape of the Atlantic storm track in DJF. At T42 it was too zonal in their model. In the southern hemisphere in both seasons the high resolution model values are higher than the climatology in the south Pacific whereas the standard resolution values are too low. In the southern Indian ocean the high resolution model is in better agreement with the climatology.

Figures 38 show the low pass filtered 500 hPa heights for DJF. The low pass filter used looks at variability on timescales of 10-90 days. High values tend to occur at the end of the storm tracks in the northern hemisphere. The high resolution model tends to agree better with the analysis having higher values than the standard resolution model. Both models lack variability over Canada. The models have high values over Northern Europe agreeing with the findings of Deque and Piedelievre (1995), though both their runs have lower values than observed. In JJA, figure 39, the high resolution model has more variability in the southern hemisphere giving better agreement with the analyses. In the northern hemisphere over the Pacific the standard resolution model is in better agreement with the analyses.

4.9.2 Blocking

Figure 40 a shows the blocking index for the northern hemisphere calculated using a slightly modified form of the Tibaldi and Molteni (1990) blocking index. At both resolutions the models lack blocking over the Pacific where the flow tends to be too westerly.

Over the Atlantic the high resolution model has the peak in blocking at 30°E whereas the analysis peaks at about 15°E. In MAM both models do well in the Atlantic, lack blocking over the Pacific but have too much blocking at the end of the Pacific storm track. In JJA and SON the models agree fairly well with the analyses but have a tendency to too much blocking between 30° to 70°E over Europe. There are suggestions, (Ferranti et al. (1994)) that a lack of precipitation/ diabatic heating over the Indonesian region in DJF is linked to less blocking over the Pacific. Both the models lack precipitation over the Indonesian region in both DJF and MAM. An experiment increasing the SSTs by 2°C around Indonesia for 5 DJF simulations at high resolution using an earlier version of the Hadley Centre GCM, in a similar way to the experiment described by Ferranti et al., gave an increase in the blocking over the Pacific. The anomaly runs also showed a reduction in the mean sea level bias in the North Pacific. These results suggest that the lack of blocking in the Pacific and the large error in the mean sea level pressure in the North Pacific are linked and are partly due to a lack of precipitation/diabatic heating in the model over the warm pool.

5. Conclusions

Most of the main systematic errors (ie those in winds, temperature, heights and mean sea level pressure) in the AMIP simulation appear to be almost independent of resolution. An exception to this is the change in westerly winds in the northern hemisphere stratosphere in DJF and the difference in the DJF mean sea level pressure errors over Northern Europe and Asia. The simulation of mean sea level pressure at high resolution is lower over the north pole in DJF than that at standard resolution and in better agreement with the ECMWF reanalysis. This difference may be due to the better resolution of orography and therefore gravity wave drag at high resolution or it may be due to the high resolution model being better able to simulate flow near the pole. There is a polewards shift in the westerly jets, related to the change in temperature gradient at mid-latitudes.

Increasing the resolution of the Hadley Centre climate model HadAM2b enables the model to resolve smaller scale features increasing the magnitude of the vertical motion in the model. More vigorous vertical motion leads to moist air ascending more rapidly, reaching supersaturation, condensing, releasing heat and producing more large scale precipitation. At high resolution the large scale precipitation occurs as more intense bursts. The total mean precipitation remains almost independent of resolution, increases in the large scale rainfall being compensated for by decreases in convective rainfall. The only evidence of this change in the mean fields can be seen in the total runoff which is larger at high resolution. The increase in vertical motion and warming of the atmosphere leads to a reduction in the relative humidity particularly at mid-latitudes, though the specific humidity in the same regions increases slightly. The amount of layer cloud is reduced. Some of these changes are beneficial; the cold bias is reduced slightly, changes in cloud improve the short and long wave cloud forcing over mid-latitude land.

Some of the differences between the high and standard resolution models are complicated by the fact that some of the physics schemes, i.e. convection and to a small degree ice fallout, are timestep dependent. This has made the analysis of the changes in cloud and radiation more difficult particularly in the tropics and implies that the behaviour of this model may not be typical of the behaviour of other high resolution models in this area. In this model the amount of convection over the tropical oceans increases at high resolution, but the same result is seen in a run at standard resolution with the same shorter timestep. The

reduction in convection at mid-latitudes is not seen in the shorter timestep standard resolution run suggesting that this change in convection is due to the change in resolution.

Increased resolution increases the variability of the model tending to give better agreement with the ECMWF reanalysis climatology which is from a model with a similar horizontal resolution to the high resolution model. Increased variability might be expected as the higher resolution model should be better able to resolve smaller scales. The standard resolution model has difficulty resolving and therefore simulating tropical cyclones, the high resolution model may do better at this. Increased resolution increases the transient eddy kinetic energy in the latitudes of the storm tracks implying that individual storms may be more intense as they are better resolved in the high resolution model.

Many of the findings of this study are similar to those in the other published studies of resolution (Boville, 1991, Kiehl and Williams, 1991, Boyle 1993, Phillips et al. 1995 and Williams et al 1995). All studies seem to confirm that increasing resolution tends to increase the model eddy kinetic energy. Results about temperature, moisture and clouds tend to differ and depend on the model used and also the approach taken to retuning the model as resolution is increased.

Acknowledgements

The high resolution run was on the C90 at ECMWF using computer units donated by member states as part of an ECSN project. The analysis of the results from the run was funded by CEC contract number ENV4-CT95-0184.

References

Blackmon, M. L., Wallace, J.M., Lau, N-C. and Mullen, S.L., 1977, An observational study of the northern hemisphere wintertime circulation. J. Atom. Sci. **34,** 1040-1053.

Barkstrom, B., Harrison, E., Smith, G., Green, R., Kibler, J. and Cess, R., 1989. Earth Radiation Budget Experiment (ERBE) archival and April 1985 results. Bull Am. Met Soc., **70**, 1254-1262.

Boville, B.A., 1991, Sensitivity of simulated climate to model resolution. J. Clim. **4**, 469-485.

Boyle, J.S., 1993, Sensitivity of dynamical quantities to horizontal resolution for a climate simulation using the ECMWF (cycle 33) Model. J. Clim. **6**, 796-815.

Cullen, M.J.P. and Davies, T., 1991. A conservative split-explicit integration scheme with fourth-order horizontal advection. Q.J.R. Meteorol. Soc. **117**, 993-1002.

Cullen, M.J.P, 1993. The unified forecast/climate model. Meteorol. Mag., 122, 81-94.

Da Silva, A.M., Young, C.C. and Levitus, S., 1994, Atlas of surface marine data 1994. Volume 1: Algorithms and procedures. NOAA Atlas NESDIS 6.

Deque, M. and Piedelievre, J.P., 1995, High resolution climate simulation over Europe. Clim Dyn. **11**, 321-339.

ECMWF, 1996, ECMWF re-analysis workshop 8-10 July 1996. ECMWF, Shinfield Park, Reading.

Ferranti, L., Molteni, F. and Palmer, T.N., 1994, Impact of localized tropical and extratropical SST anomalies in ensembles of seasonal GCM integrations. Q.J.R.Meterol. Soc. **120,** 1613-1645.

Geleyn, J-F. and Hollingsworth, A., 1979. An economical analytical method for the computation of the interaction between scattering and line absorption of radiation. Beitr. Phys. Atmos. **52**, 1-16.

Gregory, D. and Rowntree, P R., 1990. A mass flux convection scheme with representation of cloud ensemble characteristics and stability dependent closure. Mon. wea. rev. **118,** 1483-1506.
Gregory, D. and Allen, S., 1991. The effect of convective scale downdraughts upon NWP and climate simulations. 122-123 in Ninth conference on numerical weather prediction. Denver, Colorado, Am. Meteorol. Soc.
Gregory, D., 1995. A consistent treatment of the evaporation of rain and snow for use in large-scale models. Mon. Wea. Rev. **123**, 2716-2732.
Gregory, D., Shutts G. J. and Mitchell, J. R., 1996. A new gravity wave drag scheme incorporating anisotropic orography and low level wave breaking: Impact upon the climate of the Uk Met. Office Unified Model. Met. Office, Hadley Centre CRTN 75.
Gregory, D. and Morris, D., 1996, The sensitivity of climate simulations to the specification of mixed phase clouds. Clim. Dyn. **12,** 641-651.
Han, Q., Rossow, W. B. and Lacis, A. A., 1994. Near-global survey of effective droplet radii in liquid water clouds using ISCCP data. J. Clim. **7,** 465-497.
Harrison, E. F., Minnis, P., Barkstrom, B.R., Ramanathan, V., Cess, R.D. and Gibson, G.G, 1990. Seasonal variation of cloud radiative forcing derived from the Earth Radiation Budget Experiment. J. Geophys. Res., **95**, 18687-18703.
Hoskins, B. J., Hsu, H. H., James, I. N., Masutani, M., Sardeshmukh, P. D. and White, G. H., 1989, Diagnostics of the Global Atmospheric circulation based on ECMWF analyses 1979-1989. WCRP-27 WMO/TD - No. 326.
Jones, R. G., Murphy, J. M. and Noguer, M., 1995. Simulation of climate change over Europe using a nested regional-climate model. I: Assessment of control climate, including sensitivity to location of lateral boundaries. Q.J.R. Meteorol. Soc. **121**, 1413-1449.
Keating, G.M., Young, D.F., and Pitts, M.C., 1987. Ozone reference models for CIRA. Adv. Space Res. **7,** 105-115.
Kiehl, J.T. and Williamson, D.L., 1991, Dependence of cloud amount on horizontal resolution in the national centre for atmospheric research community climate model. J. Geophys. Res. **96,** 10955-10980.
Legates, D.R. and Willmott, C.J., 1990a. Mean Seasonal and spatial variability in gauge corrected global precipitation. Int. J. Clim., **10**, 111-127.
Legates, D.R. and Willmott, C.J., 1990b. Mean seasonal and spatial variability in global surface air temperature. Theor. and Appl. Clim. **41**, 11-21.
Mason, P.J., 1985. On the parmetrization of orographic drag. 139-165 in ECMWF seminar on physical parametrization for numerical models of the atmosphere.
McPeter, R. D., Heath, D.F. and Bhartia, P.K., 1984. Averaged ozone profiles for 1979 from the Nimbus 7 SBUV instrument. J. Geophys. Res. **89**, 5199-5214.
Palmer, T.N., Shutts, G.J. and Swinbank, R., 1986. Alleviation of a systematic westerly bias in general circulation and numerical weather prediction models through an orographic gravity wave drag parametrization. Q.J.R.Meteor. Soc., **112**, 1001-1039.
Phillips, T.J., Corsetti, L.C. and Grotch S.L., 1993, The impact of horizontal resolution on moist processes in the ECMWF model. Clim. Dyn., **11,** 85-102.
Rossow, W.B. and Schiffer, R.A., 1991. ISCCP cloud data products. Bull. Amer. Met. Soc., 72, 2-20.
Senior, C.A. and Mitchell, J.F.B., 1993. CO_2 and climate: The impact of cloud parametrization. J. Climate, **6,** 393-418.
Slingo, A., 1985. Handbook of the Meteorological Office 11-layer atmospheric general circulation model. Volume I: Model description. Met. O. 20 DCTN 29 (Unpublished)

Slingo, A. and Widerspin, R.C., 1986. Development of a revised long-wave radiation scheme for an atmospheric general circulation model. Q.J.R. Meteorol. Soc. **112**, 371-386.
Slingo, A., 1989. A GCM parametrization for the shortwave radiation properties of water clouds. J. Atmos. Sci. **46**, 1419-1427.
Smith, R.N.B., 1990. A scheme for predicting layer clouds and their water content in a general circulation model. Q.J.R. Meteorol. Soc. **116**, 435-460.
Smith, R.N.B., 1993. Experience and developments with the layer cloud and boundary layer mixing schemes in the UK Meteorological Office Unified Model. In Proceedings of the ECMWF/GCSS workshop on parametrization of the cloud-topped boundary layer, 8-11 June 1993, ECMWF, Reading, England.
Tibaldi, S. and Molteni, F., 1990, On the operational predictability of blocking. Tellus **42A**, 343-365.
Warren, S.G., Hahn, C.J., London, J., Chervin, R.M. and Jenne, R.L., 1986. Global distribution of total cloud cover and cloud type amounts over land. NCAR/TN-273.
Warren, S.G., Hahn, C.J., London, J., Chervin, R.M. and Jenne, R.L., 1988. Global distribution of total cloud cover and cloud type amounts over the ocean. NCAR/TN-317.
Warrilow, D. A., Sangster, A.B. and Slingo, A., 1986. Modelling of land surface processes and their influence on European climate. Met. O. 20 DCTN 38. (Unpublished- available from Met. Office).
Wild, M., Ohmura, A., Gilgen, H. and Roeckner, E., 1995, Regional climate simulation with a high resolution GCM: surface radiative fluxes. Clim. Dyn. **11,** 469-486.
Williamson, D.L., Kiehl, J.T. and Hack, J.J., 1995, Climate sensitivity of the NCAR community climate model (CCM2) to horizontal resolution. Clim. Dyn. **11**, 377-397.
Wilson, M.F. and Henderson-Sellars, A., 1985. A global archive of land cover and soils data sets for use in general circulation models. Int. J. Clim., **5**, 119-143.
Woodruff, S. D., Slutz, R. J., Jenne, R. L. and Steurer, P. M., 1987, A comprehensive ocean-atmosphere data set. Bull. Amer. Meteor. Soc., **68**, 1239-1250.

Figure captions

1. Mean sea level pressure for DJF. (a) High resolution run. Contours every 4mb. (b) High resolution model minus the standard resolution model. Contours every 2mb with negative values shaded. (c) High resolution model minus the ECMWF analysis climatology for 1979 to 1988, with same contour interval as 2(c).
2. Same notation as figure 1 but for MAM.
3. Same notation as figure 1 but for JJA.
4. Same notation as figure 1 but for SON.
5. Plots of the zonal mean of the u component of wind for DJF.
(a) High resolution model. (Contours every 5m/s.)
(b) High resolution minus standard resolution. Contours every 2m/s with negative contour as dashed lines.
(c) High resolution minus ECMWF analysis climatology for 1979-88. Same contours as (b).
6. Same notation as figure 6 but for JJA.
7. Zonal mean plots of the v component of wind for DJF.
(a) High resolution. Contours every 0.5m/s with negative values as dashed lines.
(b) High resolution minus standard resolution. Contours every 0.2m/s.

(c) High resolution minus ECMWF analysis climatology 1979-88.
8. Same notation as figure 7 but for JJA.
9. Plots of the probability distribution of vertical velocity for July at 850mb.
(a) 40°-60°N over land (b) 40°-60°N over sea points (c) 30°N-30°S over land (d) 30°N-30°S over sea. (e) 40°-60°S over land (f) 40°-60°S over sea, and at 500mb, (g) 40°-60°N over land (h) 40°-60°N over sea points (i) 30°N-30°S over land (j) 30°N-30°S over sea (k) 40°-60°S over land (l) 40°-60°S over sea. The solid line is the high resolution values, the dotted line the standard resolution and the dashed line the ECMWF analyses.
10. Zonal mean plots of temperature for DJF
(a) High resolution. Contours every 10 Kelvin.
(b) High resolution minus standard resolution. Contours every 0.5 Kelvin.
(c) High resolution minus ECMWF analysis climatology for 1979-88. Contours every 1 Kelvin.
11. Same notation as figure 10 but for JJA.
12. Zonal mean plots of relative humidity for djf.
(a) High resolution. Contours every 5%.
(b) High resolution minus standard resolution. Contours every 2%, negative values as dashed lines.
(c) High resolution minus ECMWF analyses for 1979-88. Same contours as (b).
13. Same notation as figure 12 but for JJA.
14.Zonal mean convective cloud for (a) high resolution land points, DJF, (b) High resolution n land points, JJA, (c) high minus standard resolution over land, DJF, (d) high minus standard resolution over land, JJA, (e) high resolution sea points, DJF, (f) High resolution sea points, JJA, (g) high minus standard resolution over sea, DJF, (h) high minus standard resolution over sea, JJA,
15. Zonal mean layer cloud for DJF & JJA as land sea split, same notation as figure 14.
16. Zonal mean total cloud amount DJF. (a) all grid points, (b) land points only (c) sea points only.
17. Same notation as figure 16 but for JJA.
18. Global charts of outgoing longwave radiation for DJF.
(a) High resolution minus ERBE data.
(b) Standard resolution minus ERBE data. Contours every $10Wm^{-2}$.
19 Same notation as figure 18 but for JJA.
20. Zonal mean albedo for DJF, (a) all grid points, (b) land points only (c) sea points only.
21. Same notation as figure 20 but for JJA.
22. Global precipitation for DJF. (a) High resolution, (b) Standard resolution (c) Legates and Willmott climatology. Contours at 0.1, 0.5, 1, 2, 5, 10, 20 mm/day.
23. Same notation as figure 22 but for JJA.
24. Plots of zonal mean over land of, precipitation (a) DJF, (b) JJA, evaporation (c) DJF, (d) JJA, runoff, (e) DJF, (f) JJA and soil moisture (g) DJF, (h) JJA.
25. Plots of zonal mean rainfall (a) large scale rainfall over land for January, (b) large scale rainfall over land for July, (c) Convective rainfall over land for January (d) convective rainfall over land for July, (e) large scale rainfall over the sea for January, (f) large scale rainfall over the sea for July, (g) convective rainfall over the sea for January and (h) convective rainfall over the sea for July.
26. Zonal mean plots of the daily standard deviation of rainfall over land for (a) large scale rainfall January, (b) large scale rainfall July, (c) convective rainfall January and (d) convective rainfall July.

27. Zonal mean surface fluxes over land for Latent heat (a) DJF (b) JJA, Sensible heat (c) DJF, (d) JJA and net radiation (e) DJF and (f) JJA.
28. Annual cycle of 1.5 m temperatures for the two models and the Legates and Willmott climatology. (a) Region over Europe. (b) region over tropical South America.
29. Zonal mean surface fluxes over the sea for DJF and JJA together with Da Silva climatology, same notation as figure 27.
30. Transient eddy kinetic energy for DJF.
(a) High resolution model
(b) High resolution model minus standard resolution.
(c) High resolution minus ECMWF climatology for 1979-88.
31. Same notation as figure 30 but for JJA.
32. Transient eddy flux of northward momentum for DJF. (a) High resolution, (b) Standard resolution (c) ECMWF climatology 1979-88.
33. Same notation as figure 32 but for JJA.
34. Transient eddy heat flux for DJF. (a) High resolution, (b) Standard resolution (c) ECMWF climatology 1979-88.
35. Same notation as figure 34 but for JJA.
36. Standard deviation of band passed filtered 500mb heights for DJF.
(a) High resolution northern hemisphere, (b) High resolution southern hemisphere.
(c) Standard resolution northern hemisphere, (d) Standard resolution southern hemisphere.
(e) ECMWF analyses northern hemisphere, (f) ECMWF analyses southern hemisphere. Contours every 10m.
37 Same notation as figure 36 but for JJA.
38. Same as figure 36 but for the standard deviation of low pass filtered 500mb heights for DJF. Contours every 20m.
39. Same notation as figure 38 but for JJA.
40. Blocking index plotted against longitude for the northern hemisphere. (a) DJF, (b) MAM (c) JJA and (d) SON.

Figure 1 (a) Mean sea level pressure for djf
high resolution

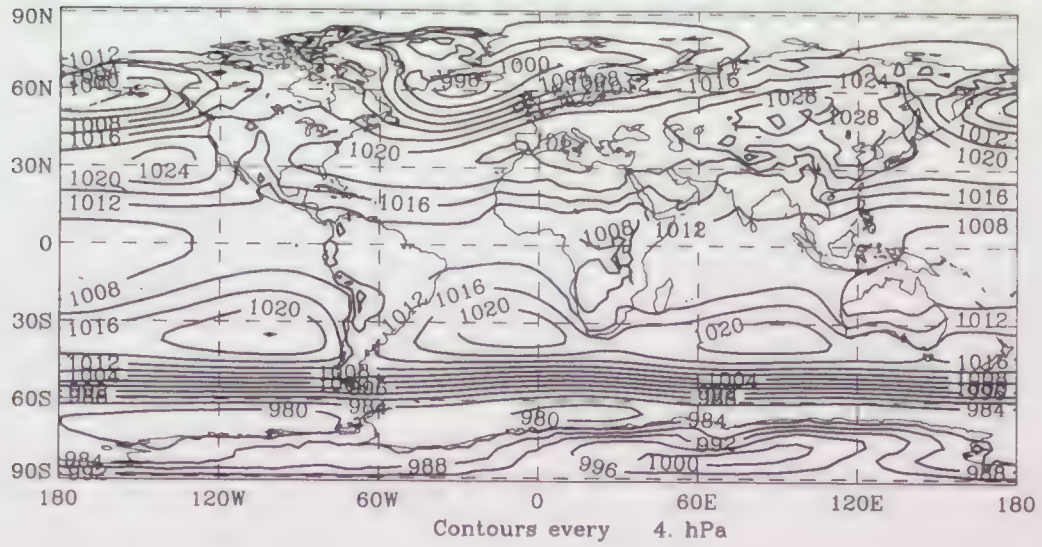

Contours every 4. hPa

(b) PMSL difference for djf
high resolution minus standard resolution

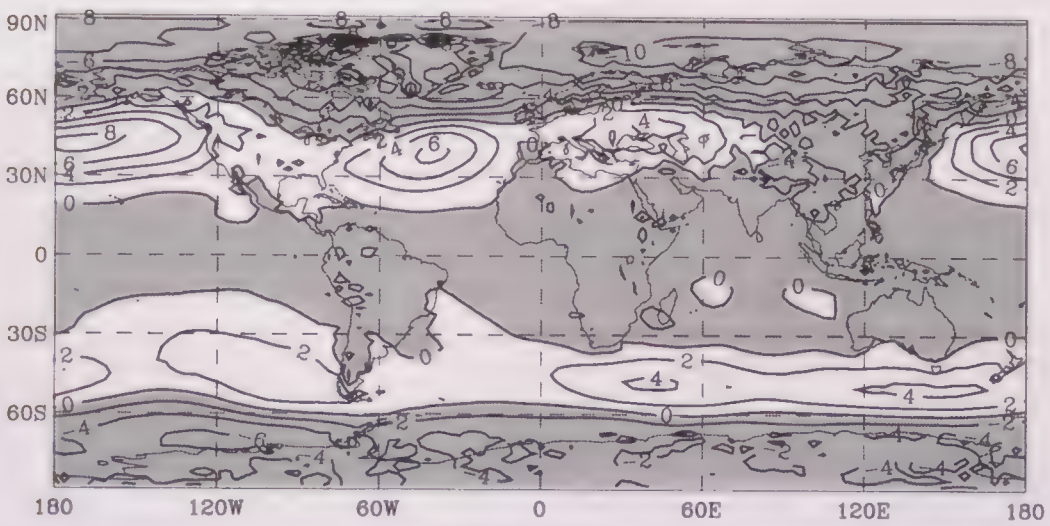

Contours every 2. hPa

(c) PMSL difference for djf
high resolution minus ECMWF climatology 1979–88

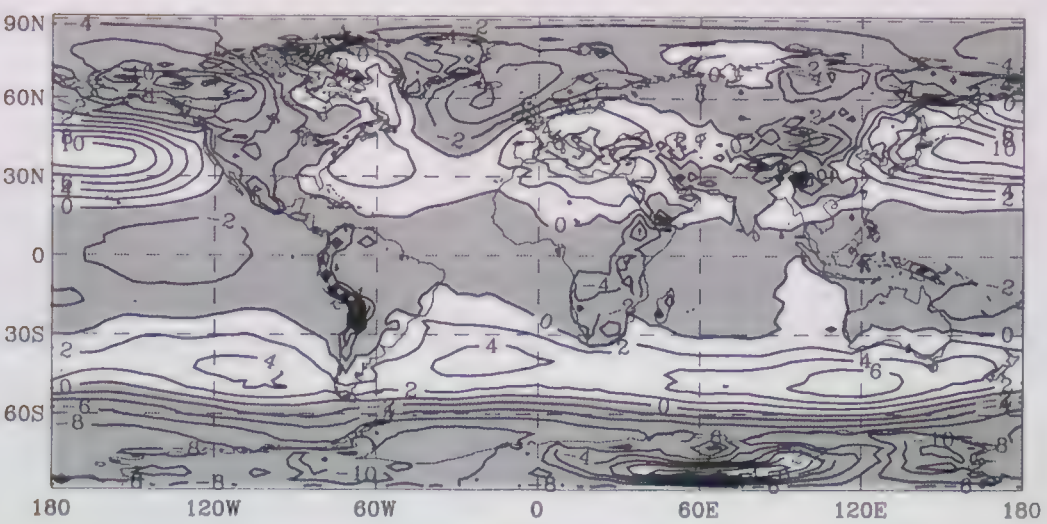

Contours every 2. hPa

Figure 2 (a) Mean sea level pressure for mam
high resolution

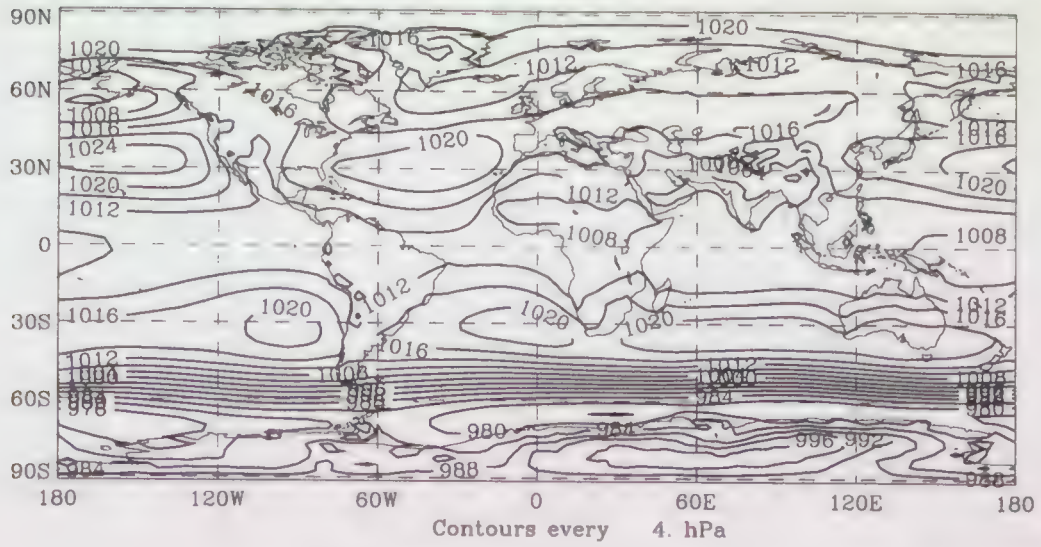

(b) PMSL difference for mam
high resolution minus standard resolution

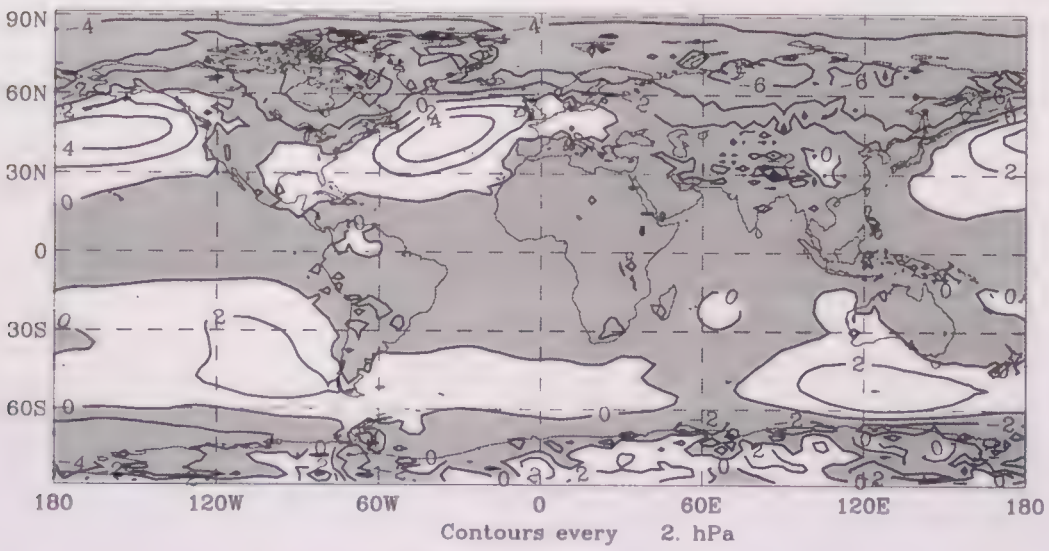

(c) PMSL difference for mam
high resolution minus ECMWF climatology 1979–88

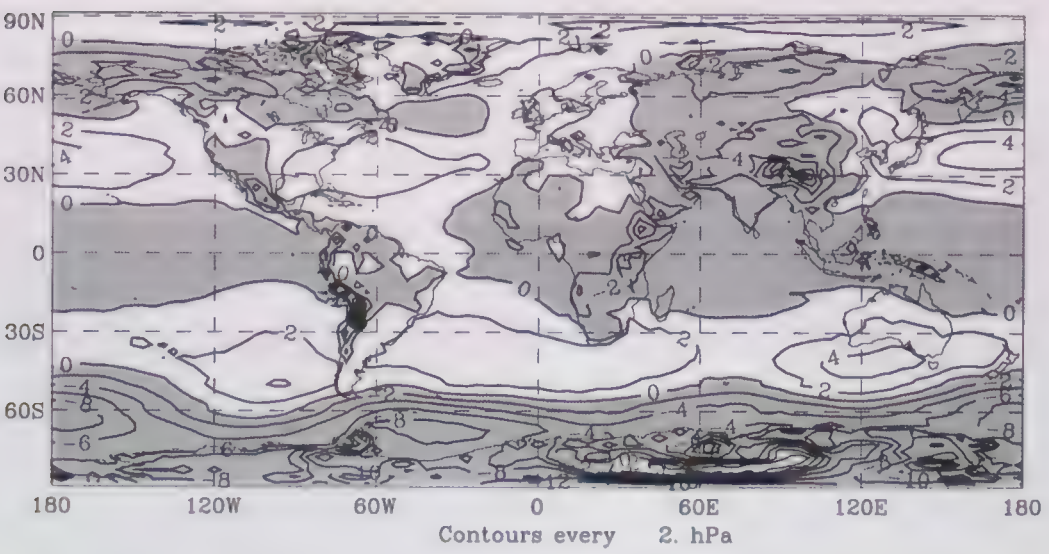

Figure 3 (a) Mean sea level pressure for jja
high resolution

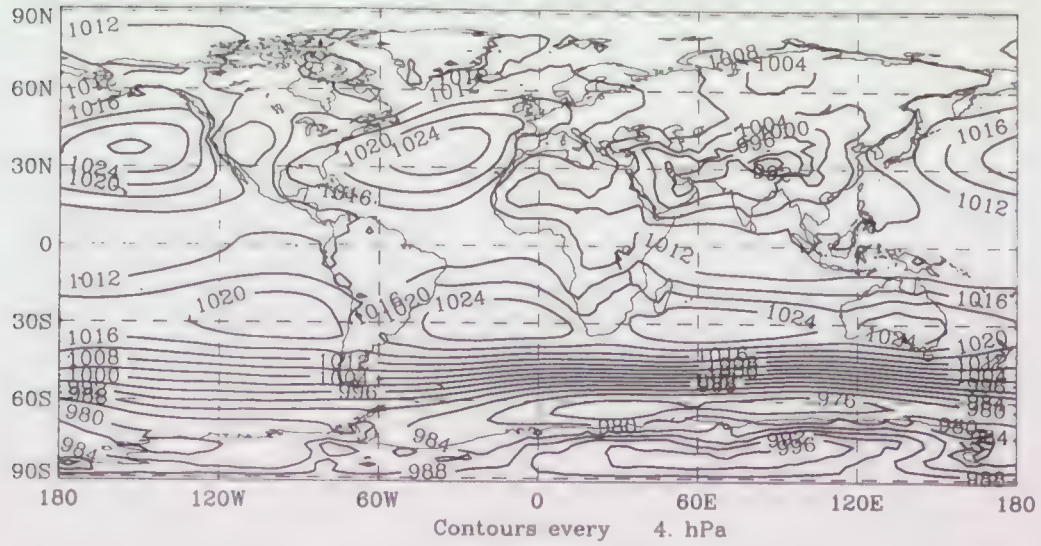

(b) PMSL difference for jja
high resolution minus standard resolution

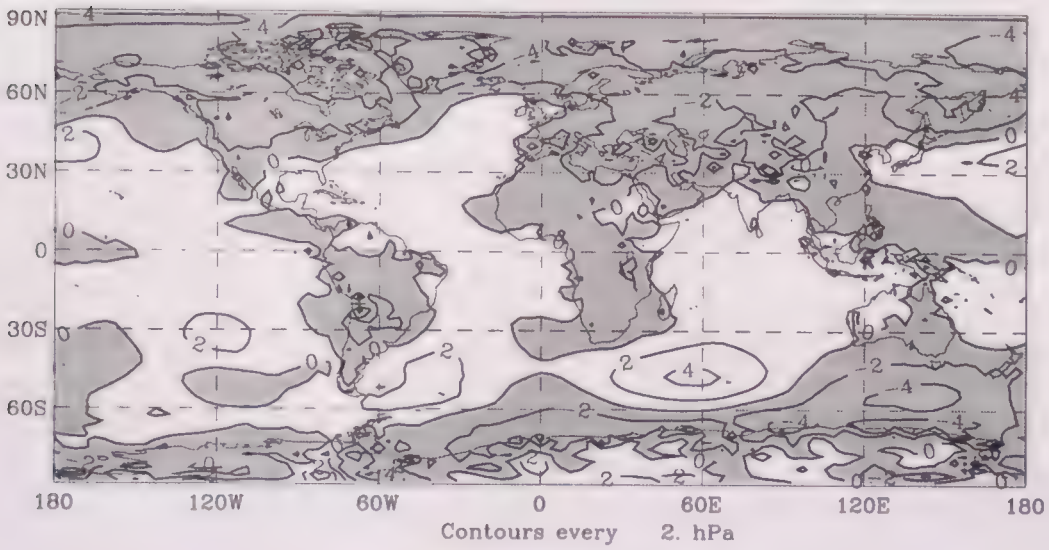

(c) PMSL difference for jja
high resolution minus ECMWF climatology 1979–88

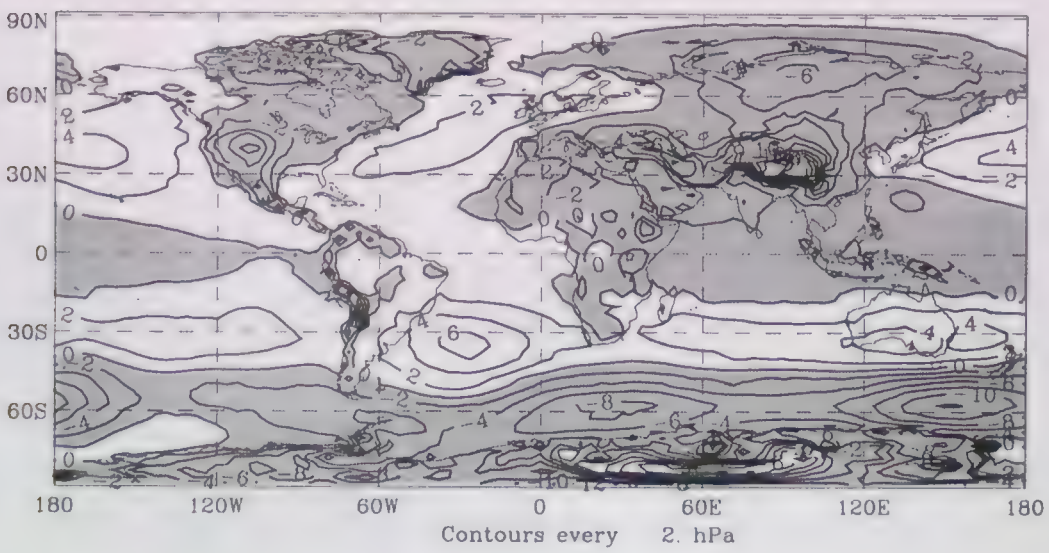

Figure 4 (a) Mean sea level pressure for son
high resolution

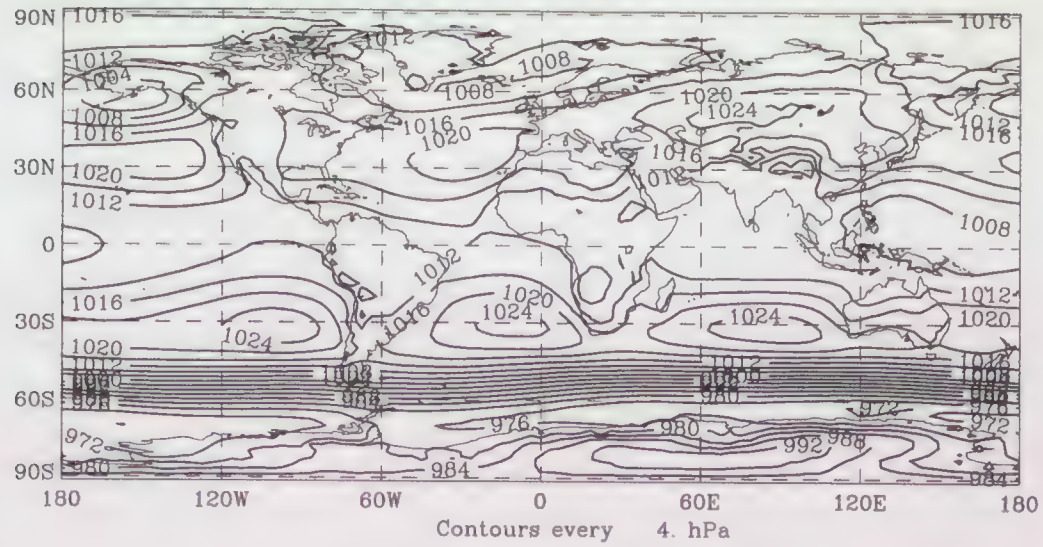

(b) PMSL difference for son
high resolution minus standard resolution

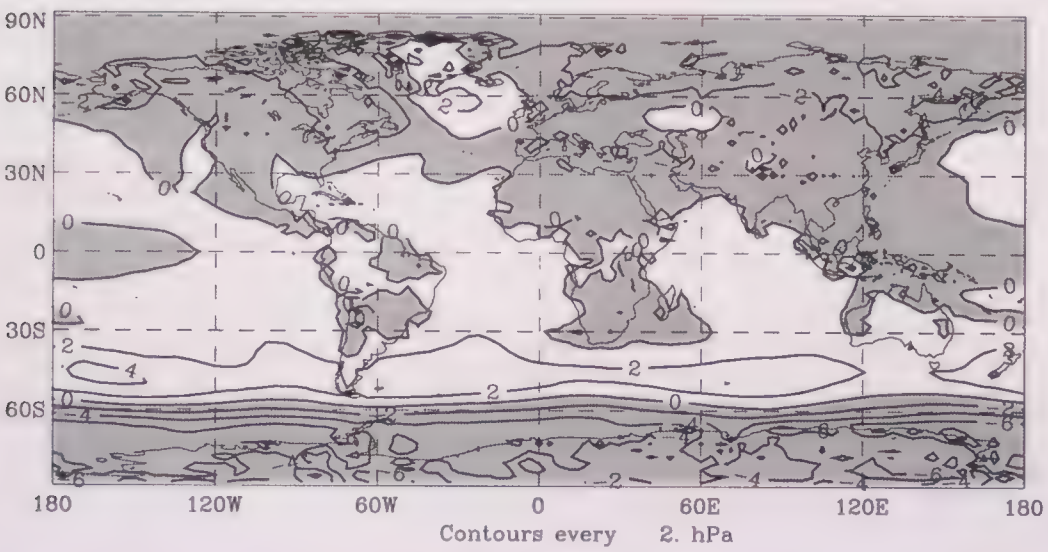

(c) PMSL difference for son
high resolution minus ECMWF climatology 1979–88

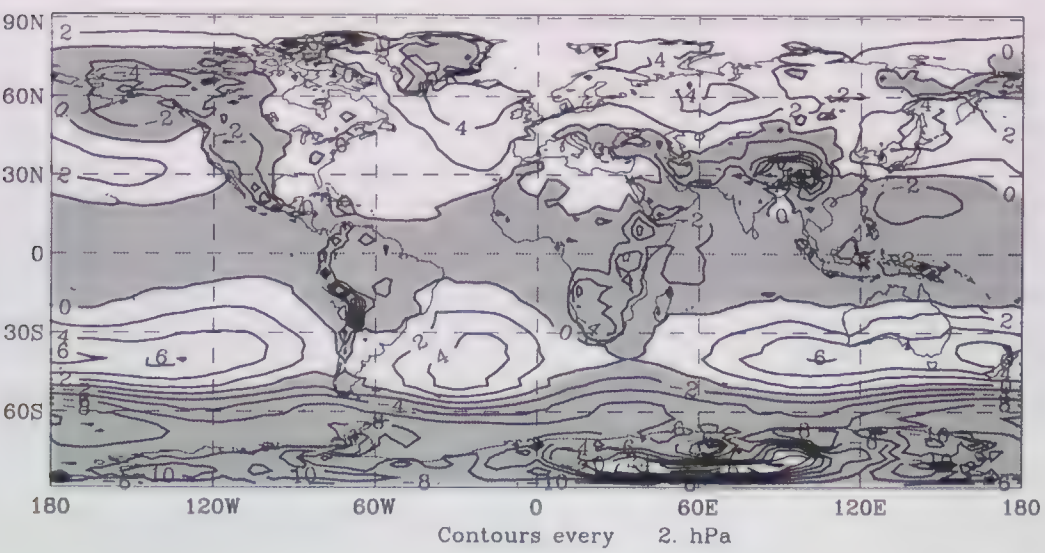

Figure 5 (a) Zonal mean cross-section of U for djf
high resolution

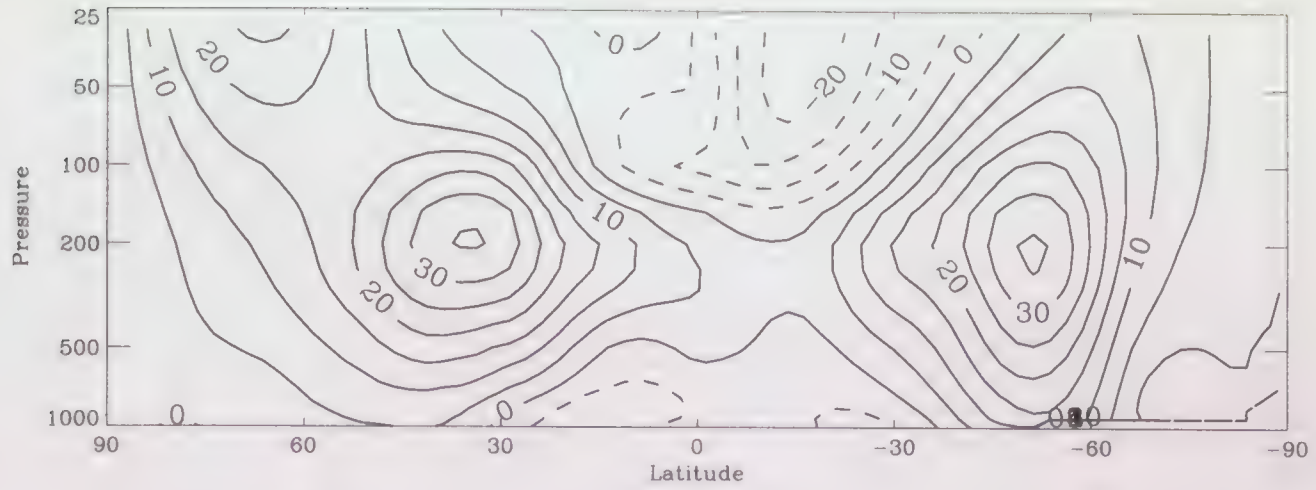

(b) Zonal mean cross-section of U difference for djf
high resolution minus standard resolution

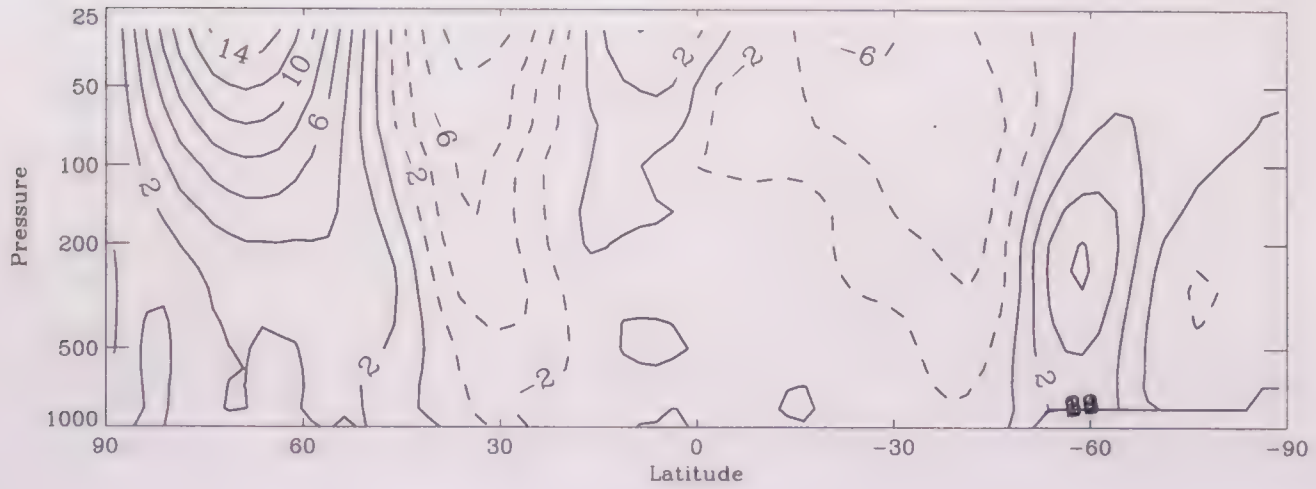

(c) Zonal mean cross-section of U difference for djf
high resolution minus ECMWF climatology 1979-88

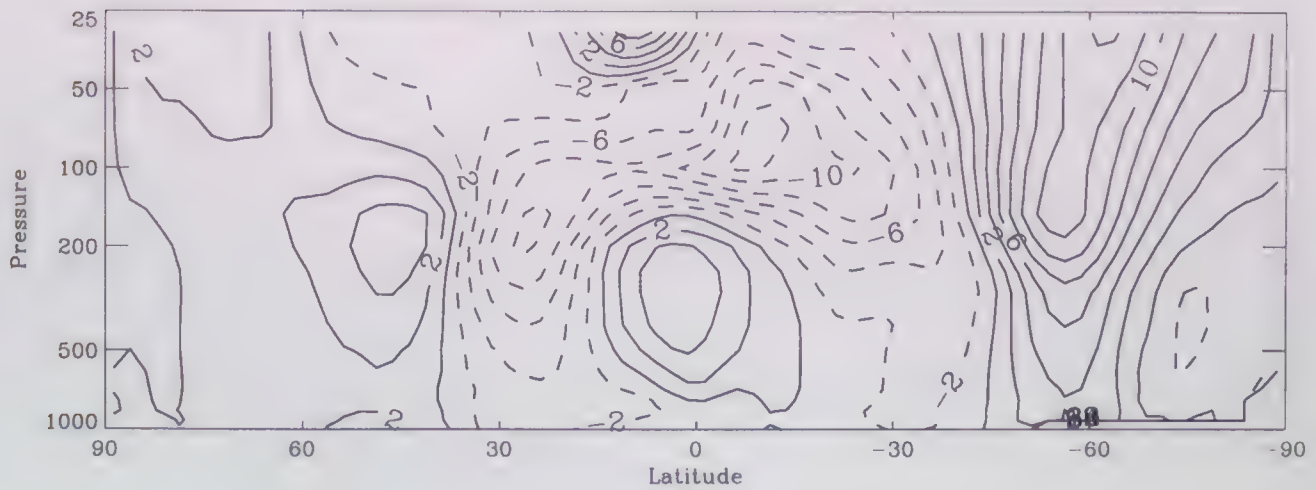

Figure 6 (a) Zonal mean cross-section of U for jja
high resolution

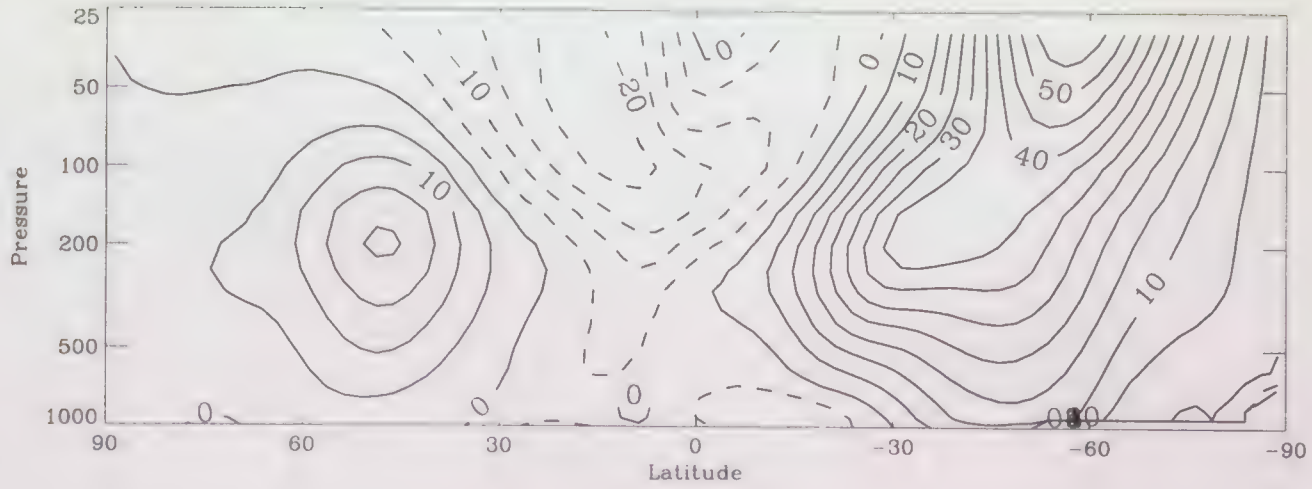

(b) Zonal mean cross-section of U difference for jja
high resolution minus standard resolution

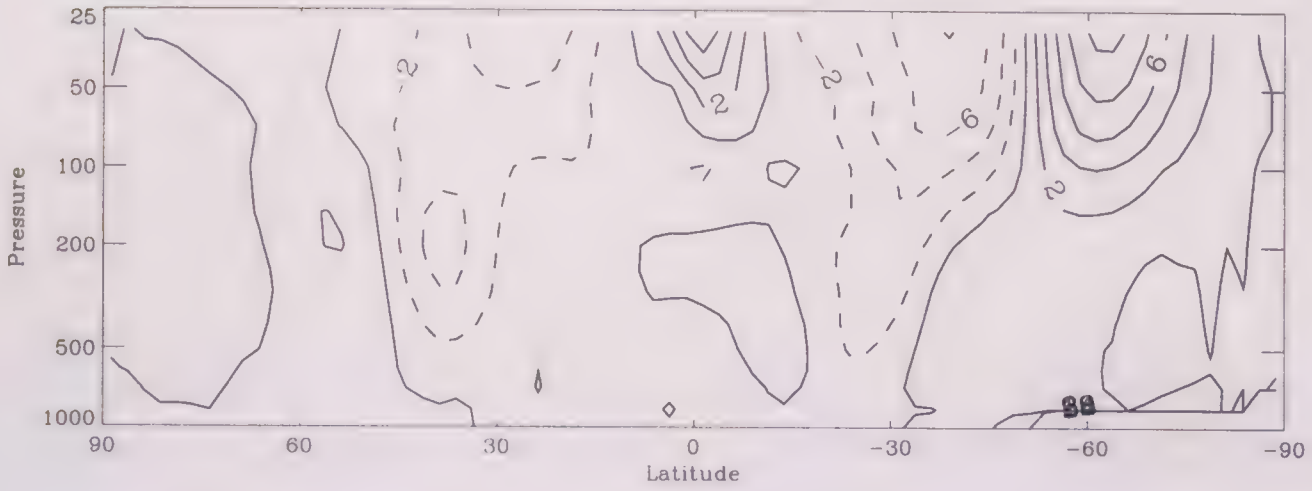

(c) Zonal mean cross-section of U difference for jja
high resolution minus ECMWF climatology 1979-88

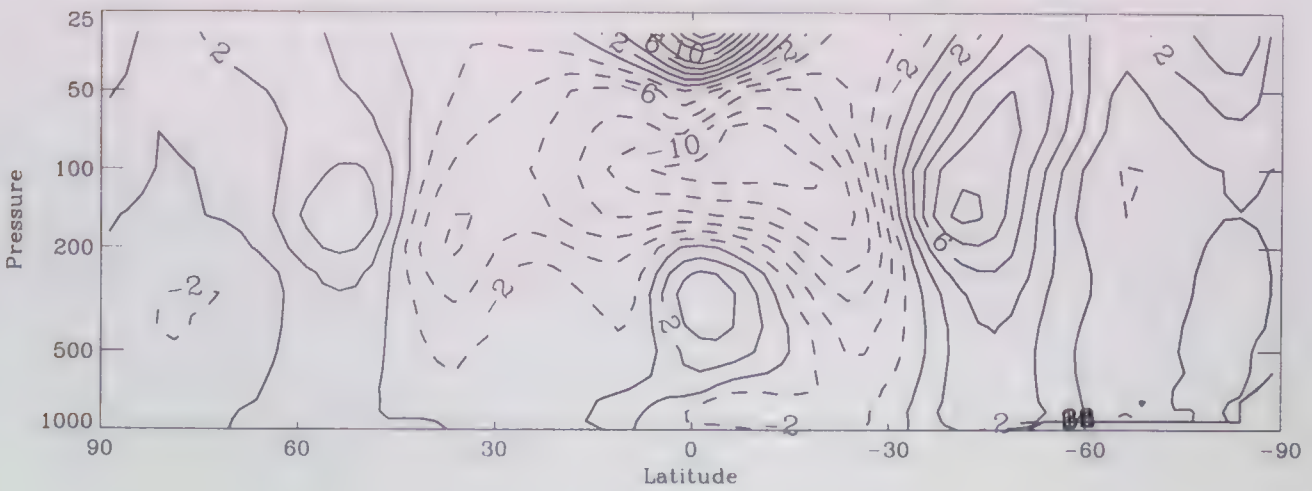

Figure 7 (a) Zonal mean cross-section of V for djf
high resolution

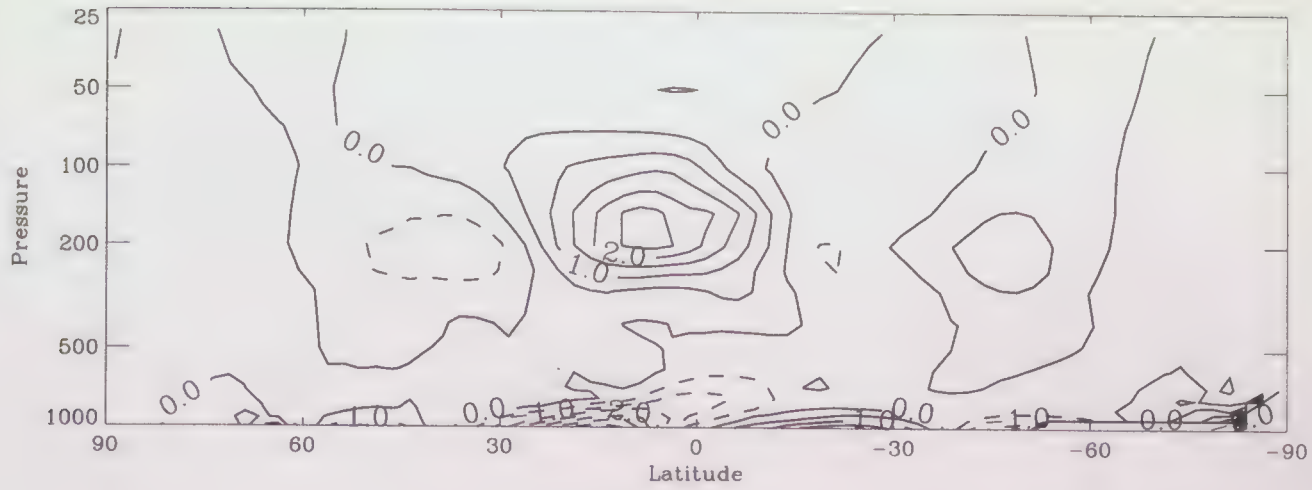

(b) Zonal mean cross-section of V difference for djf
high resolution minus standard resolution

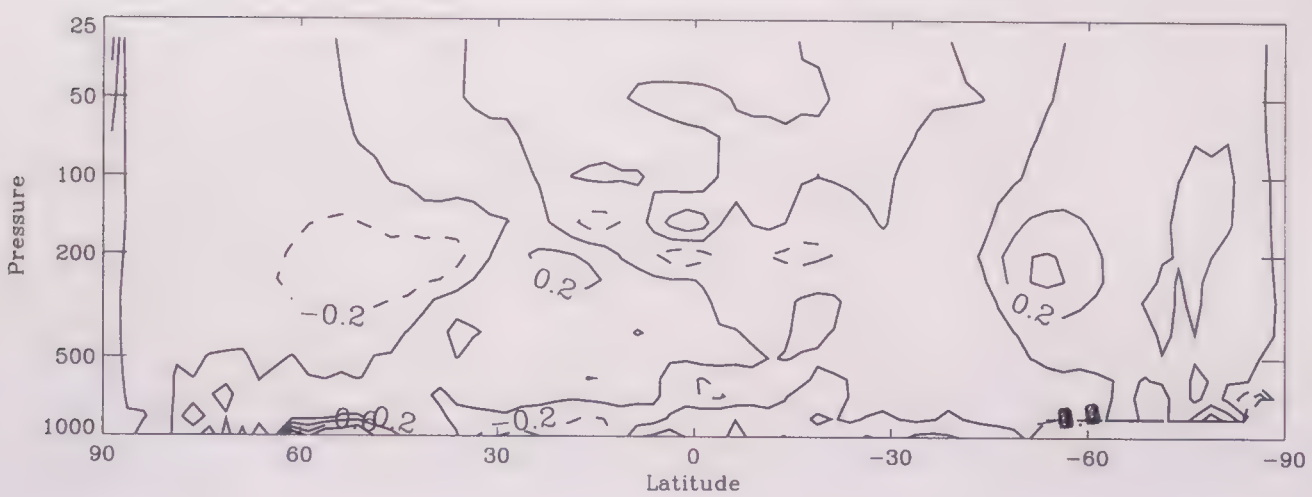

(c) Zonal mean cross-section of V difference for djf
high resolution minus ECMWF climatology 1979-88

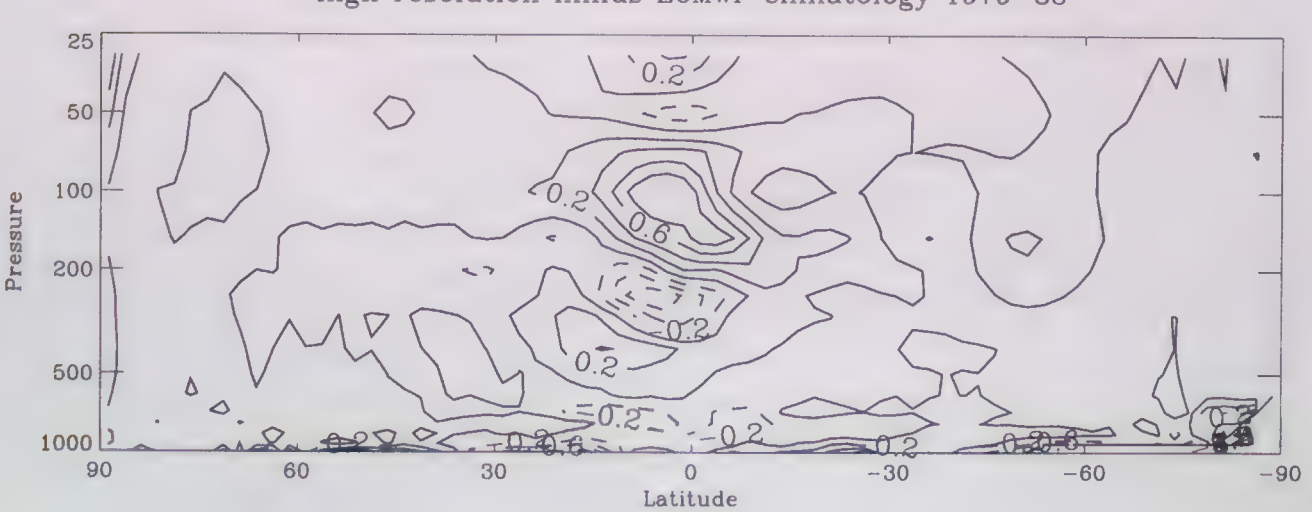

Figure 8 (a) Zonal mean cross-section of V for jja
high resolution

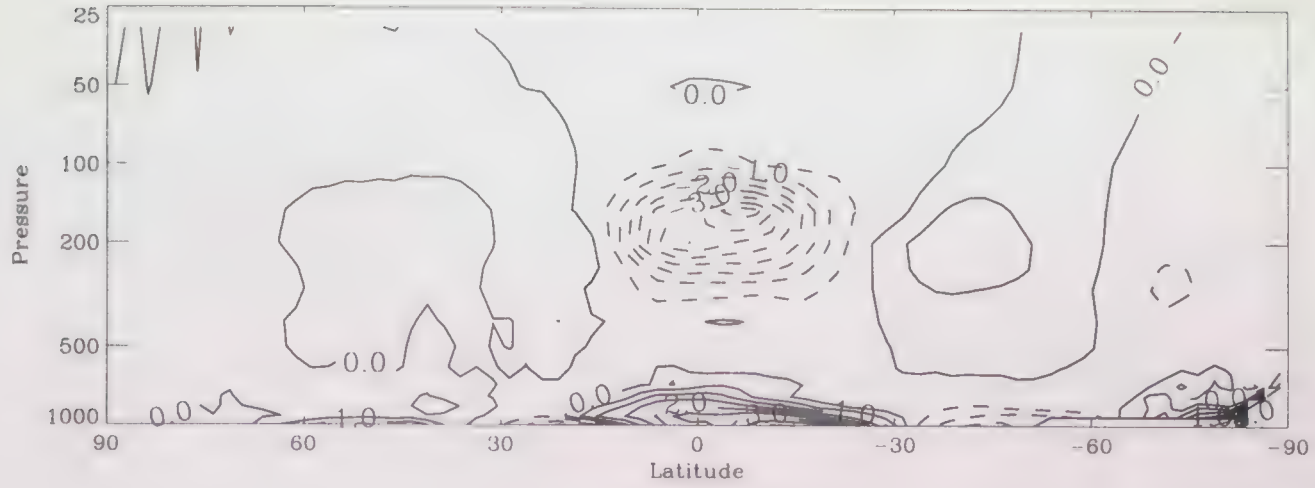

(b) Zonal mean cross-section of V difference for jja
high resolution minus standard resolution

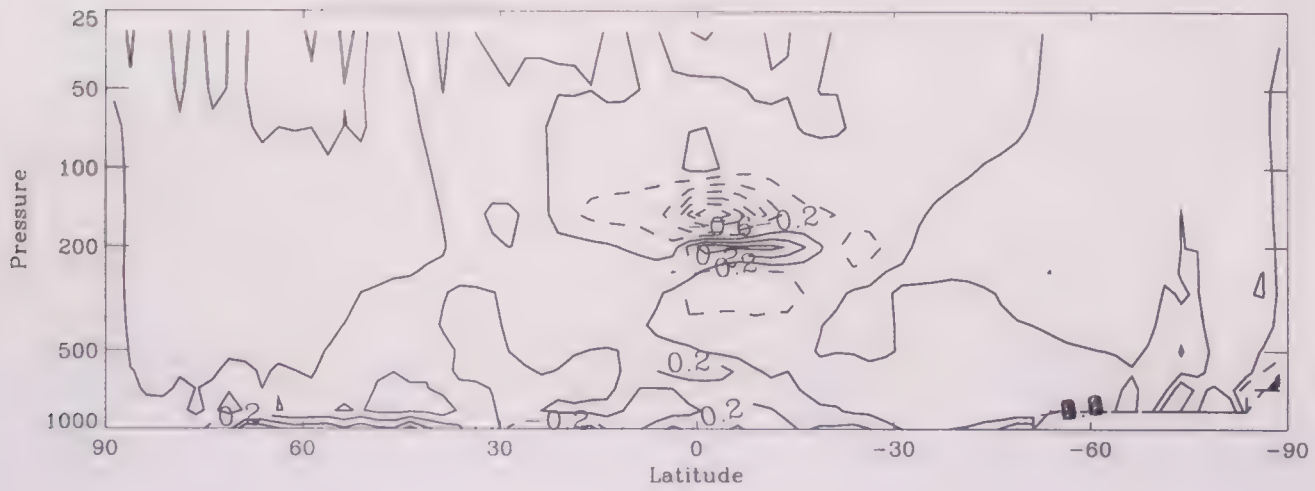

(c) Zonal mean cross-section of V difference for jja
high resolution minus ECMWF climatology 1979-88

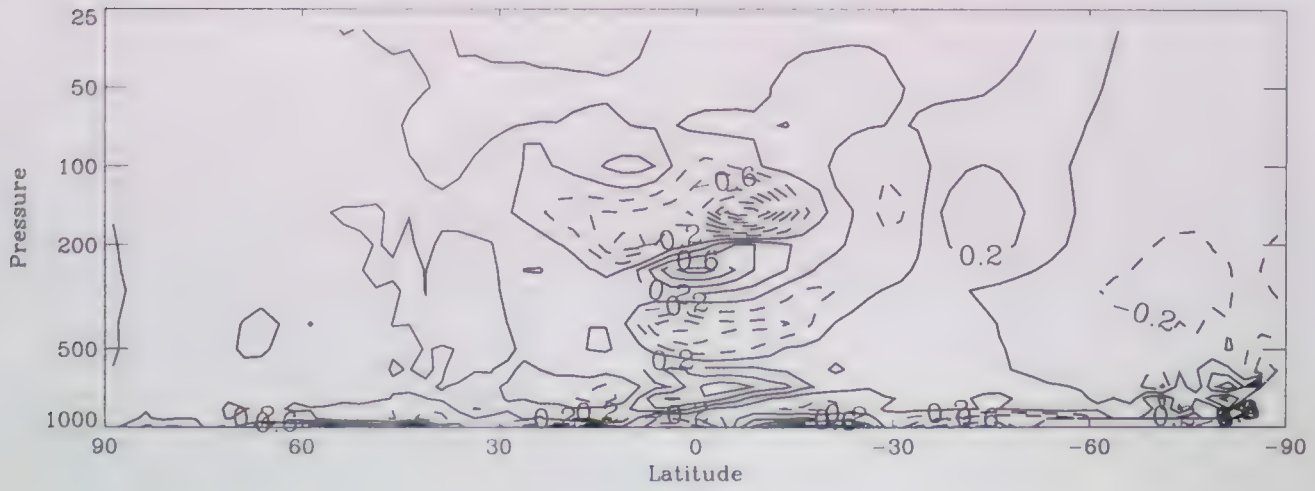

Figure 9(a) Vertical velocity at 850 hPa, in Pa/s, for jul
40–60N land

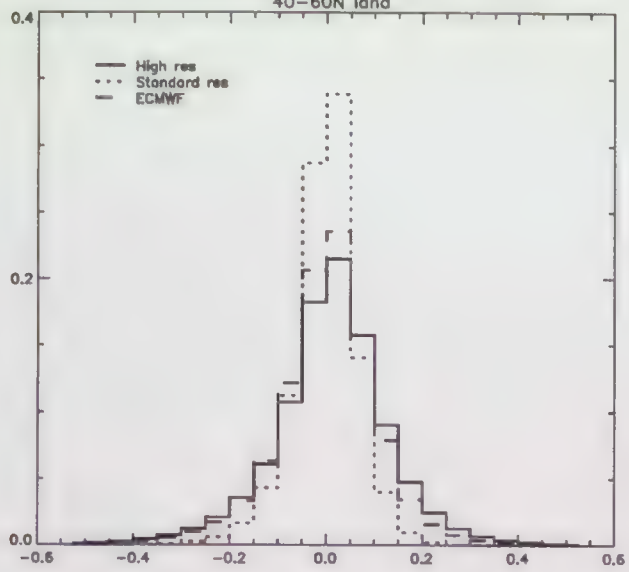

(b) Vertical velocity at 850 hPa, in Pa/s, for jul
40–60N sea

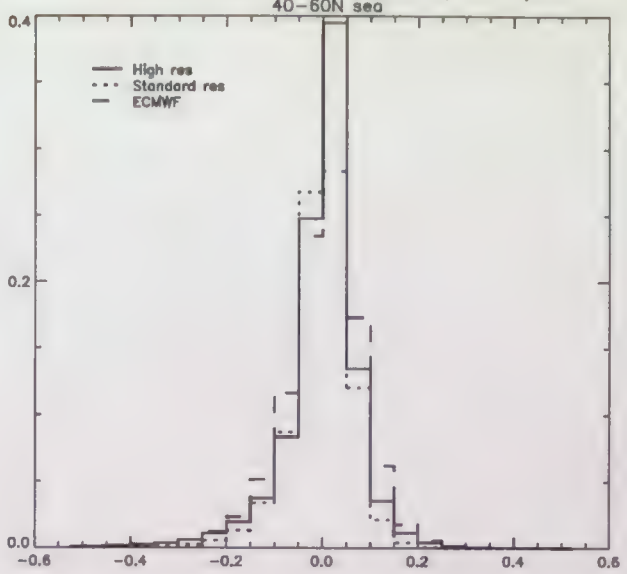

(c) Vertical velocity at 850 hPa, in Pa/s, for jul
30N–30S land

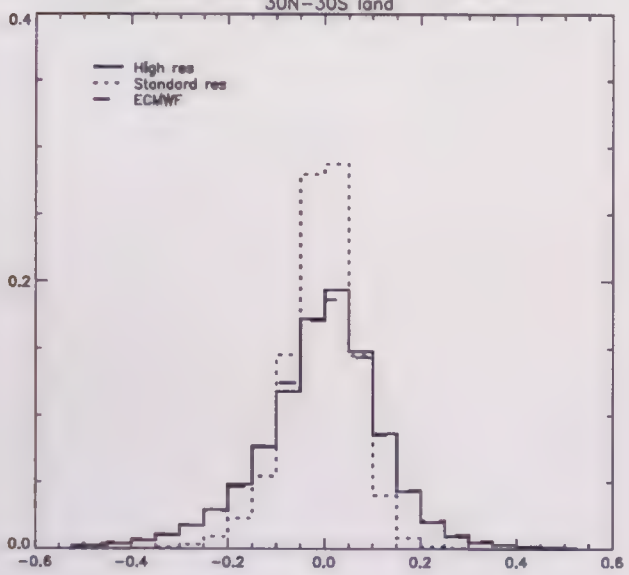

(d) Vertical velocity at 850 hPa, in Pa/s, for jul
30N–30S sea

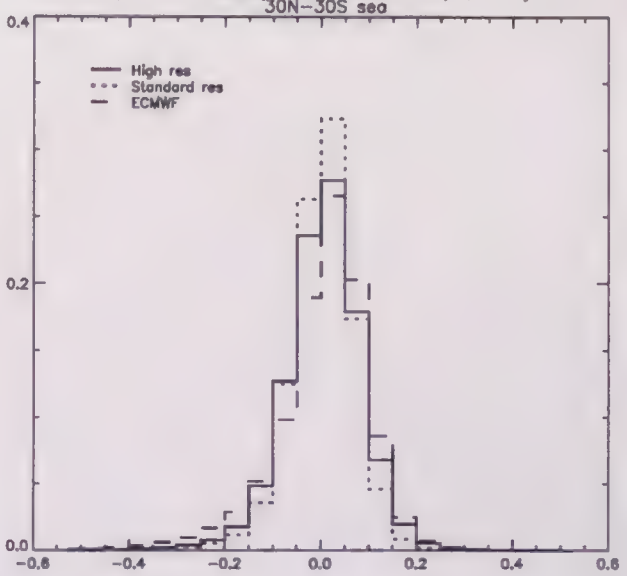

(e) Vertical velocity at 850 hPa, in Pa/s, for jul
40–60S land

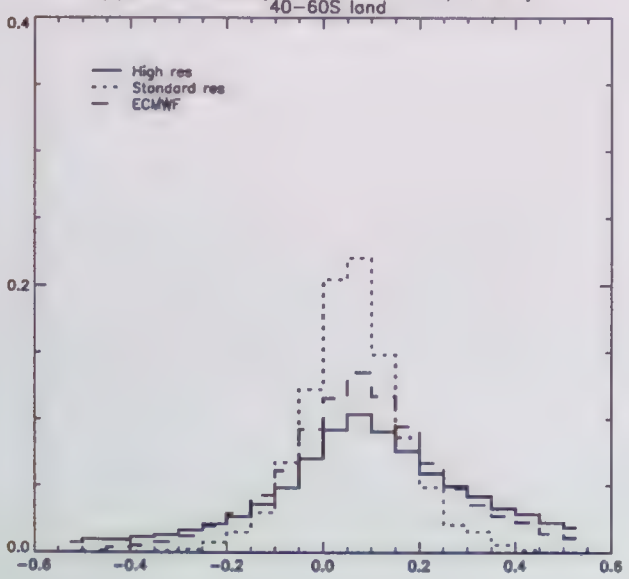

(f) Vertical velocity at 850 hPa, in Pa/s, for jul
40–60S sea

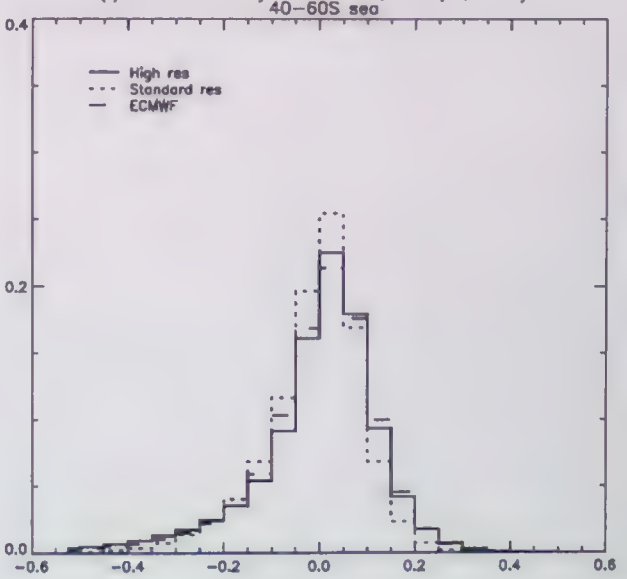

Figure 9(g) Vertical velocity at 500 hPa, in Pa/s, for jul
40–60N land

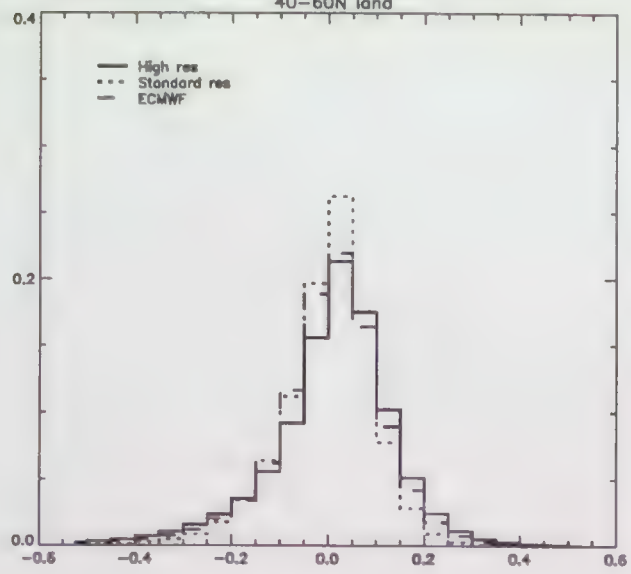

(h) Vertical velocity at 500 hPa, in Pa/s, for jul
40–60N sea

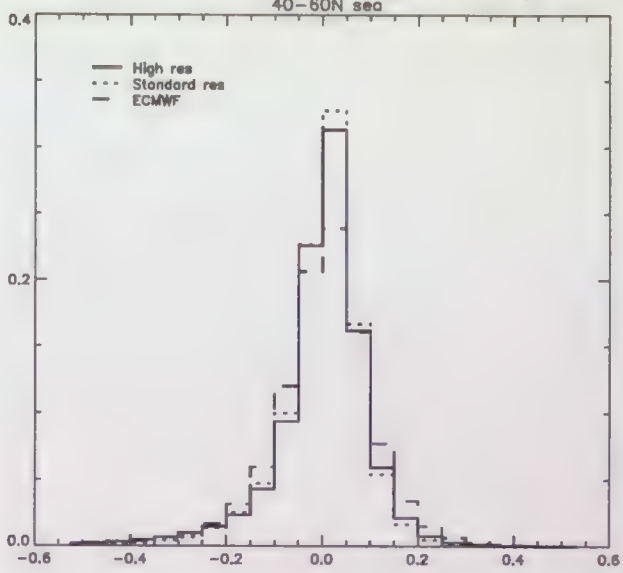

(i) Vertical velocity at 500 hPa, in Pa/s, for jul
30N–30S land

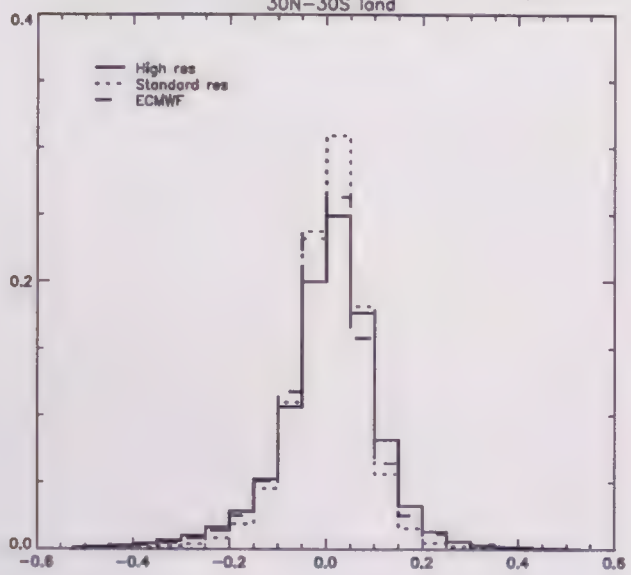

(j) Vertical velocity at 500 hPa, in Pa/s, for jul
30N–30S sea

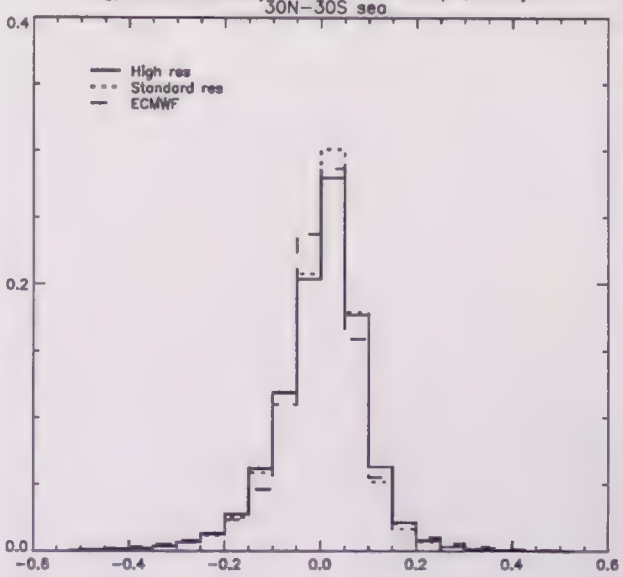

(k) Vertical velocity at 500 hPa, in Pa/s, for jul
40–60S land

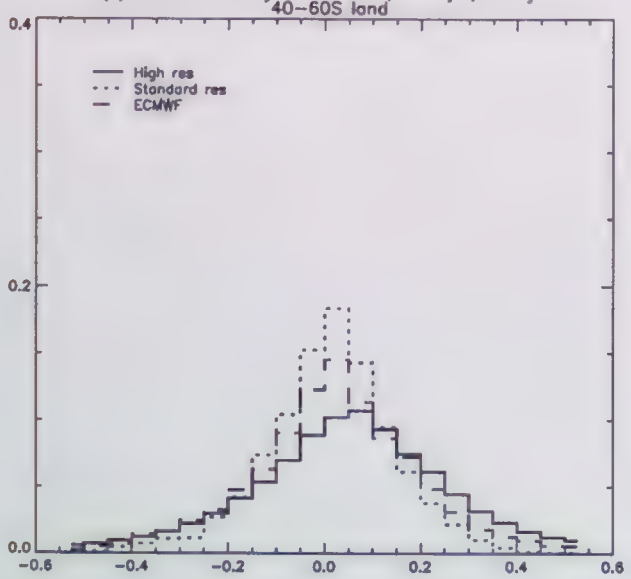

(l) Vertical velocity at 500 hPa, in Pa/s, for jul
40–60S sea

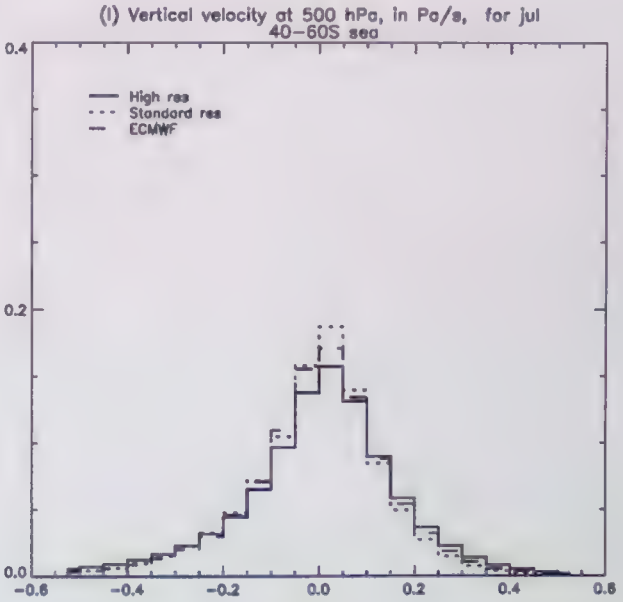

Figure 10 (a) Zonal mean cross–section of temperature for djf high resolution

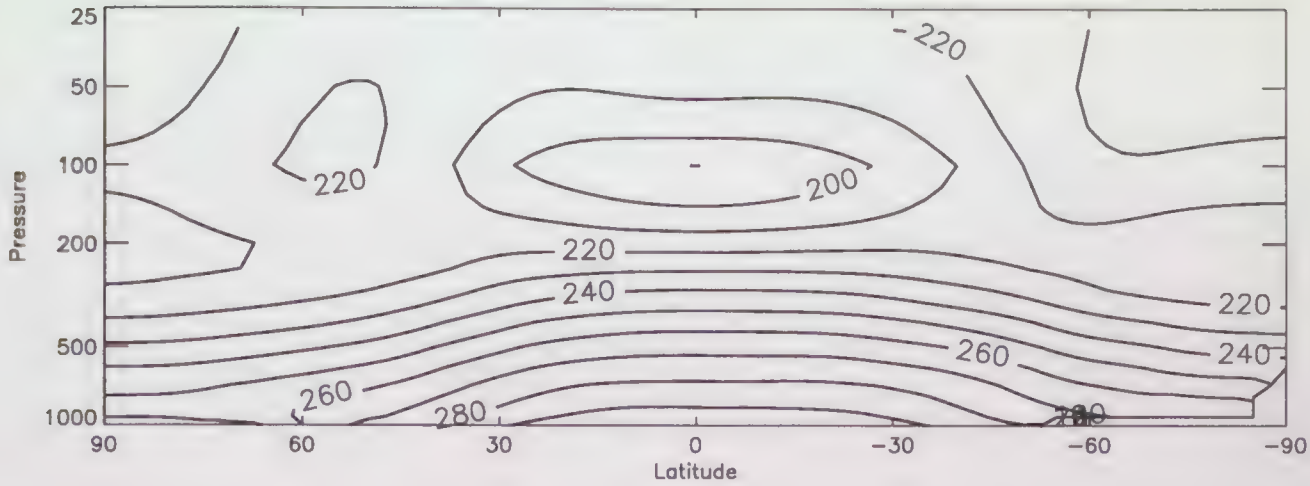

(b) Zonal mean cross–section of temperature difference for djf high resolution minus standard resolution

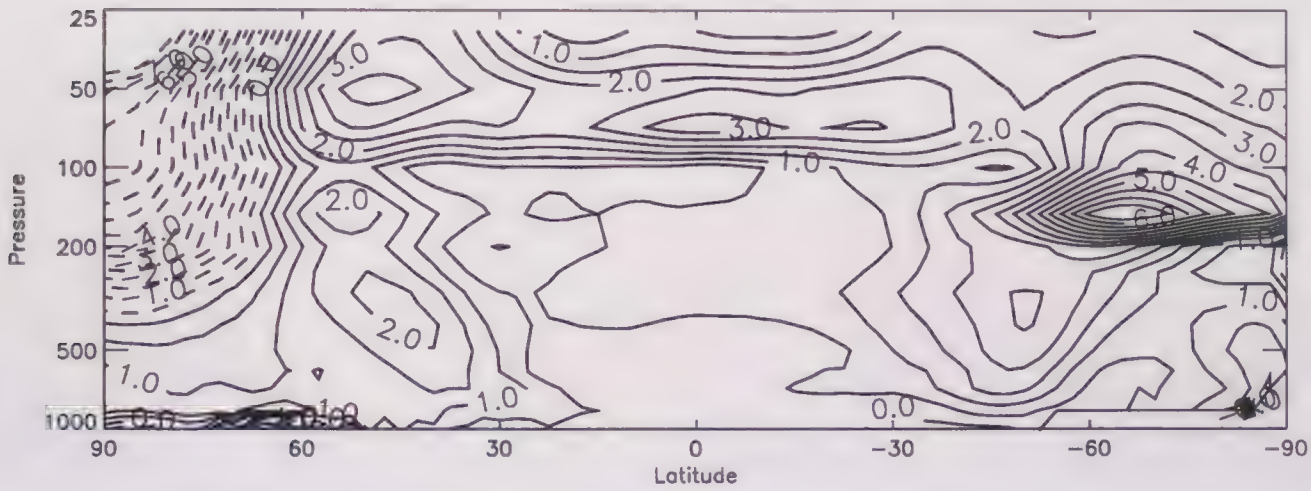

(c) Zonal mean cross–section of temperature difference for djf high resolution minus ECMWF climatology 1979–88

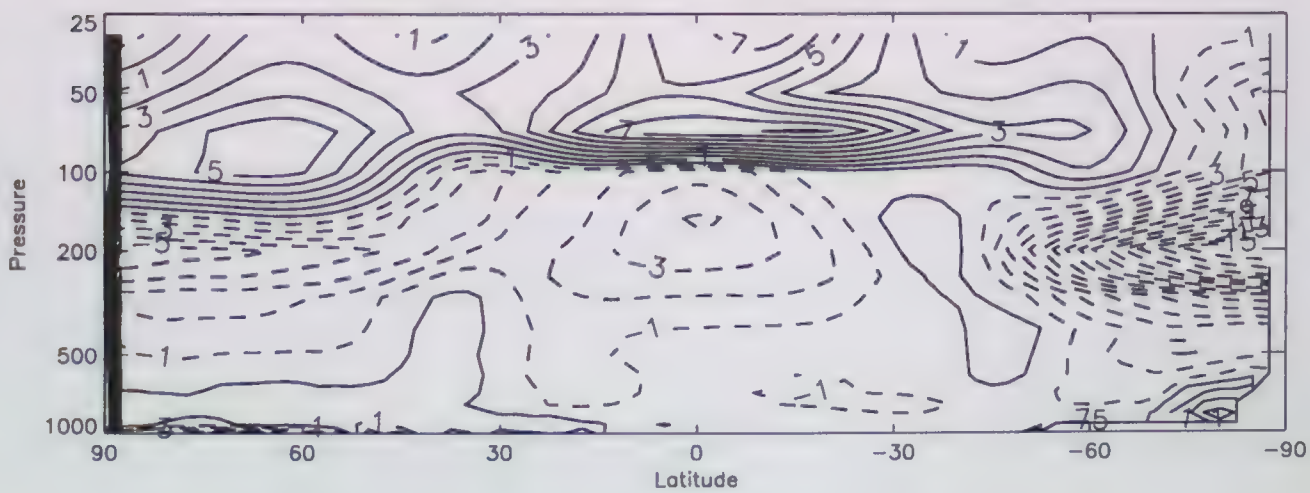

Figure 11 (a) Zonal mean cross-section of temperature for jja high resolution

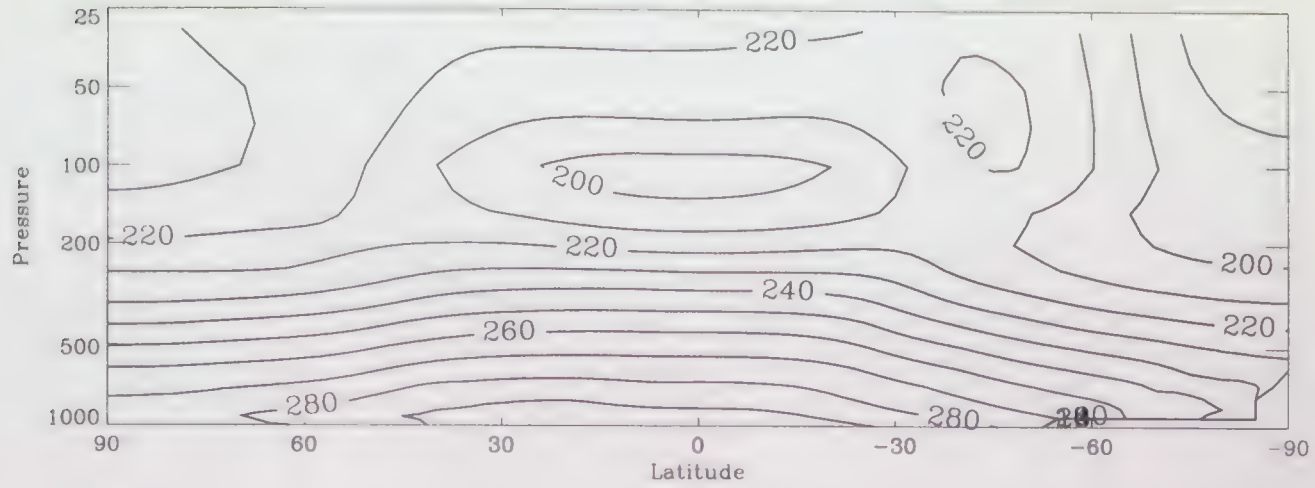

(b) Zonal mean cross-section of temperature difference for jja high resolution minus standard resolution

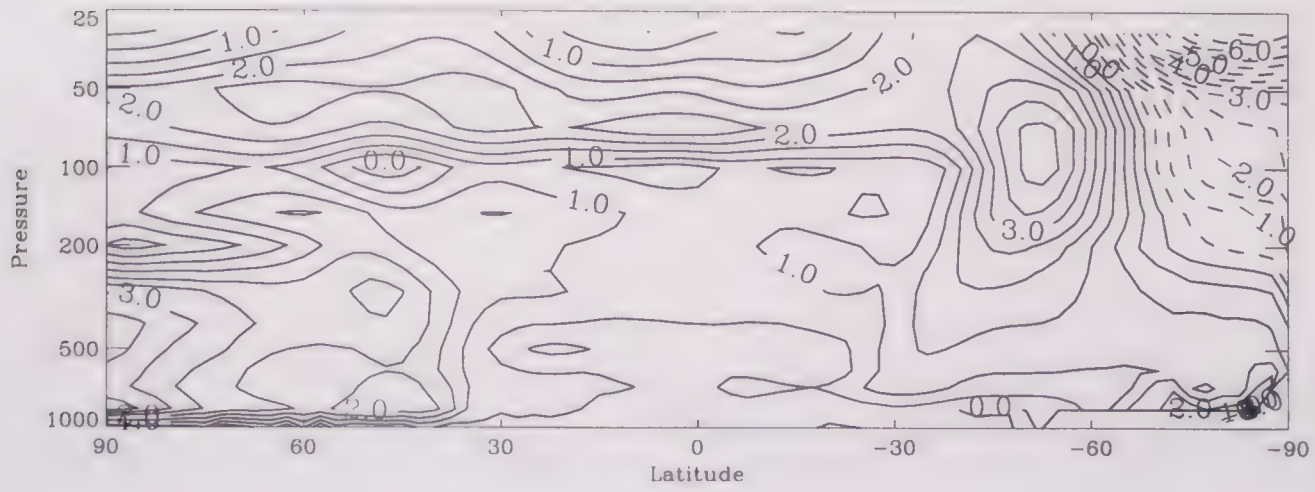

(c) Zonal mean cross-section of temperature difference for jja high resolution minus ECMWF climatology 1979-88

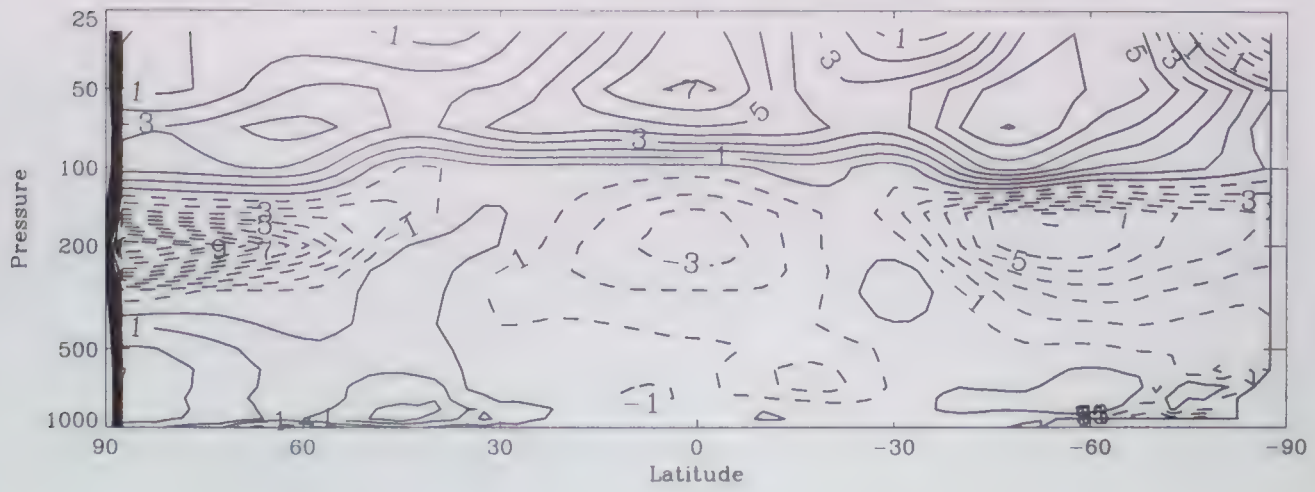

Figure 12 (a) Zonal mean relative humidity for djf
high resolution

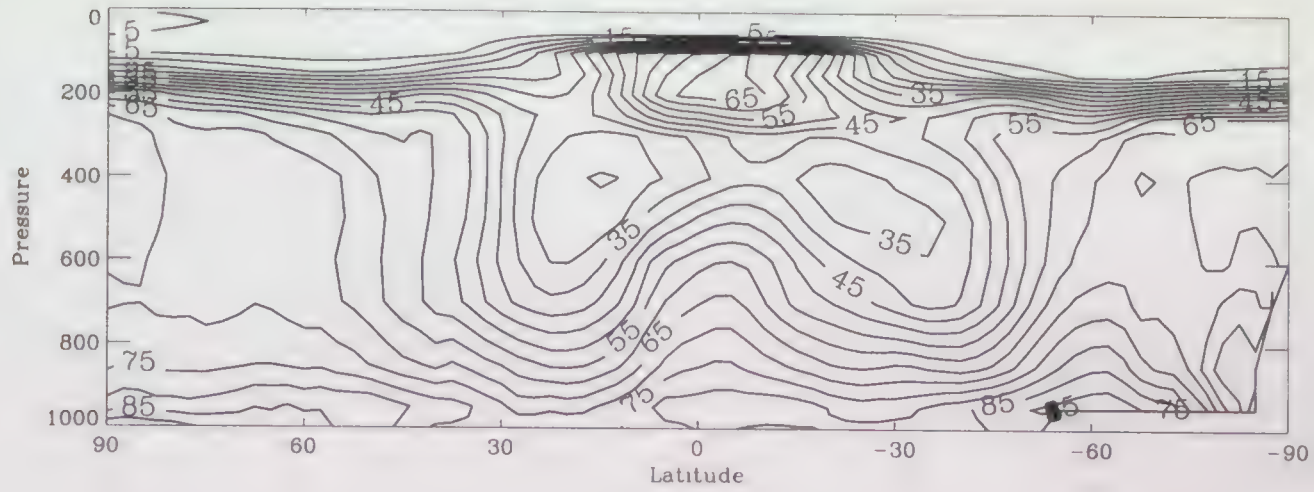

(b) Zonal mean relative humidity difference for djf
high resolution minus standard resolution

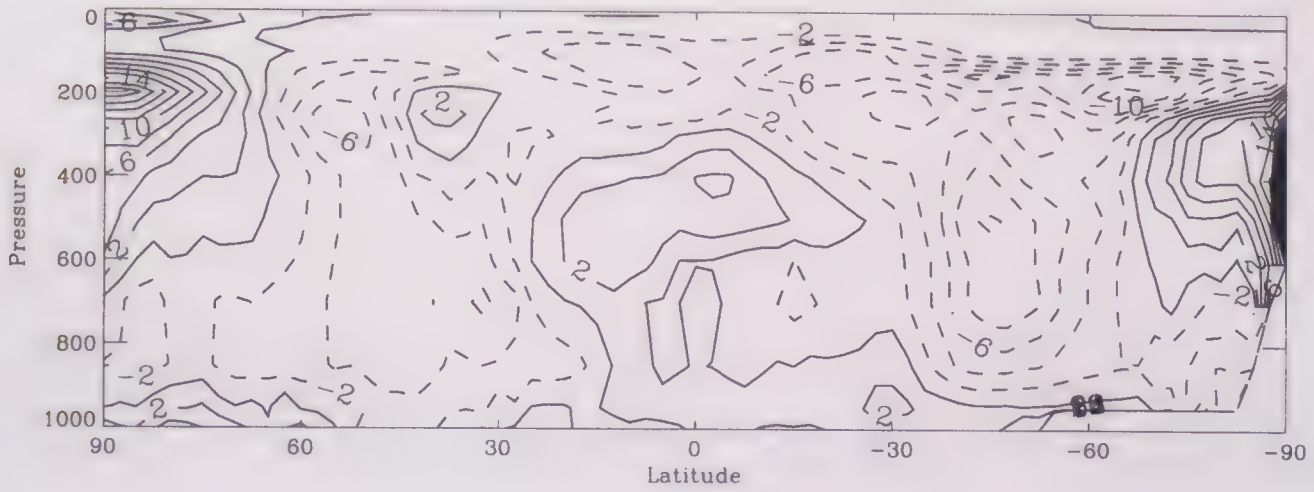

(c) Zonal mean relative humidity difference for djf
high resolution minus ECMWF climatology 1979-88

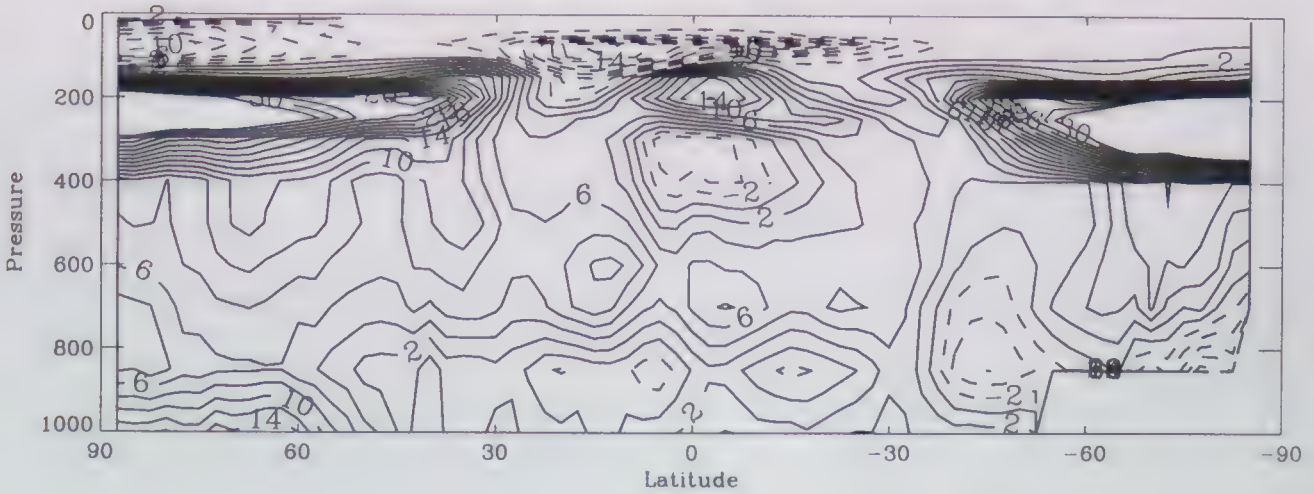

Figure 13 (a) Zonal mean relative humidity for jja
high resolution

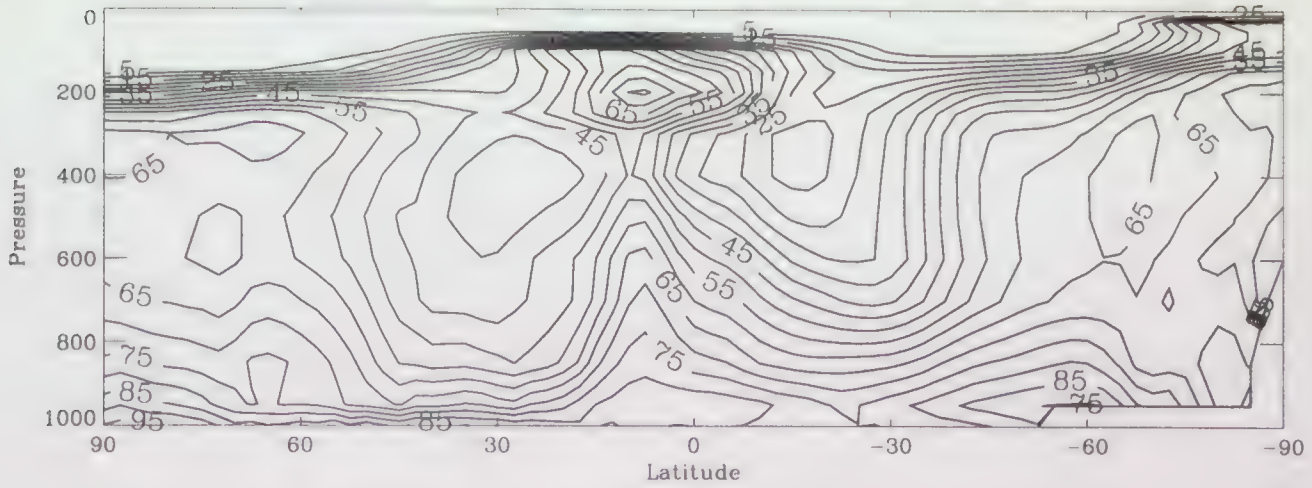

(b) Zonal mean relative humidity difference for jja
high resolution minus standard resolution

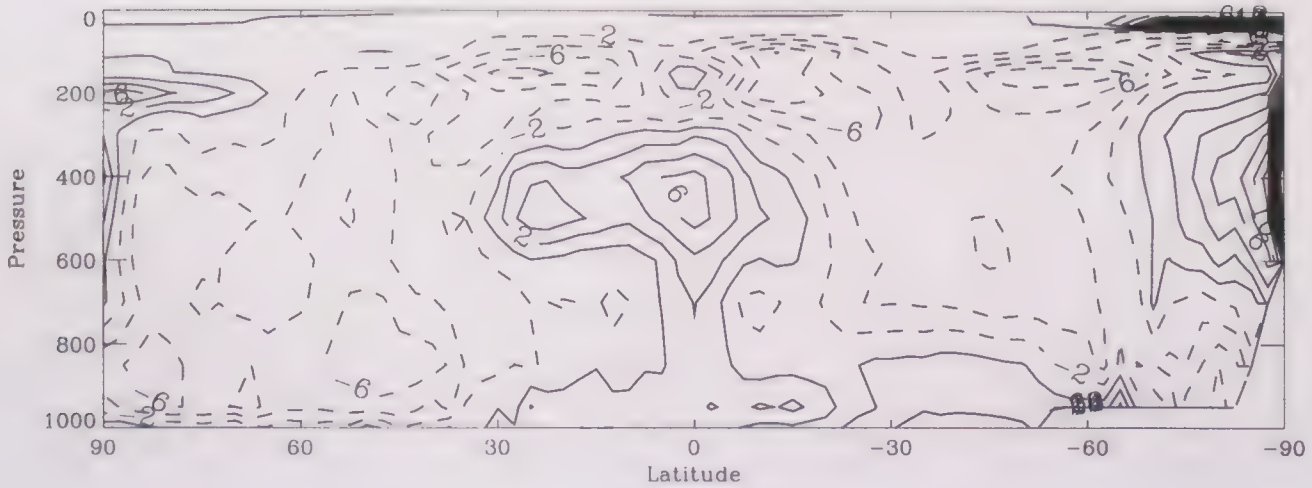

(c) Zonal mean relative humidity difference for jja
high resolution minus ECMWF climatology 1979–88

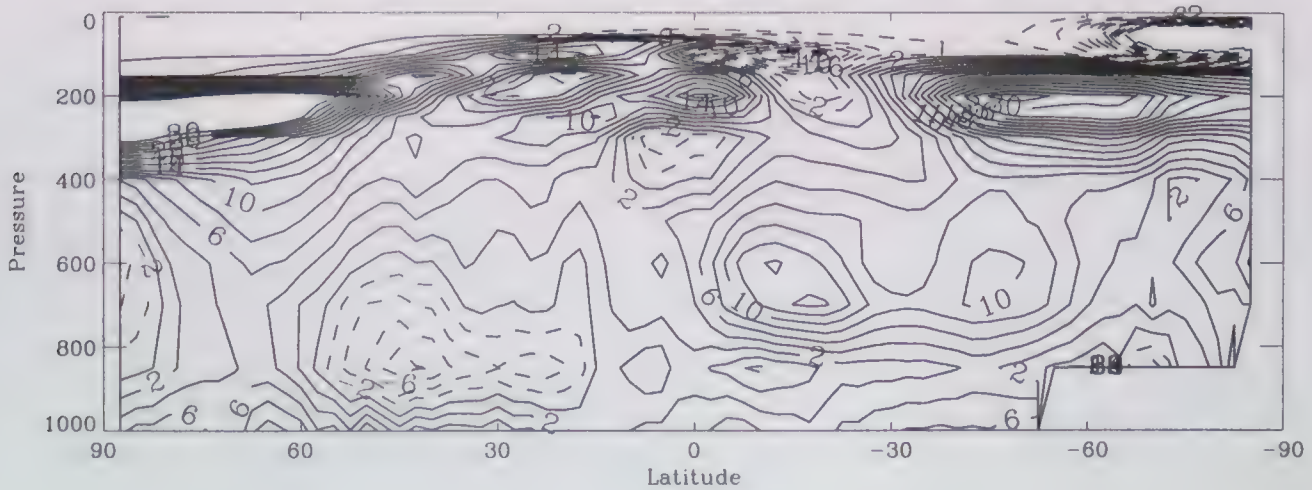

Figure 14 (a) Convective cloud amount over land for DJF high resolution

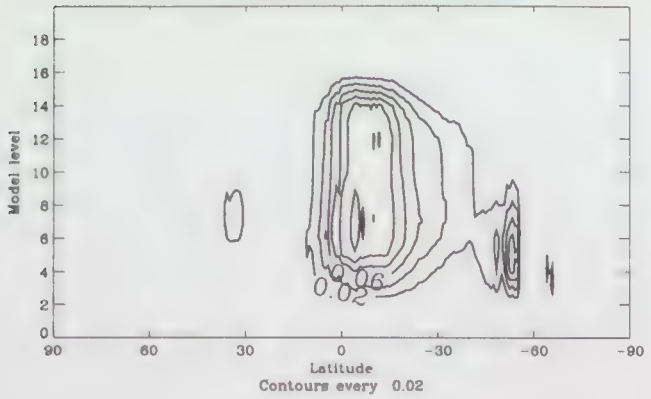

(b) Convective cloud amount over sea for DJF high resolution

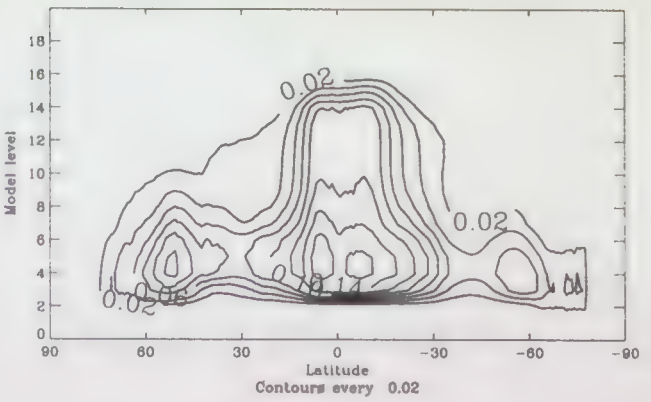

(c) Convective cloud amount over land for DJF high resolution minus standard resolution

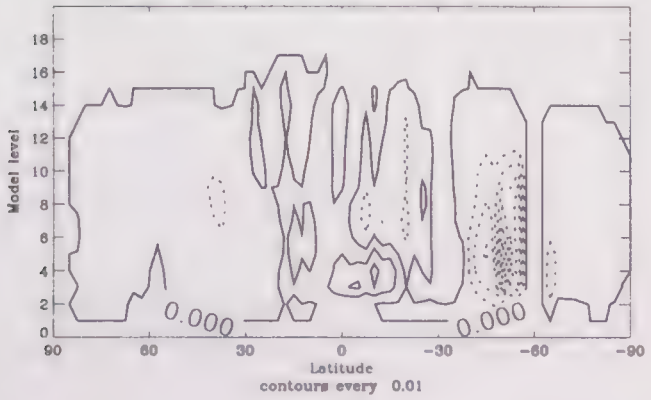

(d) Convective cloud amount over sea for DJF high resolution minus standard resolution

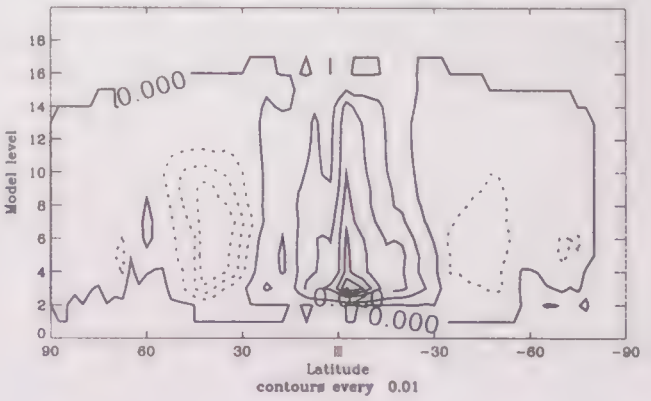

(e) Convective cloud amount over land for JJA high resolution

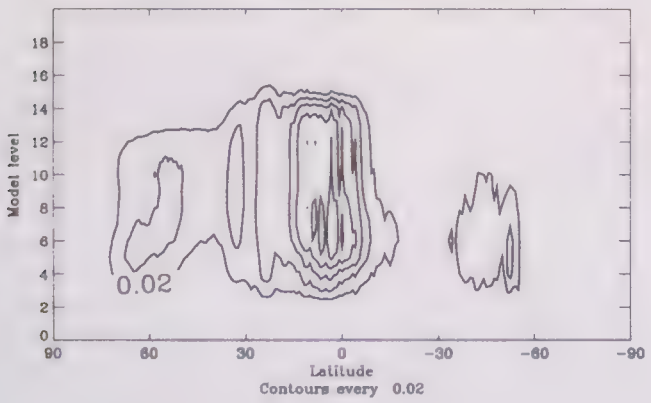

(f) Convective cloud amount over sea for JJA high resolution

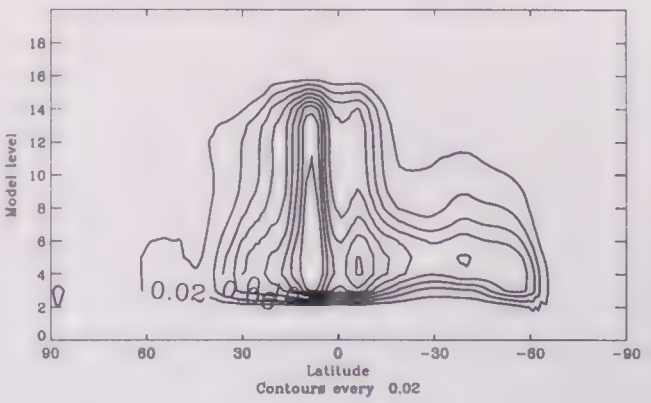

(g) Convective cloud amount over land for JJA high resolution minus standard resolution

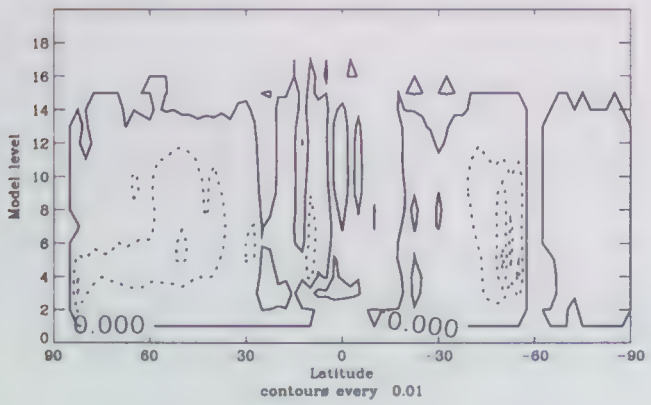

(h) Convective cloud amount over sea for JJA high resolution minus standard resolution

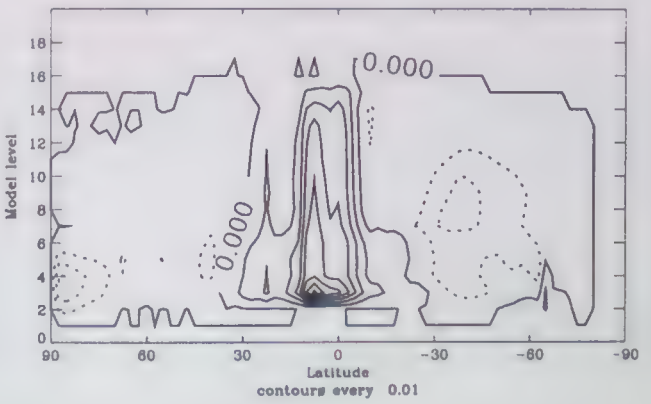

Figure 15 (a) Layer cloud amount over land for DJF high resolution

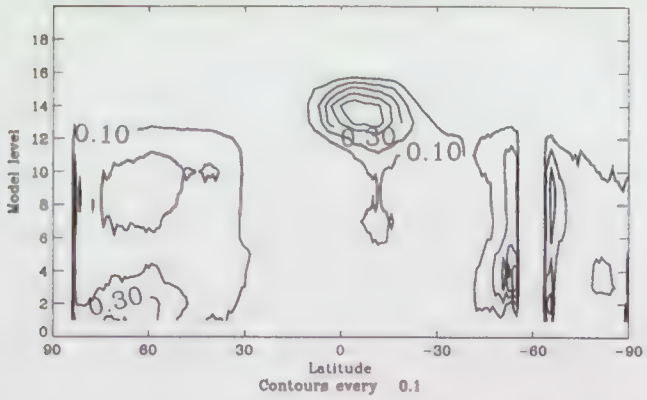

(b) Layer cloud amount over sea for DJF high resolution

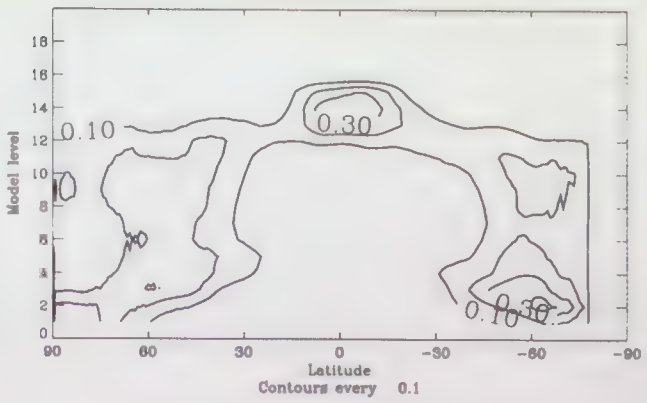

(c) Layer cloud amount over land for DJF high resolution minus standard resolution

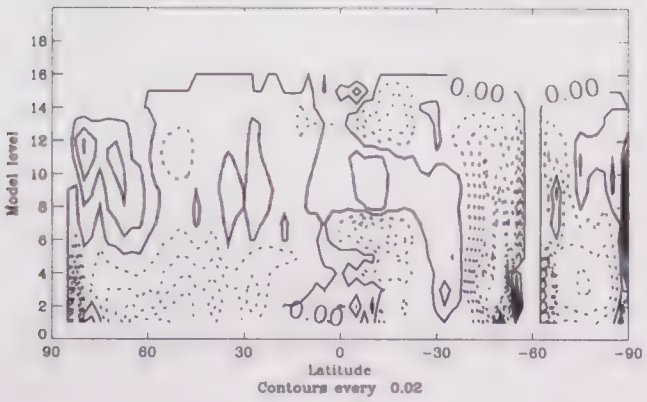

(d) Layer cloud amount over sea for DJF high resolution minus standard resolution

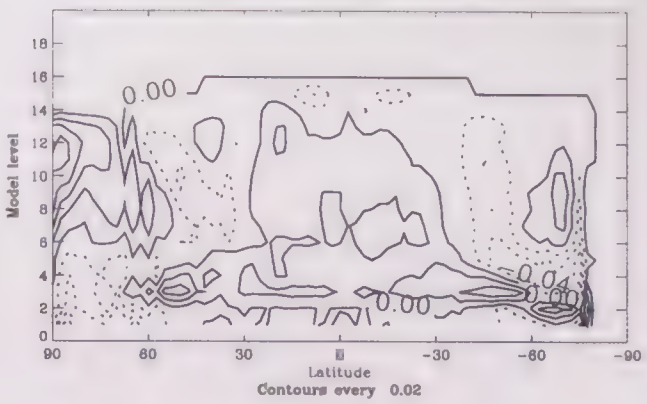

(e) Layer cloud amount over land for JJA high resolution

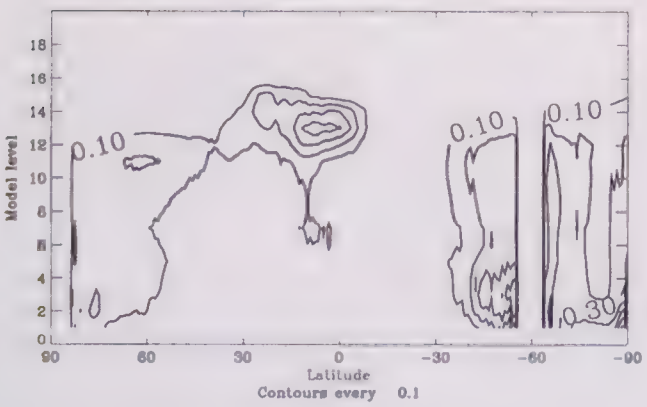

(f) Layer cloud amount over sea for JJA high resolution

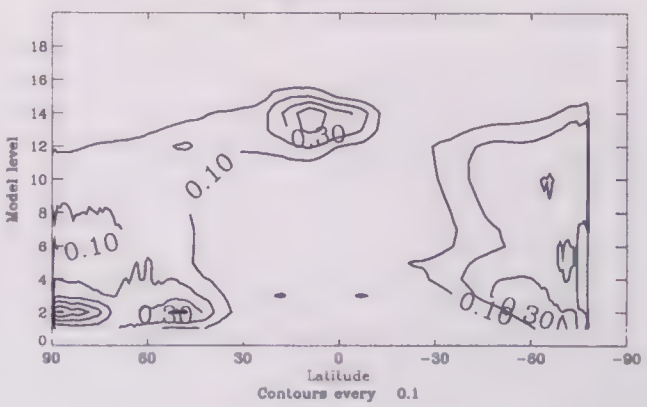

(g) Layer cloud amount over land for JJA high resolution minus standard resolution

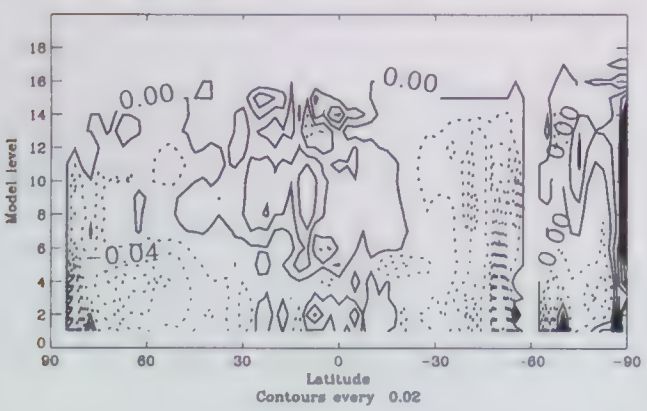

(h) Layer cloud amount over sea for JJA high resolution minus standard resolution

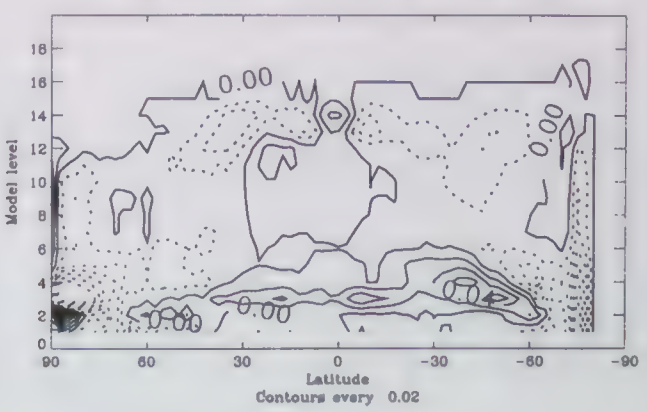

Figure 16 (a) Zonal mean total cloud amount for djf for all points.

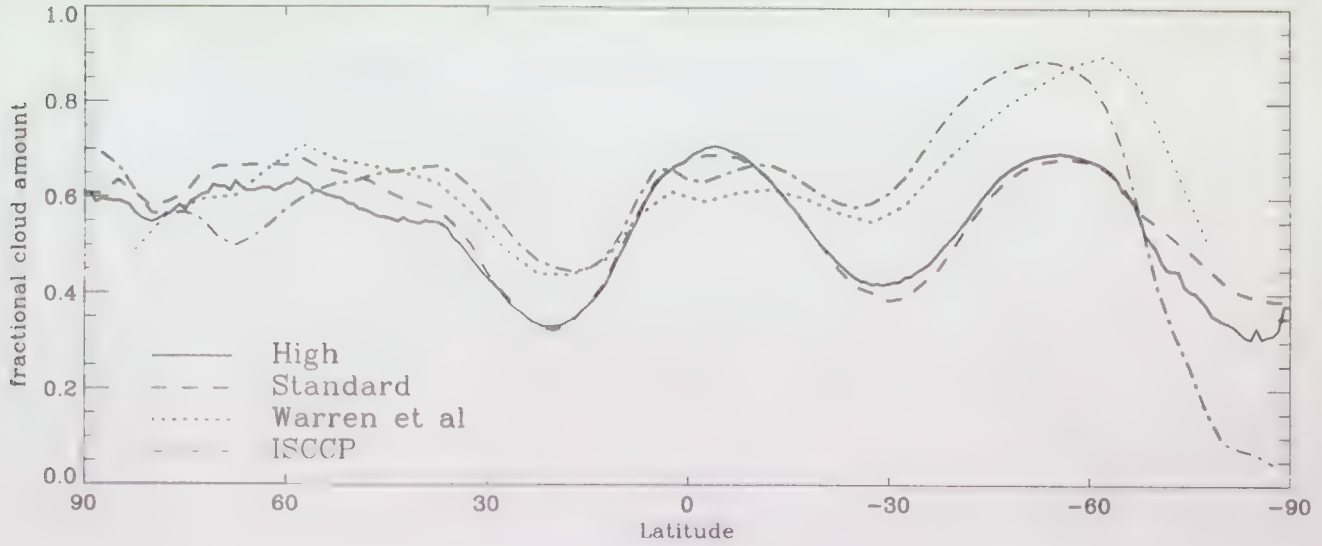

(b) Zonal mean total cloud amount for djf for land only.

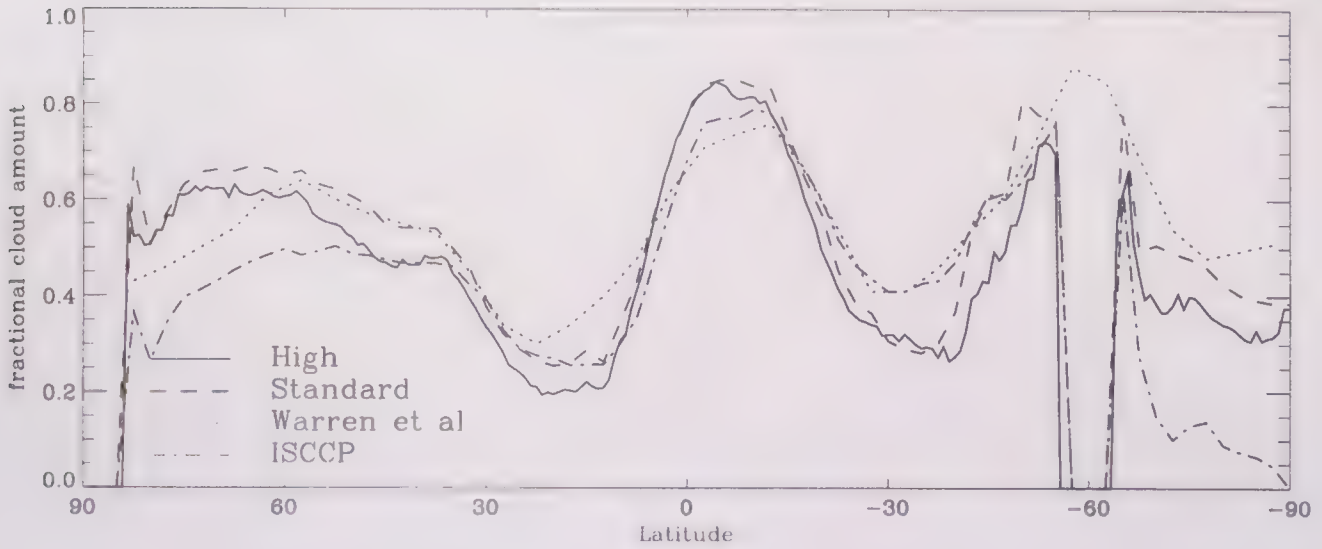

(c) Zonal mean total cloud amount for djf for sea only.

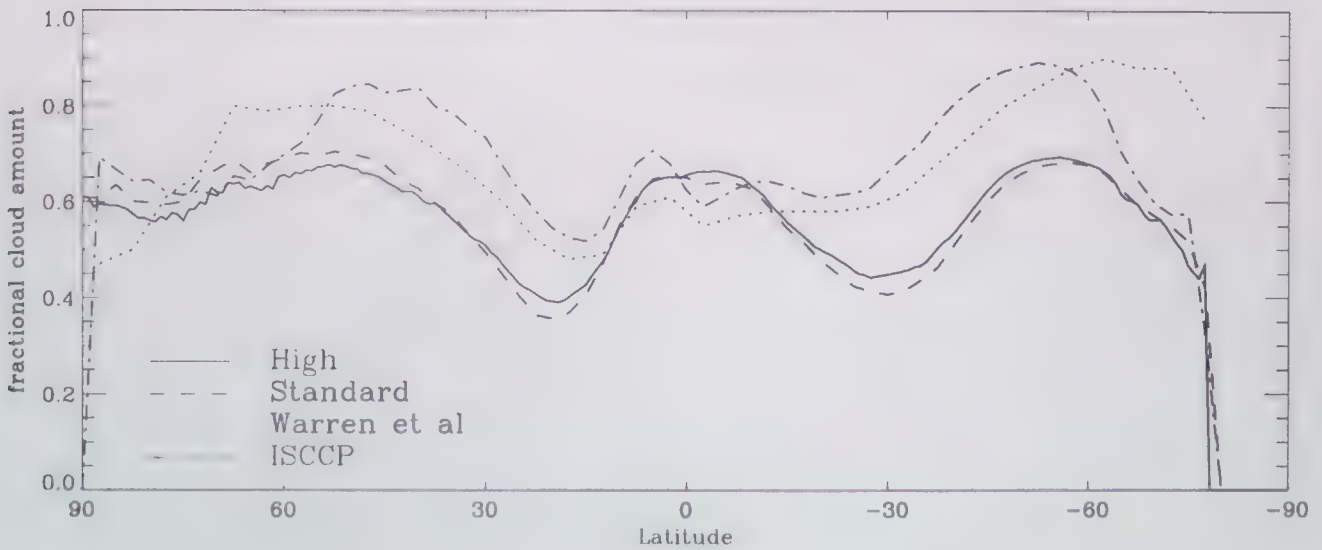

Figure 17 (a) Zonal mean total cloud amount for jja for all points.

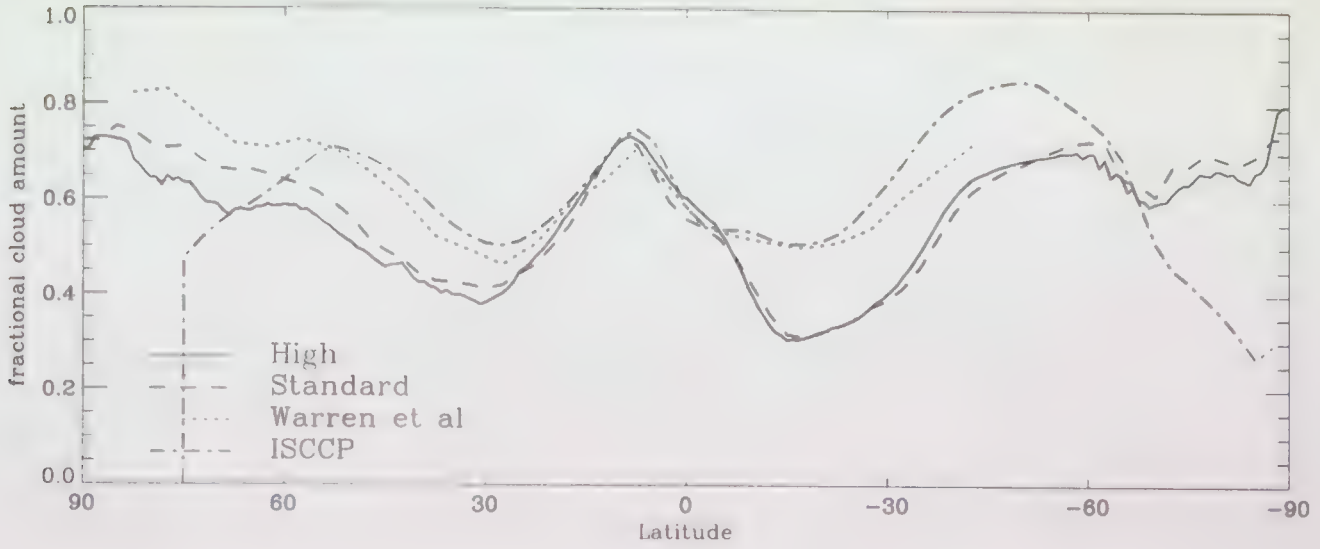

(b) Zonal mean total cloud amount for jja for land only.

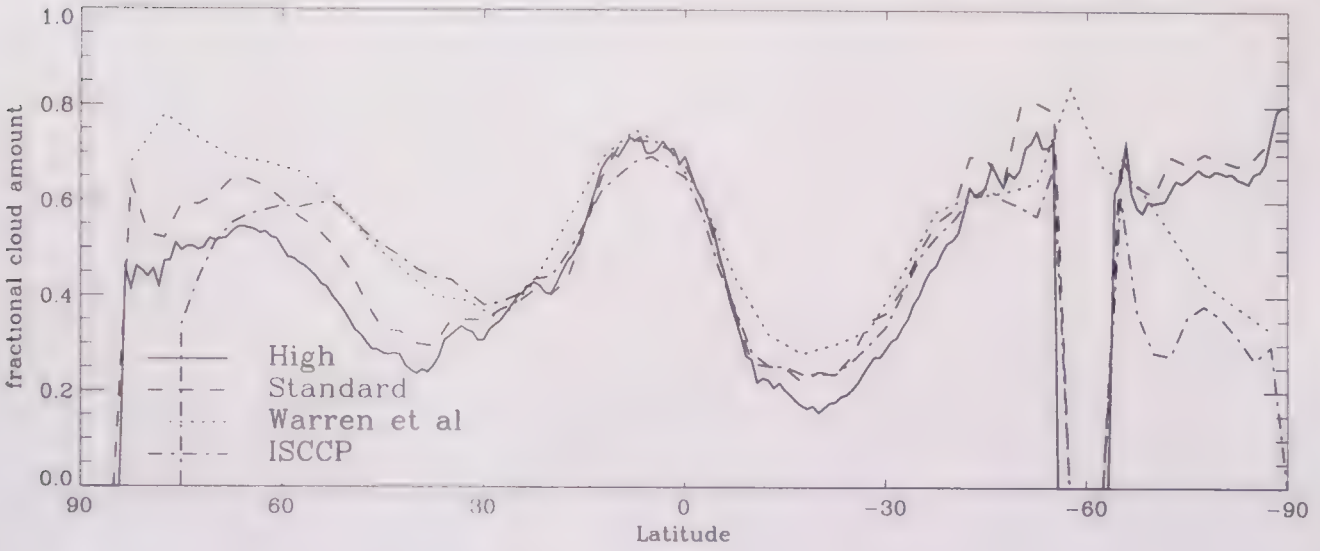

(c) Zonal mean total cloud amount for jja for sea only.

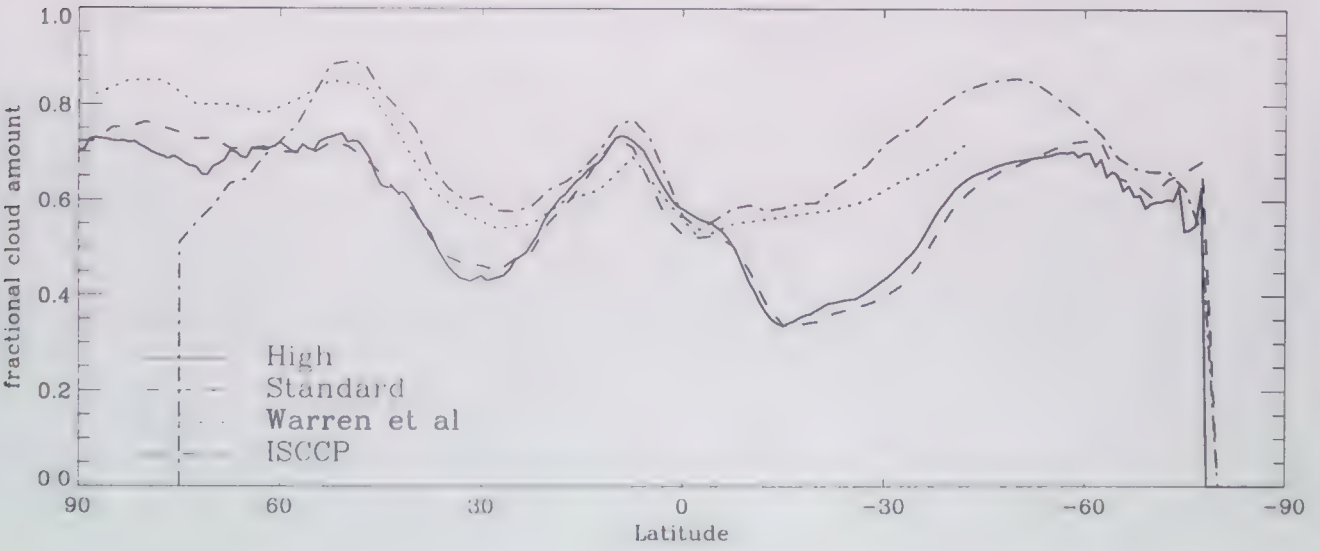

Figure 18(a) Outgoing longwave for djf
high resolution minus ERBE

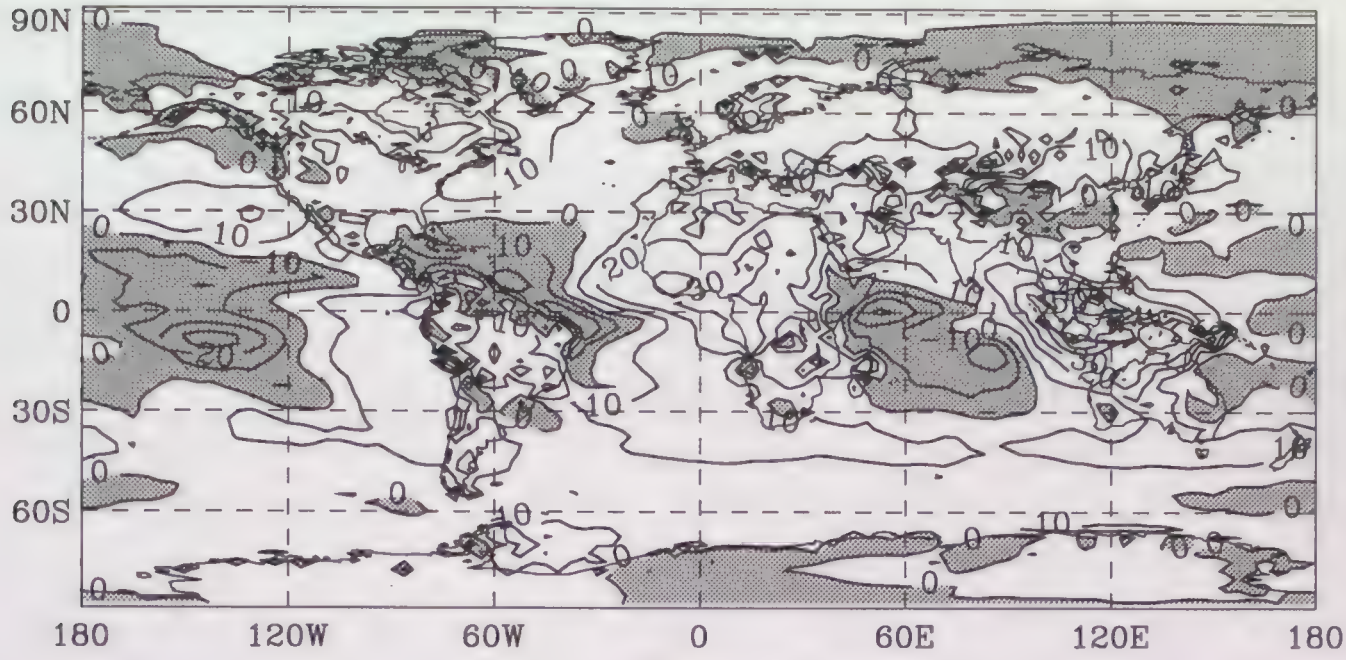

Contours every 10. W/m2

(b) Outgoing longwave for djf
standard resolution minus ERBE

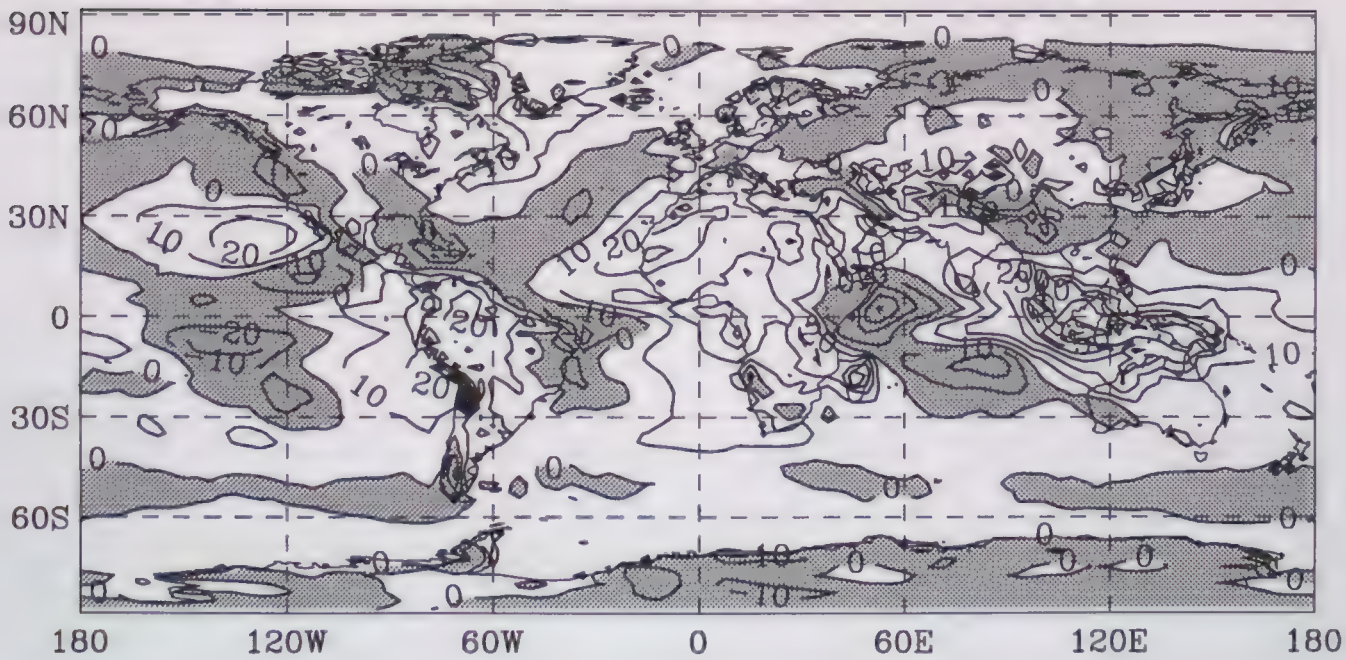

Contours every 10. W/m2

Figure 19(a) Outgoing longwave for jja
high resolution minus ERBE

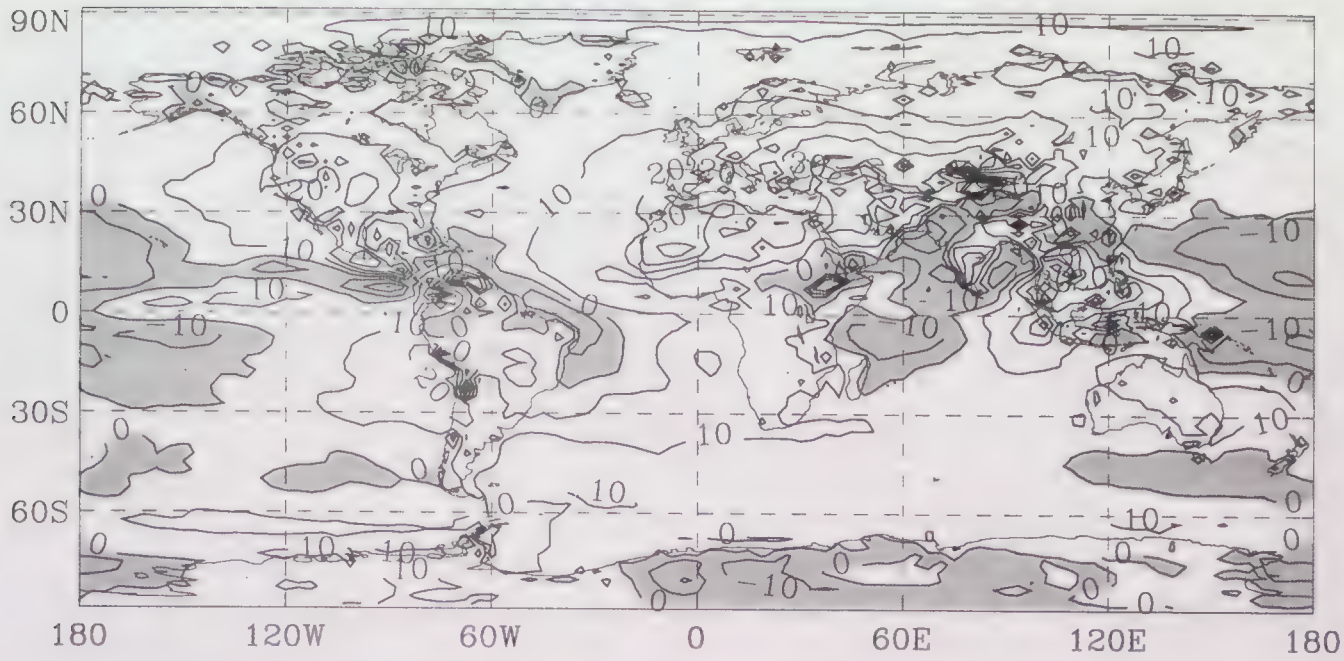

Contours every 10. W/m2

(b) Outgoing longwave for jja
standard resolution minus ERBE

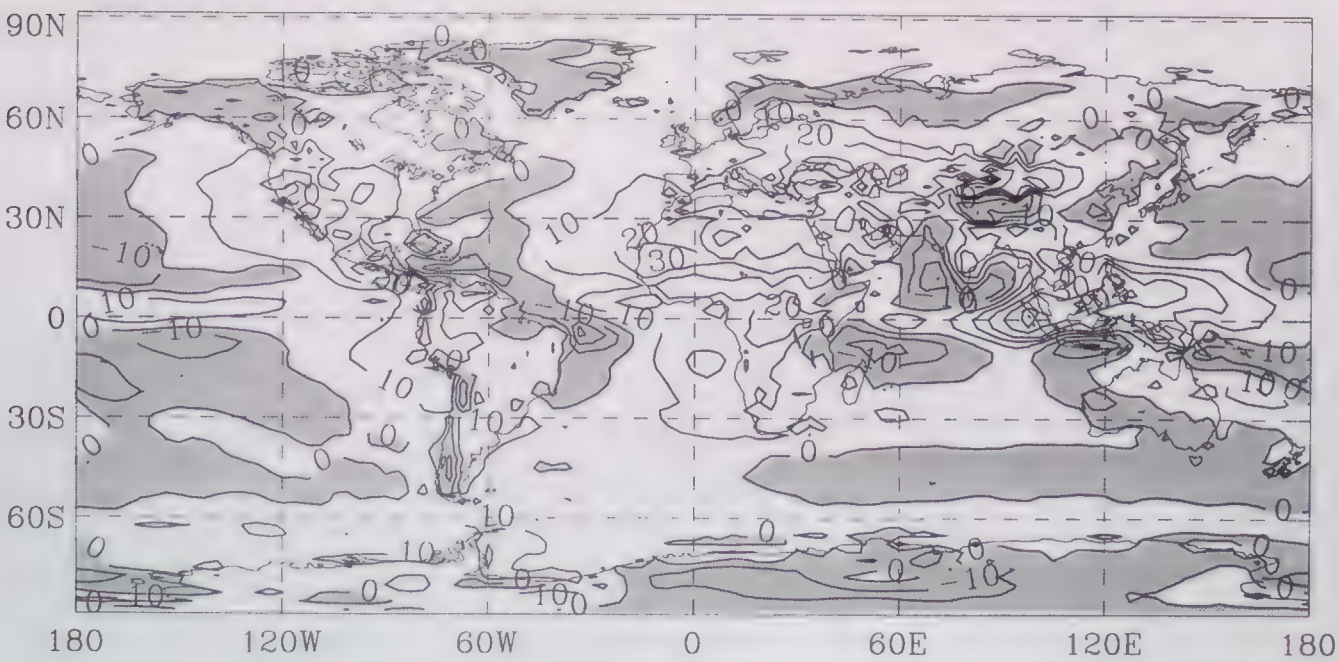

Contours every 10. W/m2

Figure 20 (a) Zonal mean albedo – djf, for all points.

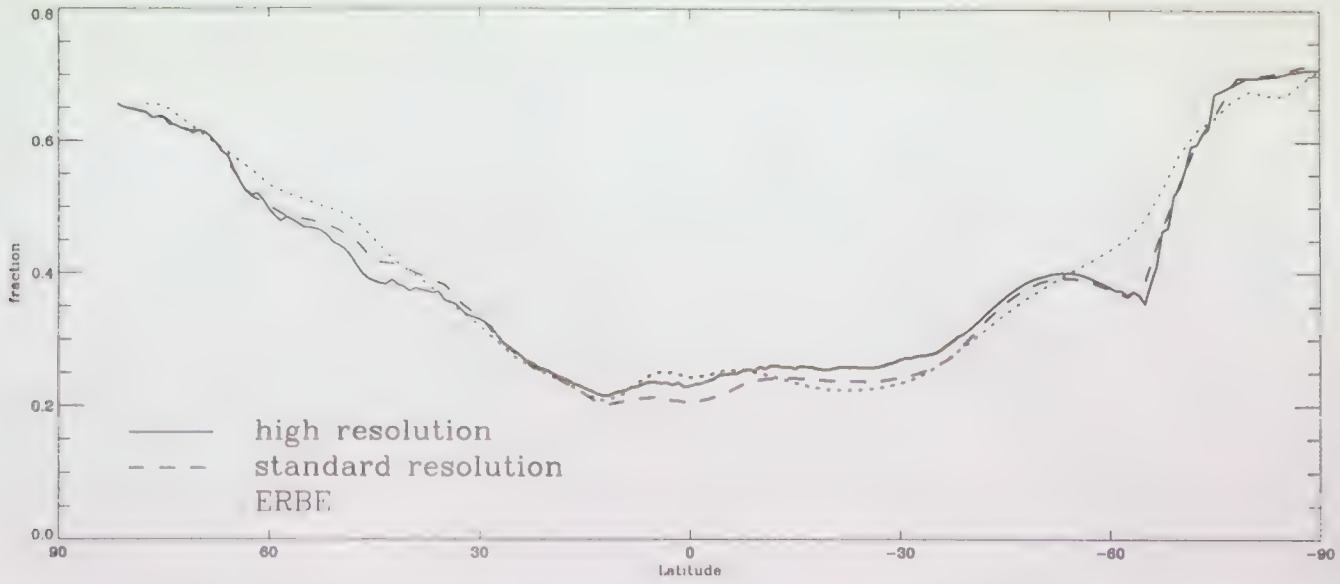

(b) Zonal mean albedo – djf, for land only.

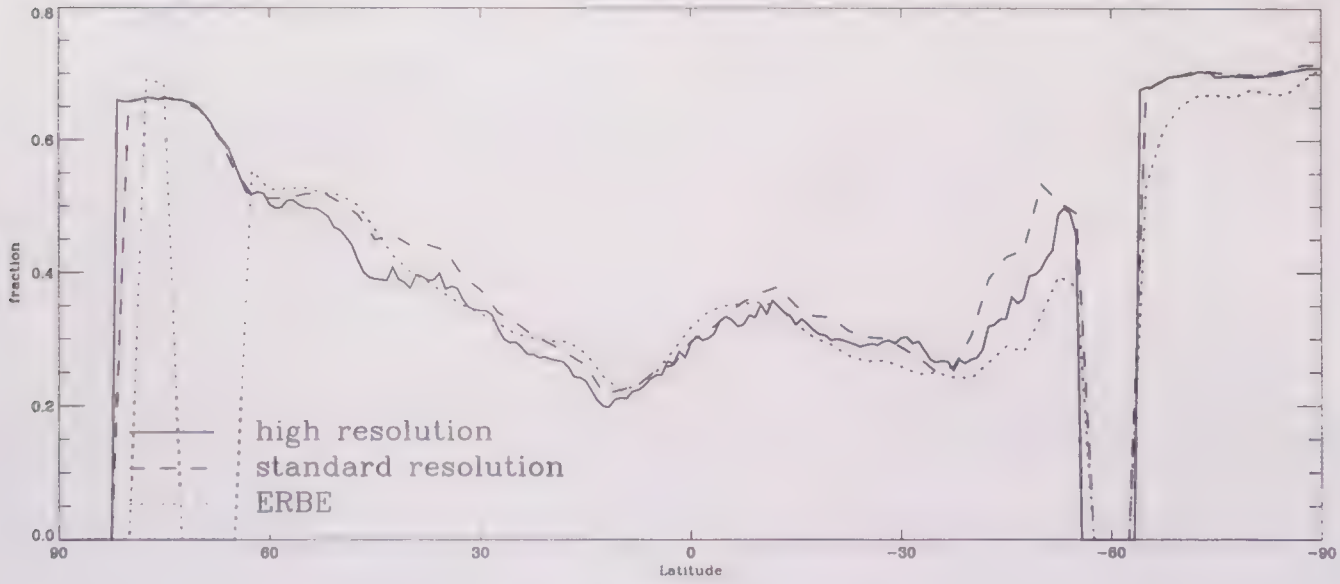

(c) Zonal mean albedo – djf, for sea only.

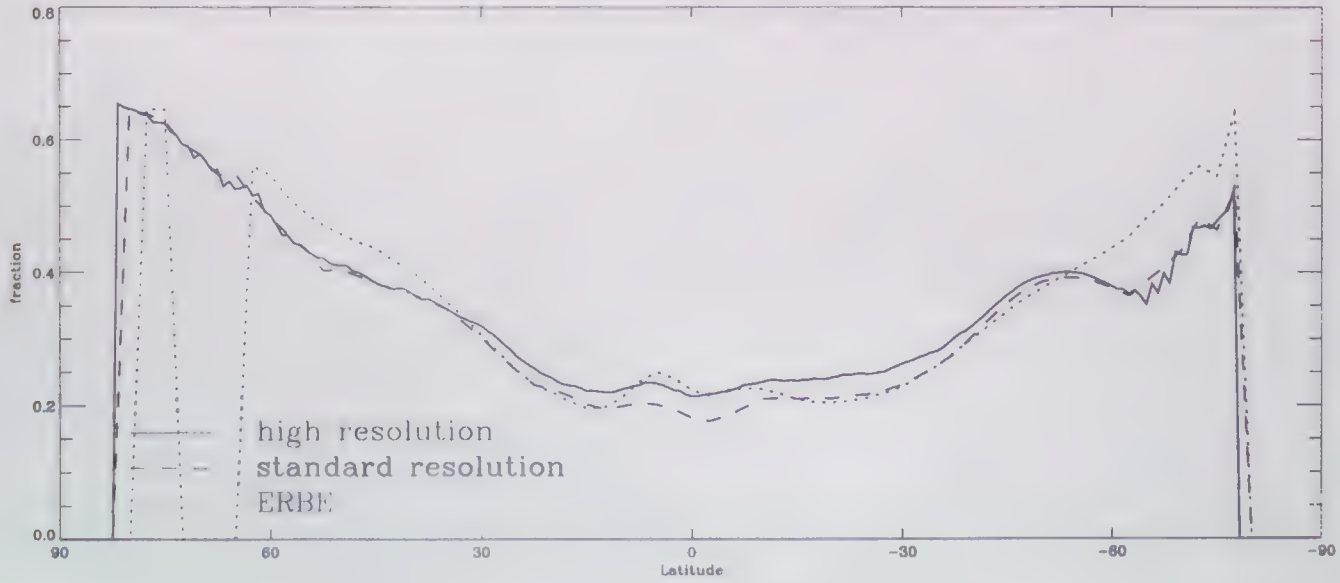

Figure 21 (a) Zonal mean albedo – jja, for all points.

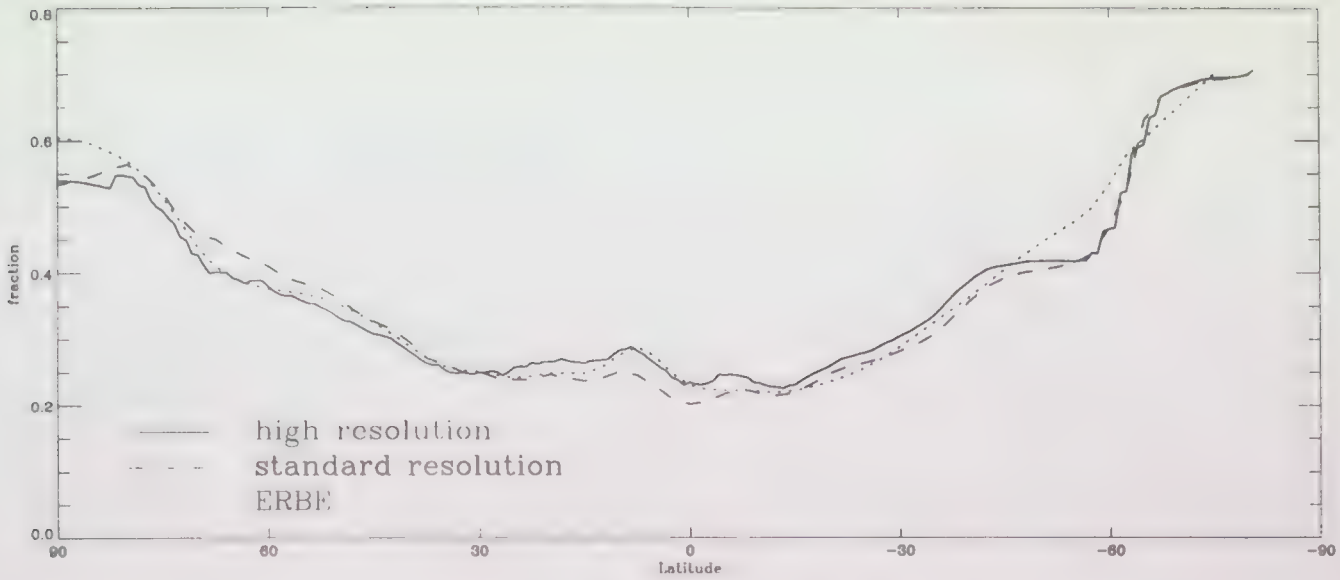

(b) Zonal mean albedo – jja, for land only.

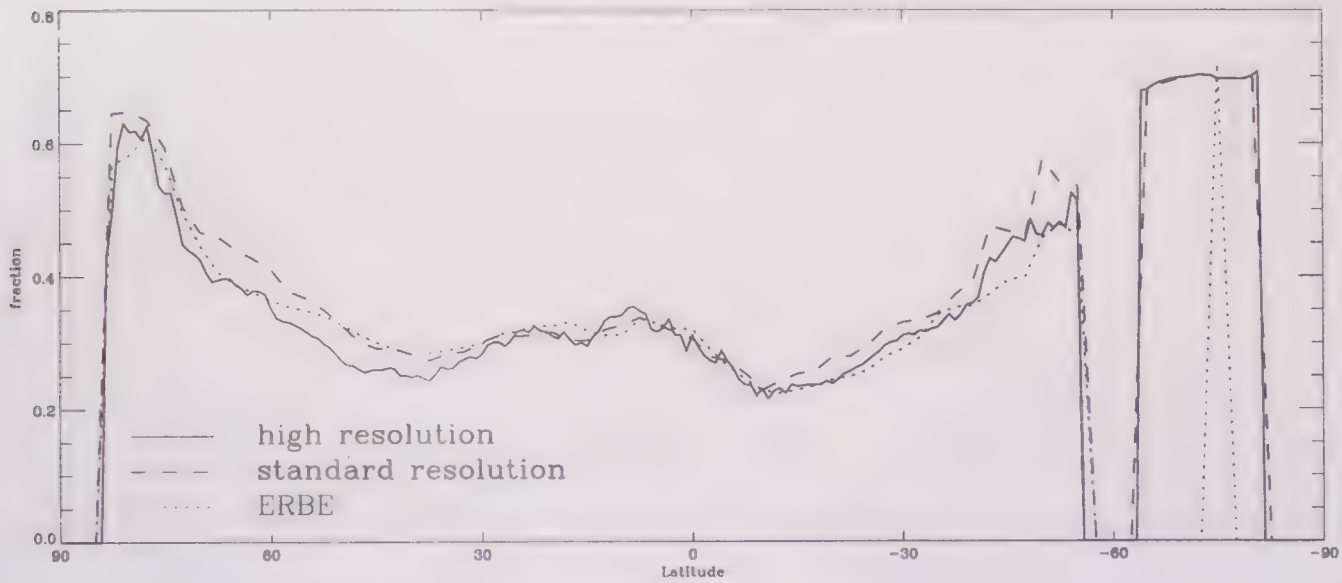

(c) Zonal mean albedo – jja, for sea only.

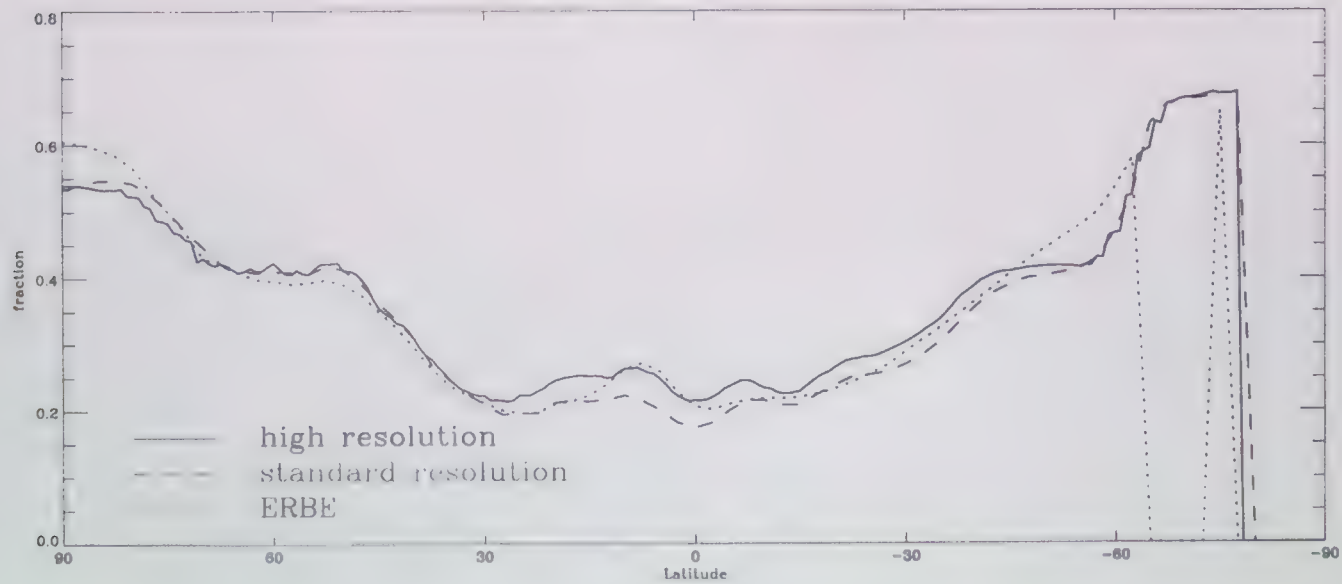

Figure 22(a) Precipitation for djf high resolution

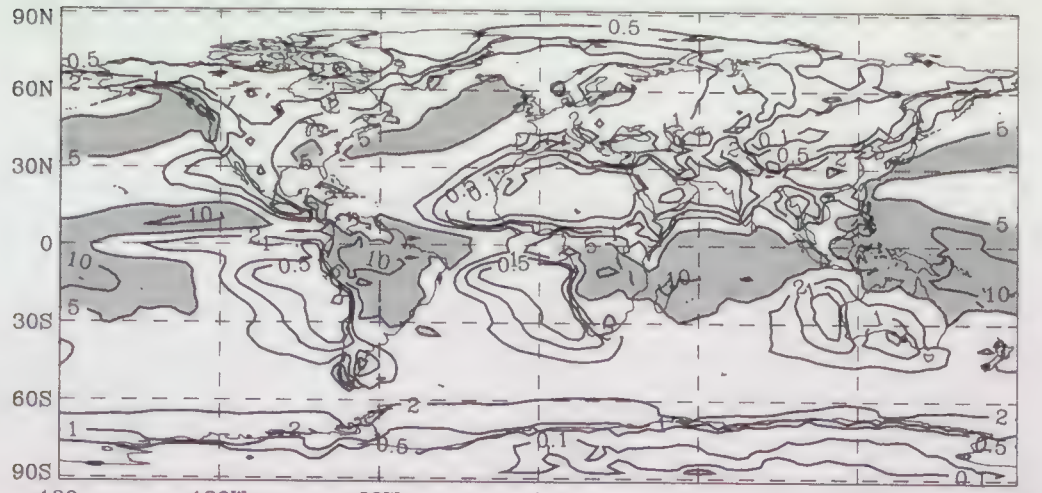

(b) Precipitation for djf standard resolution

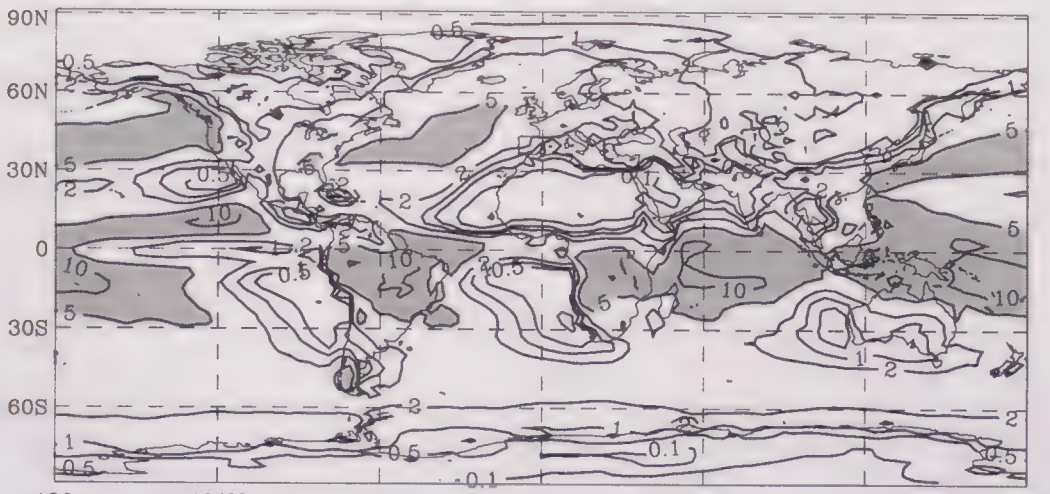

(c) Precipitation for djf
Legates and Willmott climatology

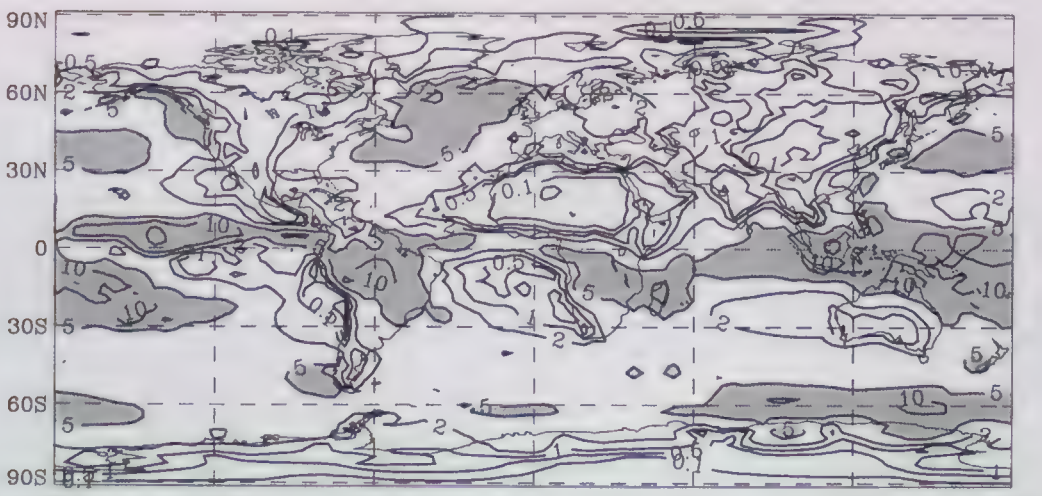

Figure 23(a) Precipitation for jja high resolution

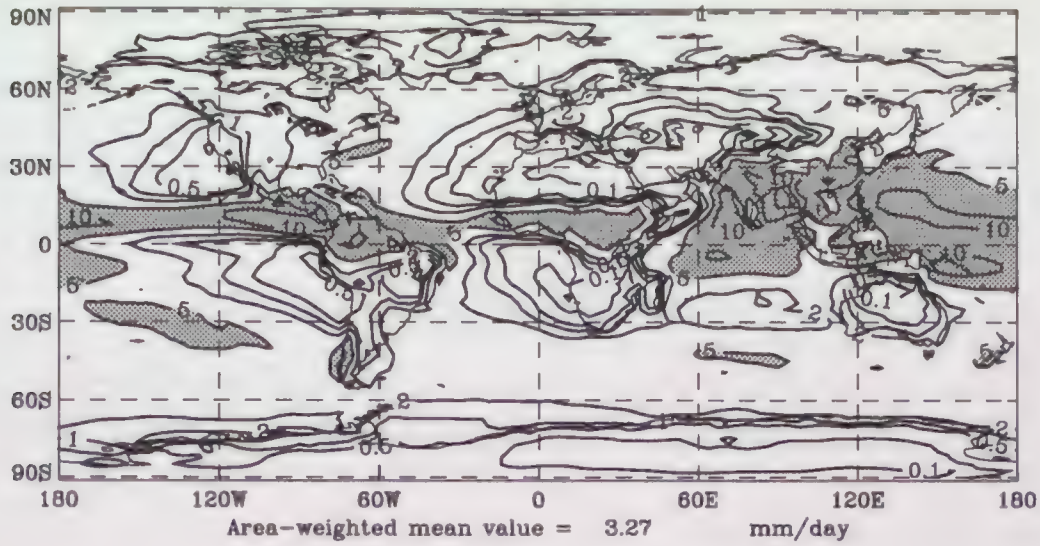

Area-weighted mean value = 3.27 mm/day

(b) Precipitation for jja standard resolution

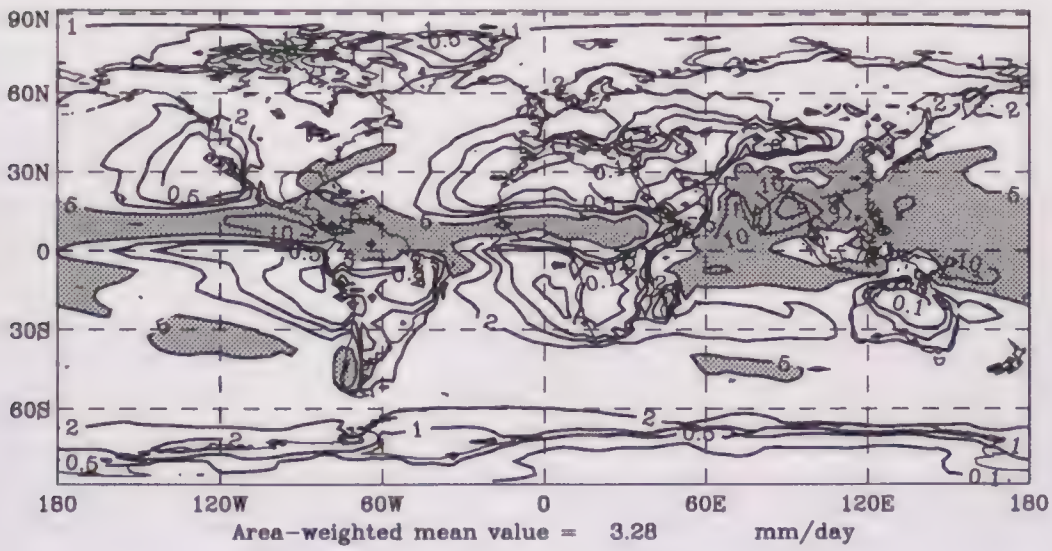

Area-weighted mean value = 3.28 mm/day

(c) Precipitation for jja
Legates and Willmott climatology

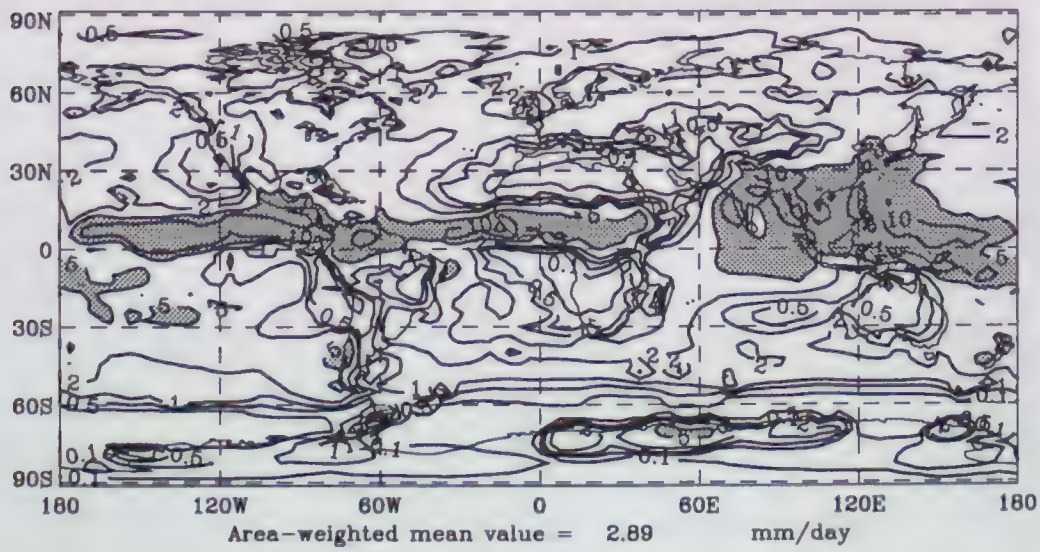

Area-weighted mean value = 2.89 mm/day

Figure 24 (a) Zonal mean precipitation over land for Dec/Jan/Feb 1979–88

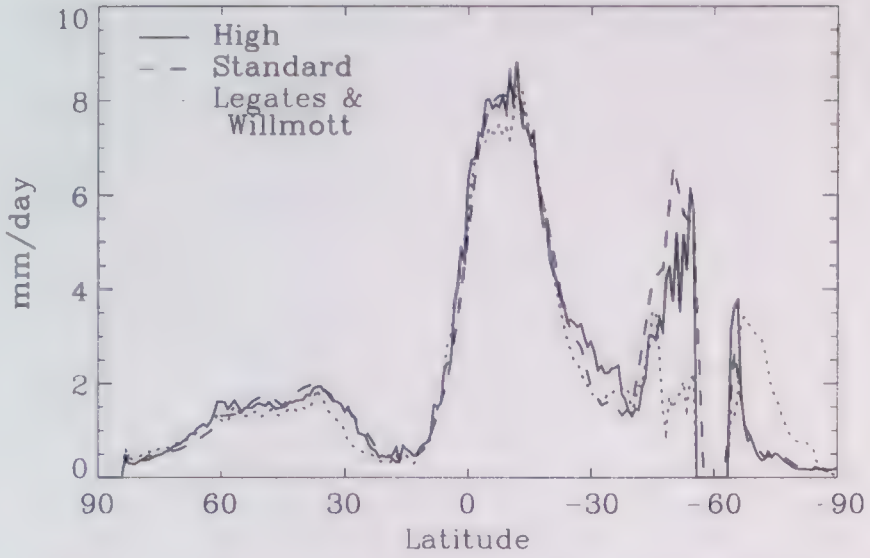

(b) Zonal mean precipitation over land for Jun/Jul/Aug 1979–88

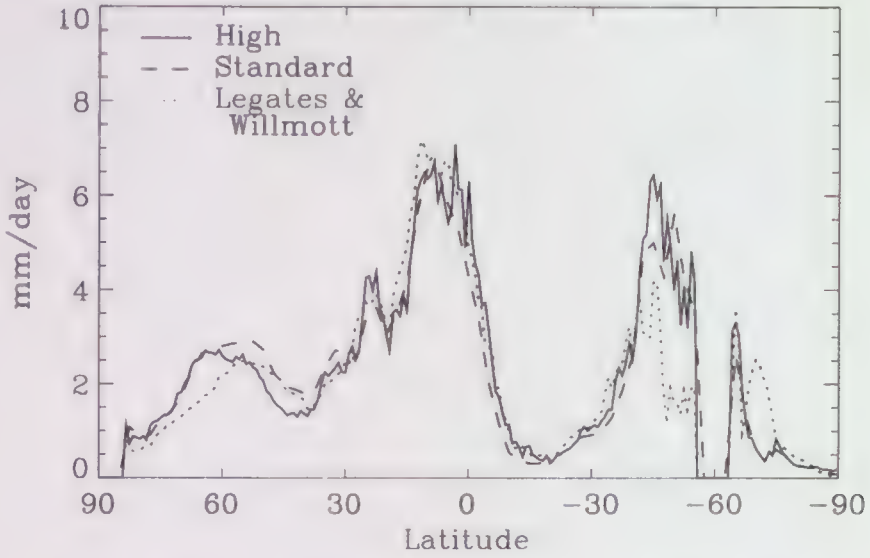

(c) Zonal mean evaporation over land for Dec/Jan/Feb 1979–88

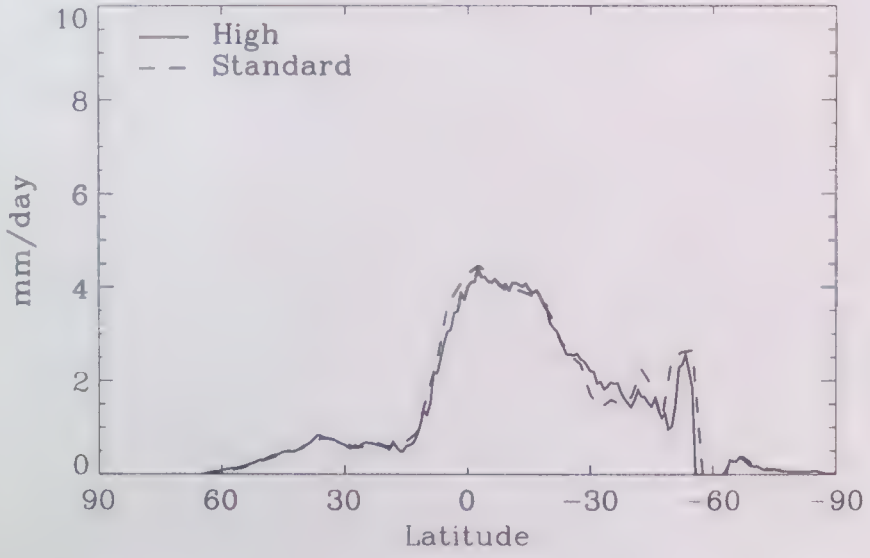

(d) Zonal mean evaporation over land for Jun/Jul/Aug 1979–88

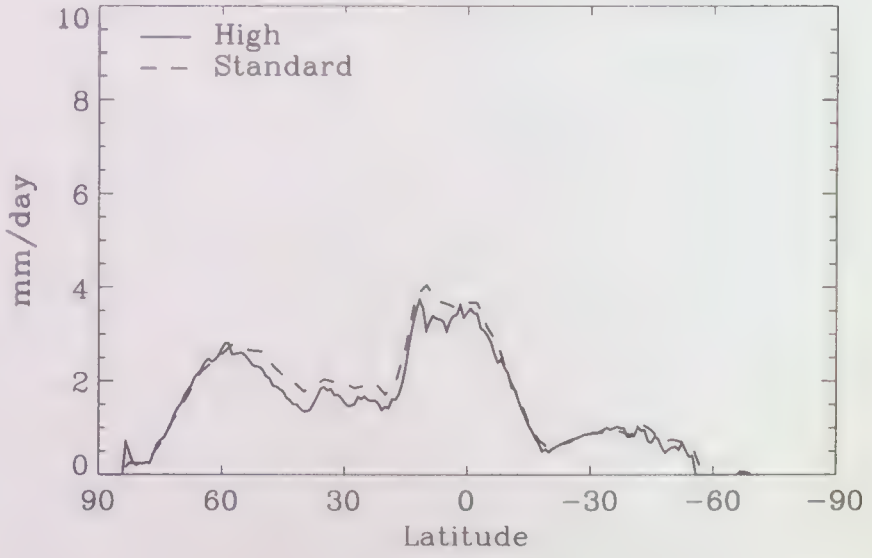

Figure 24 (e) Zonal mean runoff
for Dec/Jan/Feb 1979–88

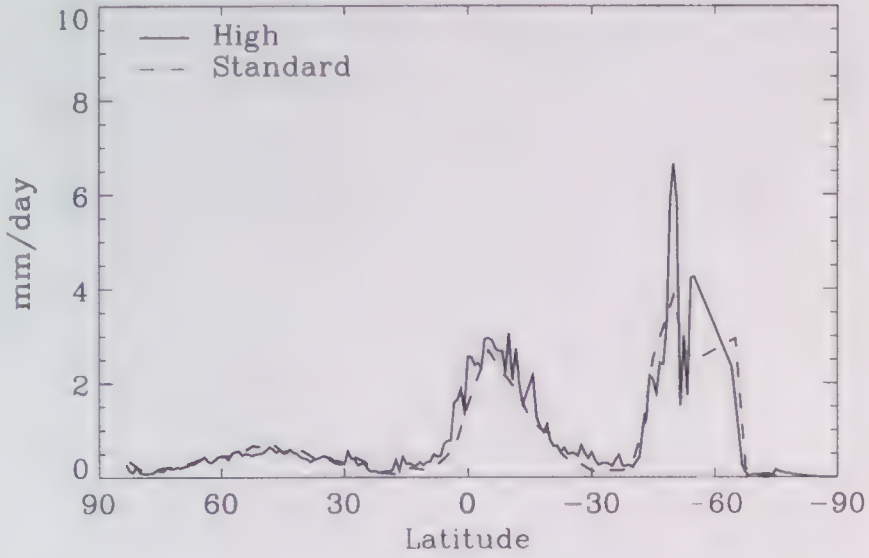

(f) Zonal mean runoff
for Jun/Jul/Aug 1979–88

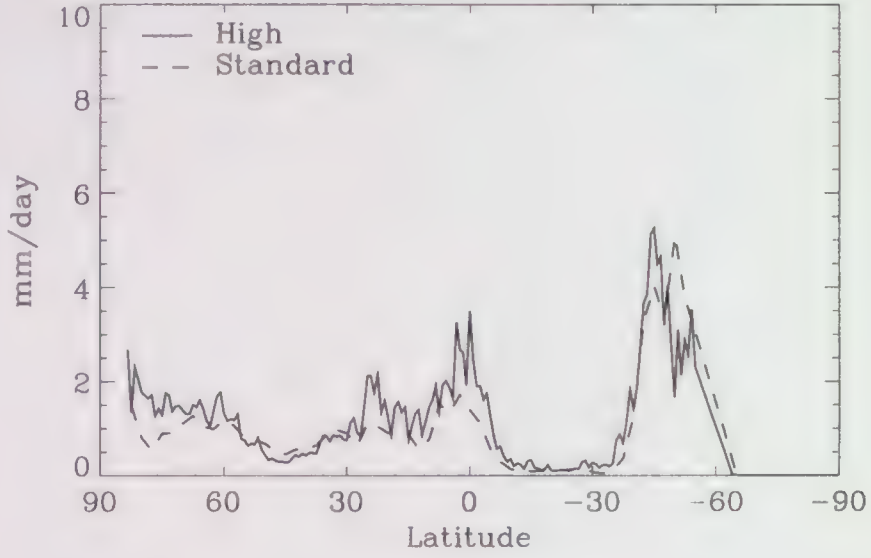

(g) Zonal mean soil moisture
for Dec/Jan/Feb 1979–88

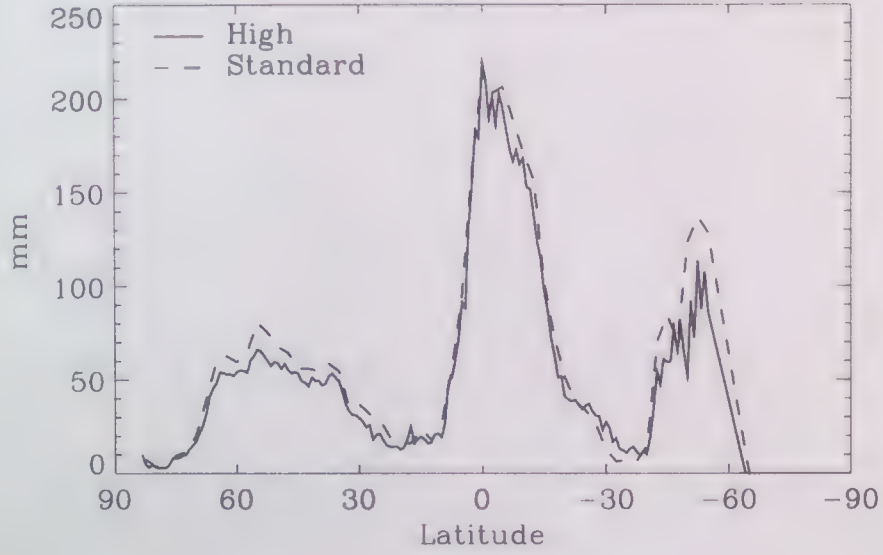

(h) Zonal mean soil moisture
for Jun/Jul/Aug 1979–88

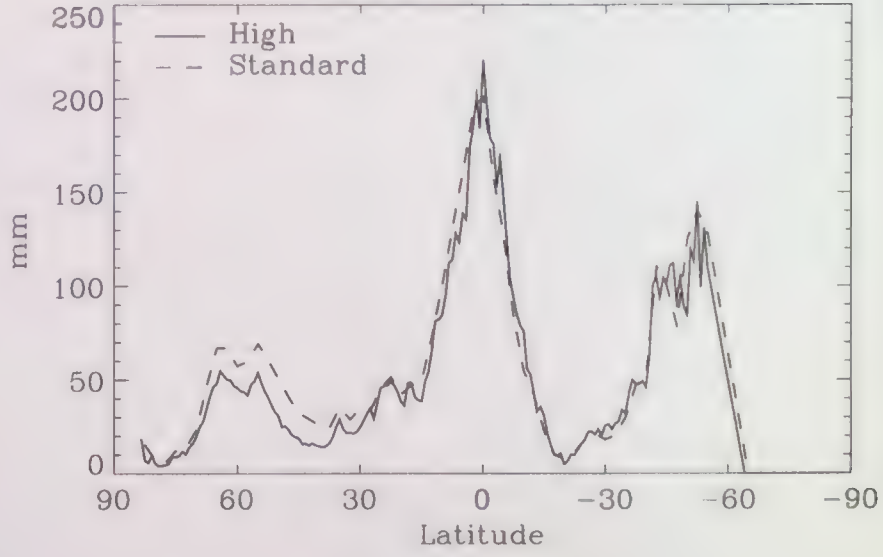

Figure 25(a) Zonal mean large scale rainfall for January over land

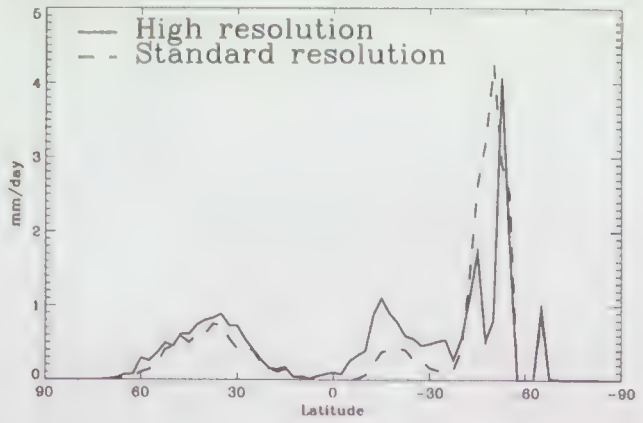

(b) Zonal mean large scale rainfall for July over land

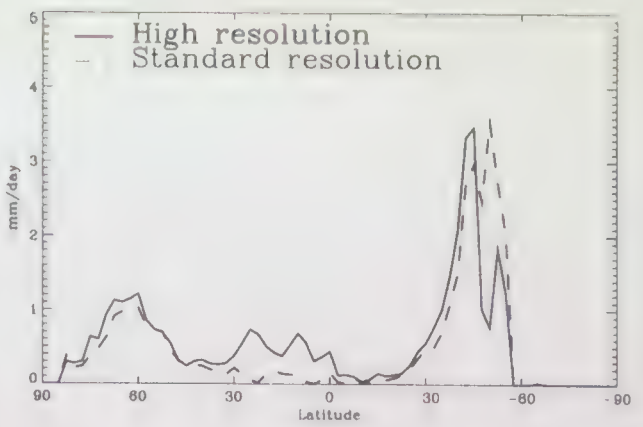

(c) Zonal mean convective rainfall for January over land

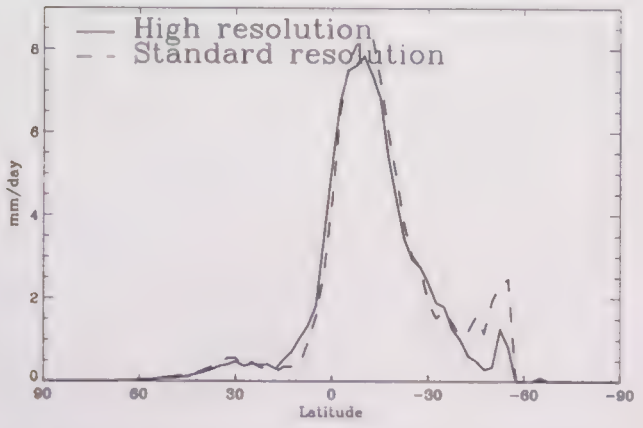

(d) Zonal mean convective rainfall for July over land

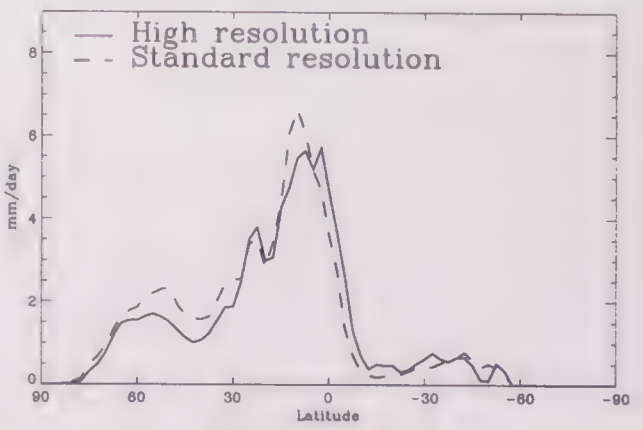

(e) Zonal mean large scale rainfall for January over sea

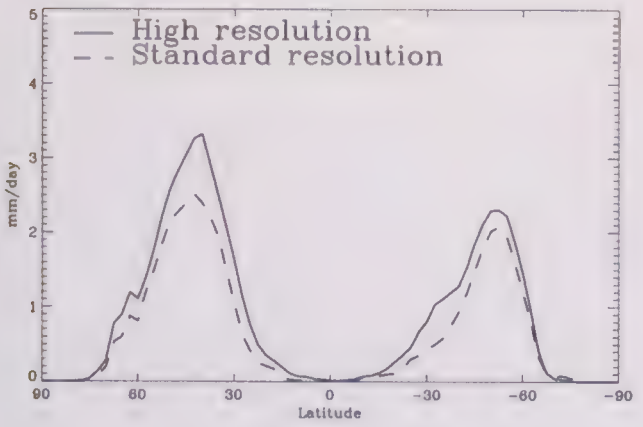

(f) Zonal mean large scale rainfall for July over sea

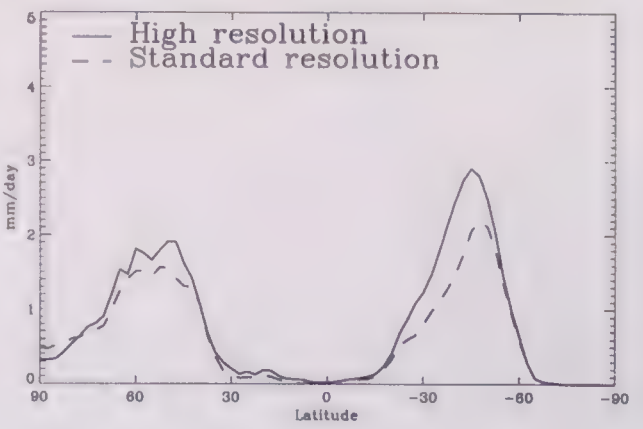

(g) Zonal mean convective rainfall for January over sea

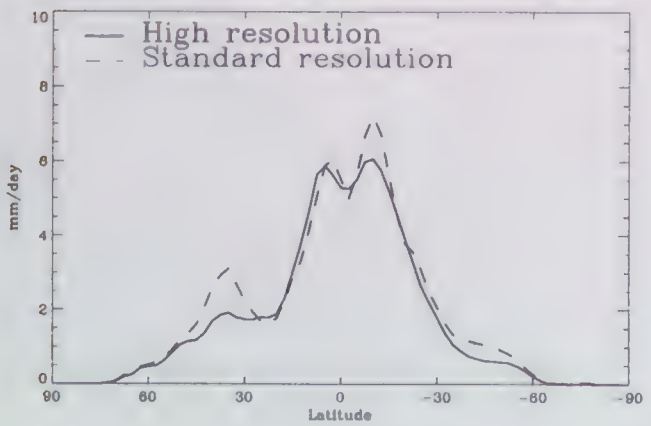

(h) Zonal mean convective rainfall for July over sea

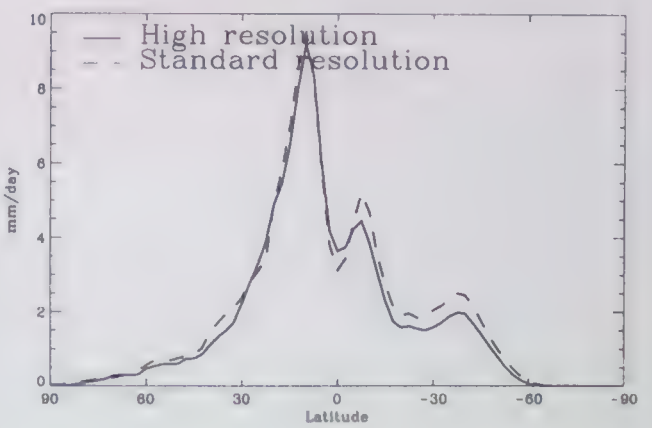

Figure 26(a) Zonal mean of the s.d. of daily mean large scale rainfall for January over land

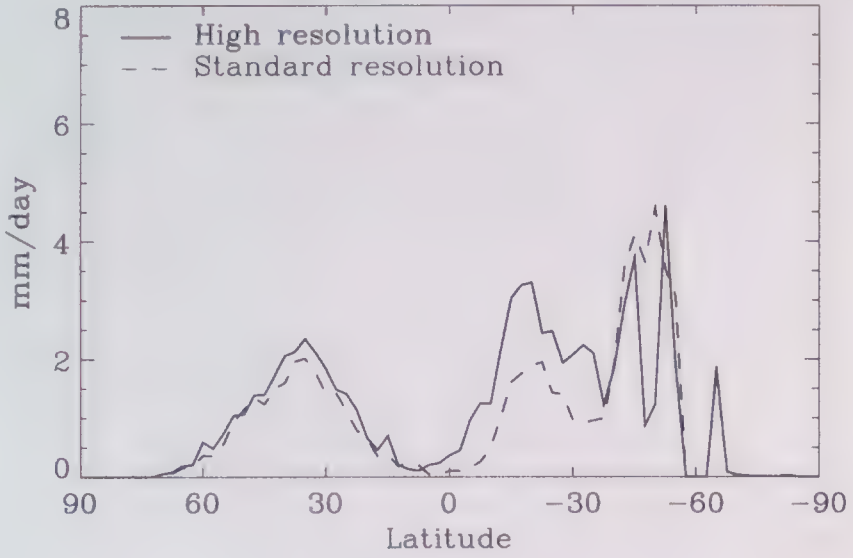

(b) Zonal mean of the s.d. of daily mean large scale rainfall for July over land

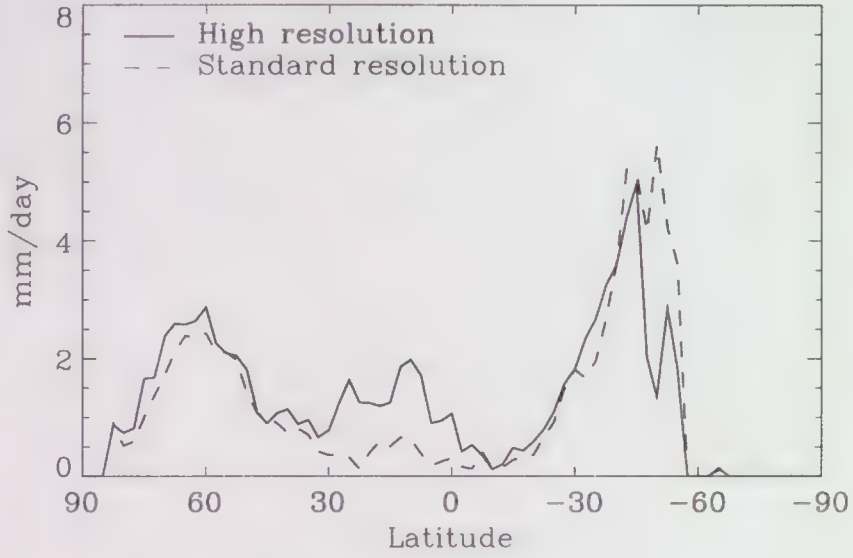

(c) Zonal mean of the s.d. of daily mean convective rainfall for January over land

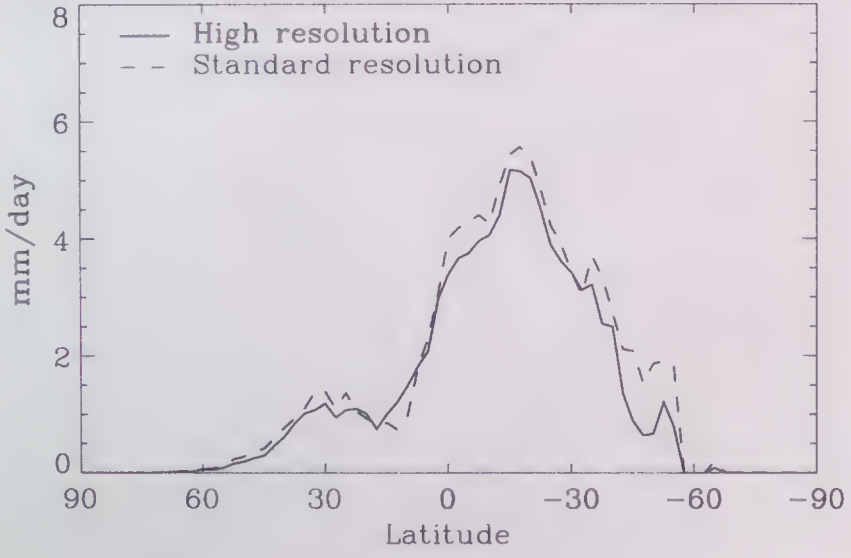

(d) Zonal mean of the s.d. of daily mean convective rainfall for July over land

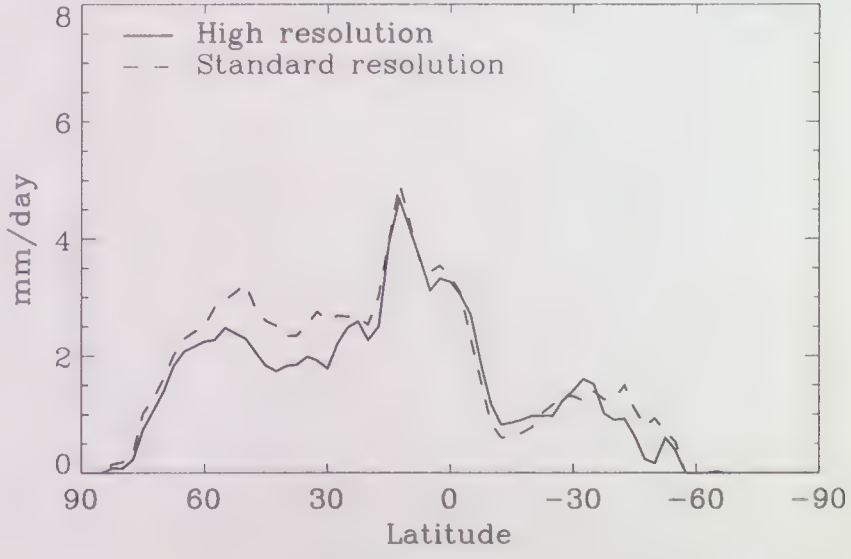

Figure 27(a) Zonal mean latent heat flux over land for Dec/Jan/Feb 1979–88

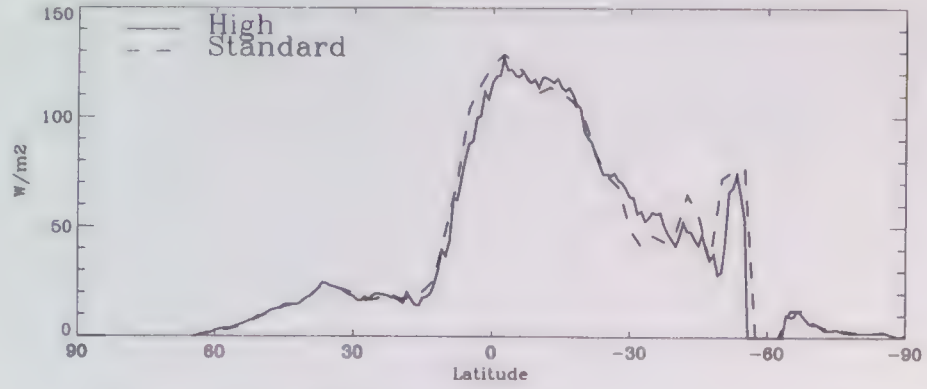

(b) Zonal mean latent heat flux over land for Jun/Jul/Aug 1979–88

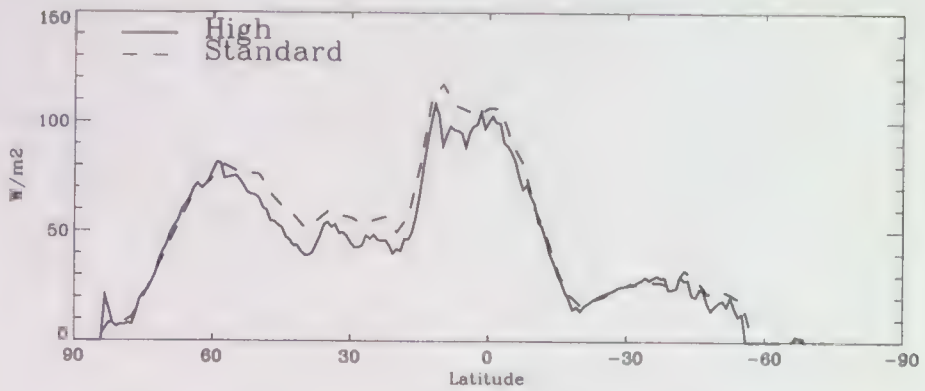

(c) Zonal mean sensible heat flux over land for Dec/Jan/Feb 1979–88

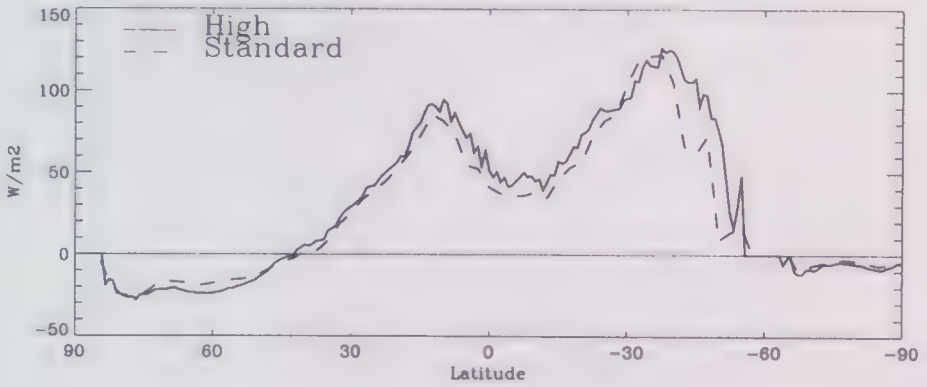

(d) Zonal mean sensible heat flux over land for Jun/Jul/Aug 1979–88

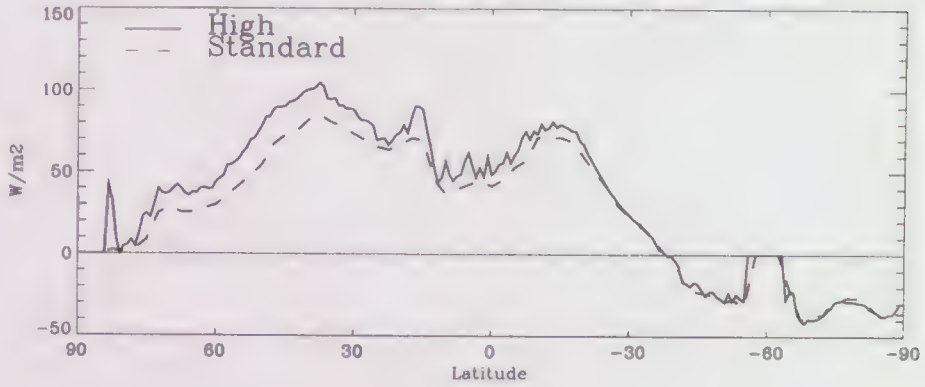

(e) Zonal mean net surface radiation over land for Dec/Jan/Feb 1979–88

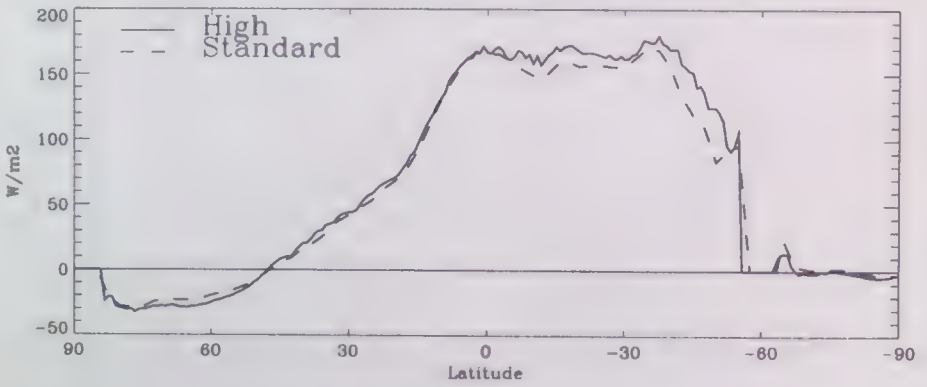

(f) Zonal mean net surface radiation over land for Jun/Jul/Aug 1979–88

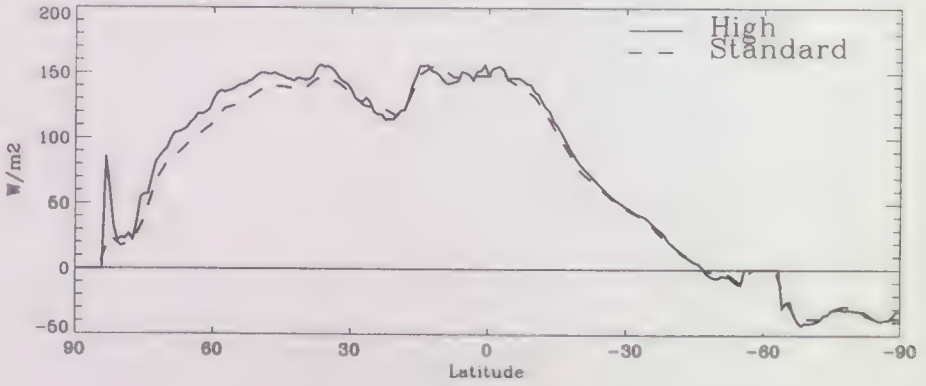

Figure 28 (a) Europe 40–55N 0–30E
10 year mean screen temperature

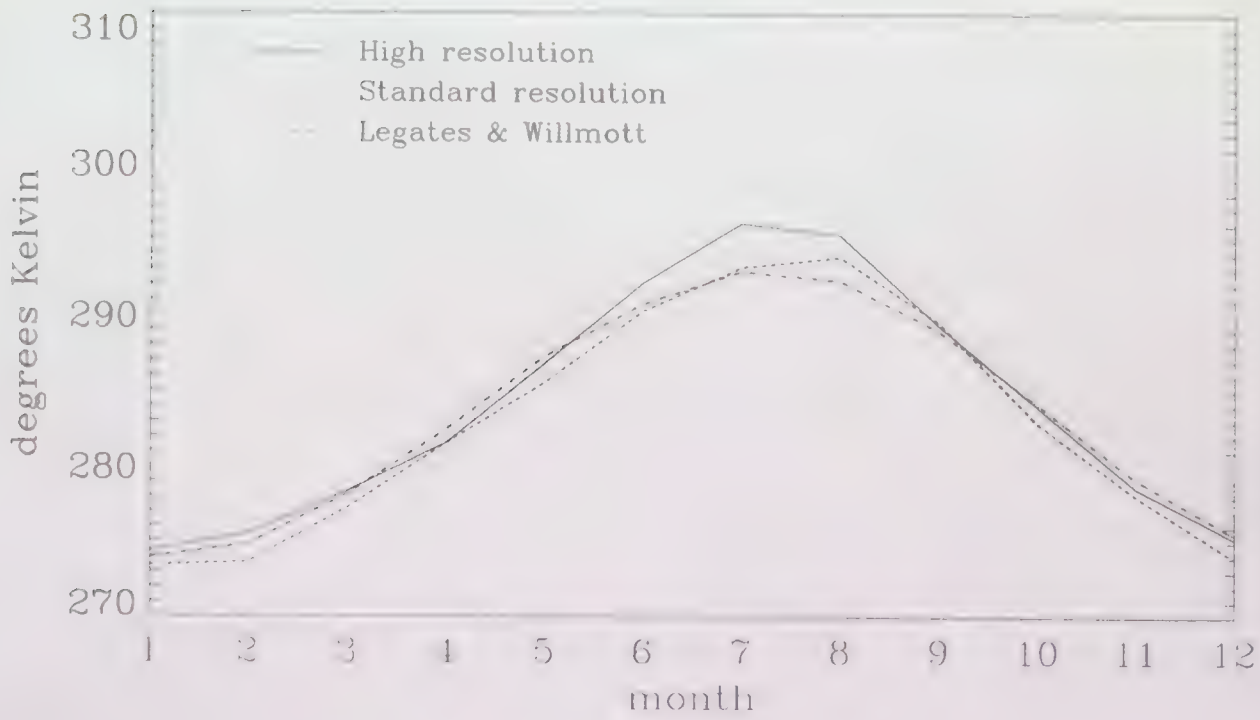

(b) South America 15–20S 45–65W
10 year mean screen temperature

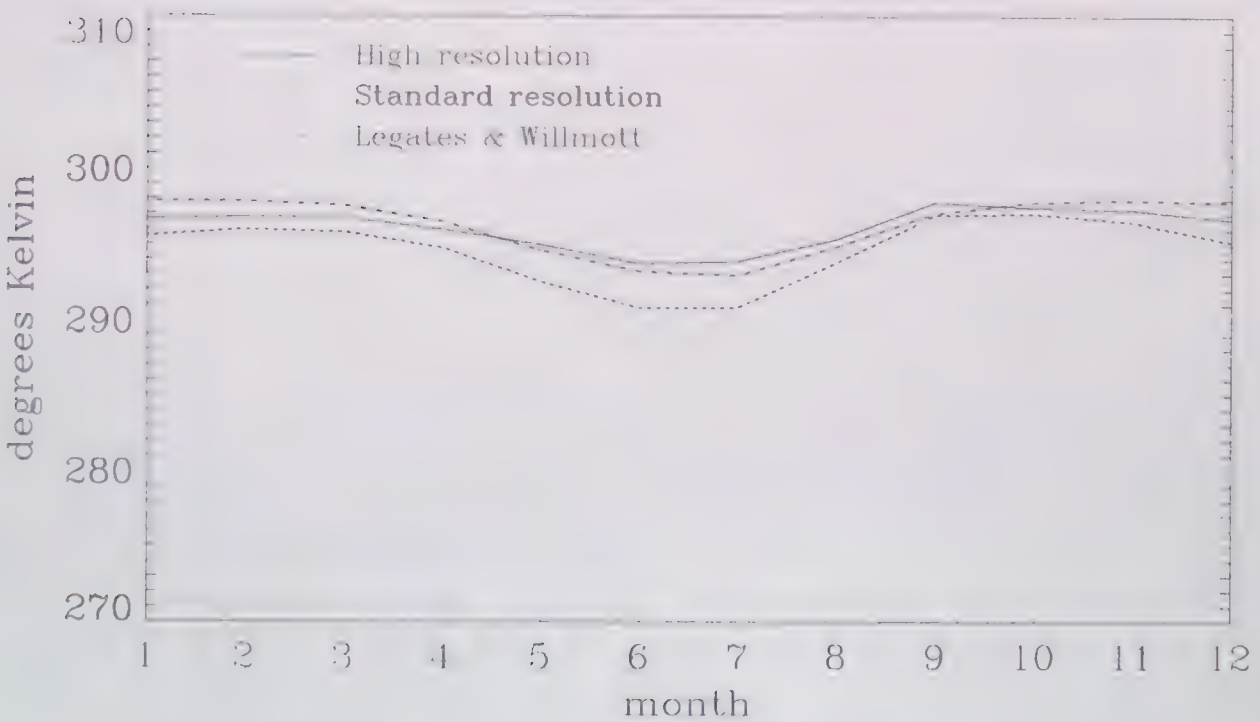

Figure 29(a) Zonal mean latent heat flux over sea for Dec/Jan/Feb 1979-88

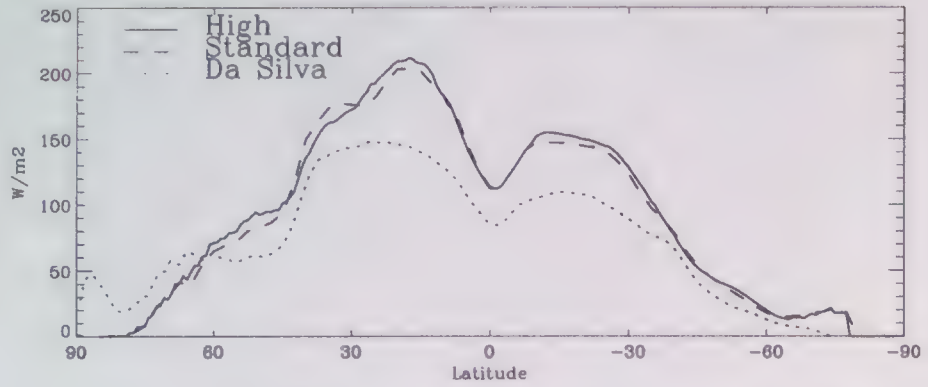

(b) Zonal mean latent heat flux over sea for Jun/Jul/Aug 1979-88

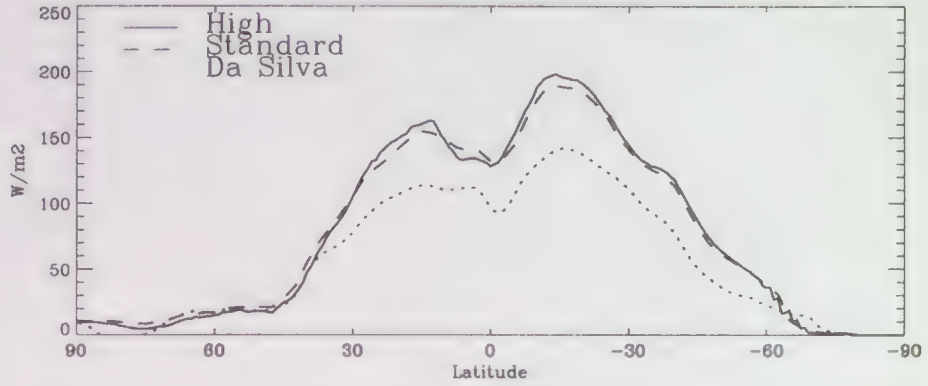

(c) Zonal mean sensible heat flux over sea for Dec/Jan/Feb 1979-88

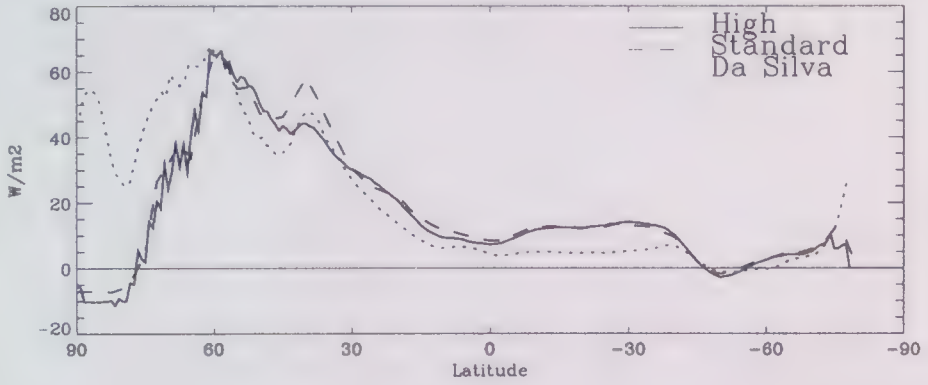

(d) Zonal mean sensible heat flux over sea for Jun/Jul/Aug 1979-88

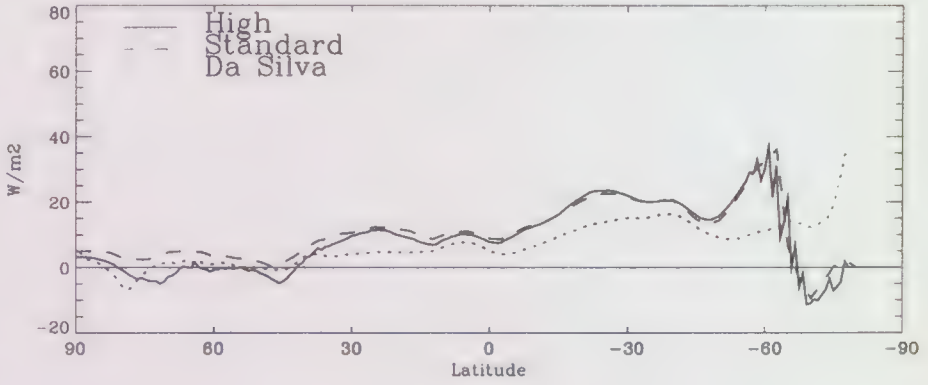

(e) Zonal mean net surface radiation over sea for Dec/Jan/Feb 1979-88

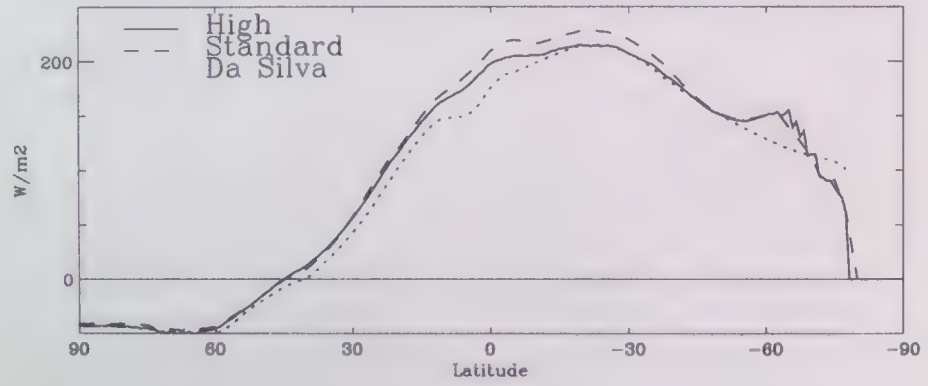

(f) Zonal mean net surface radiation over sea for Jun/Jul/Aug 1979-88

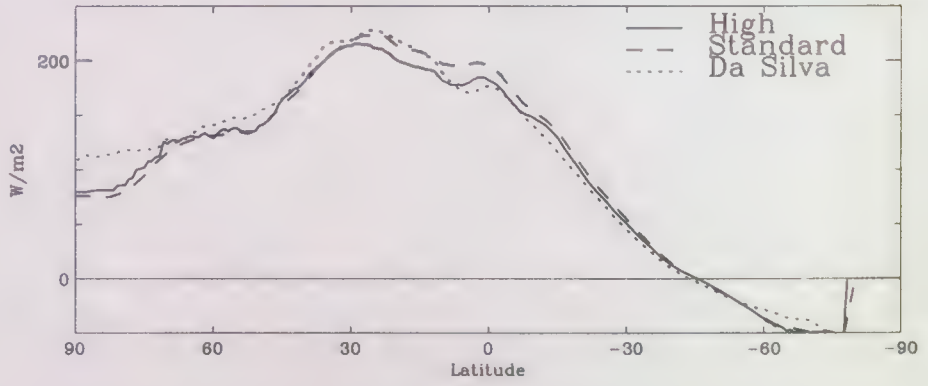

Figure 30 (a) Transient eddy kinetic energy for djf
high resolution

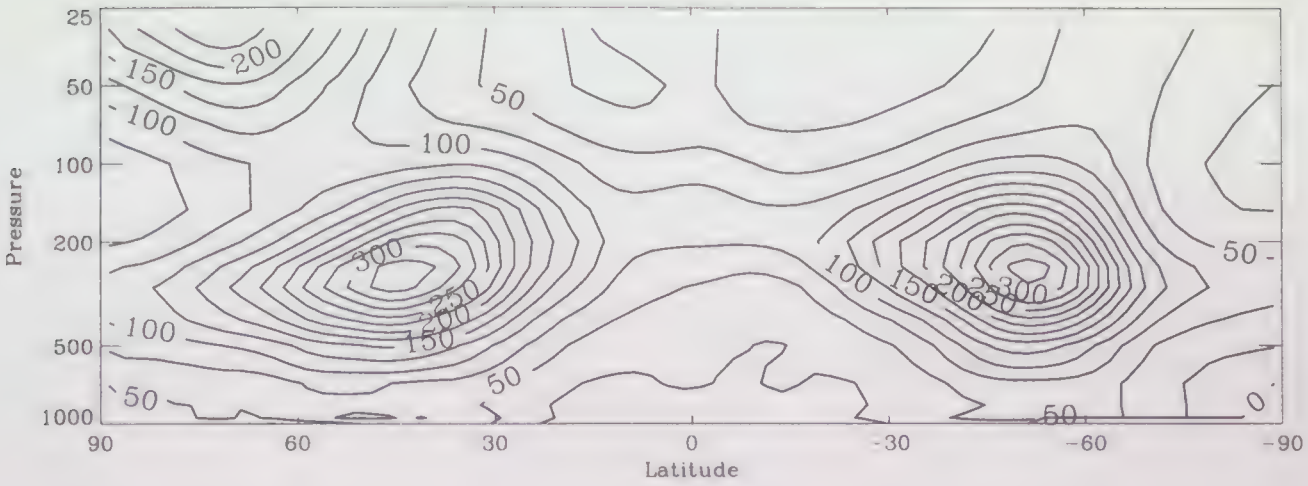

(b) Transient eddy kinetic energy for djf
standard resolution

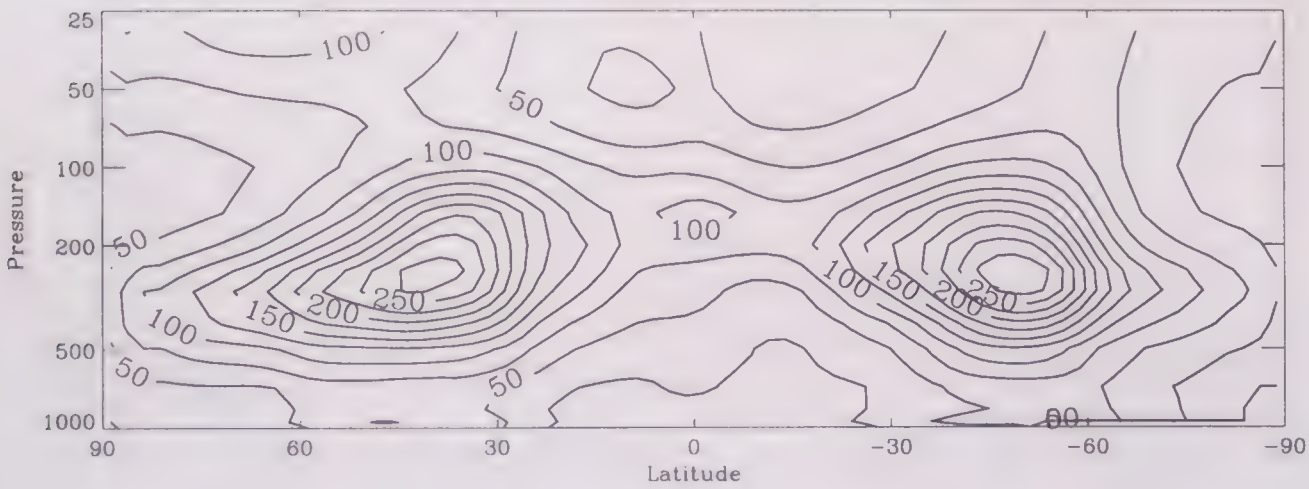

(c) Transient eddy kinetic energy for djf
ECMWF reanalysis climatology 1979–88

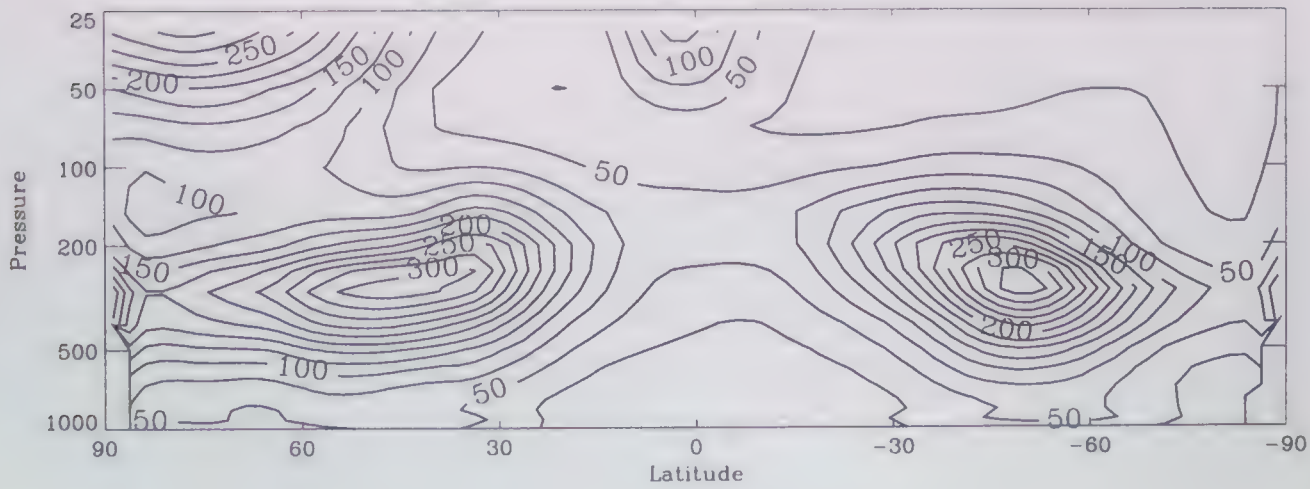

Figure 31 (a) Transient eddy kinetic energy for jja
high resolution

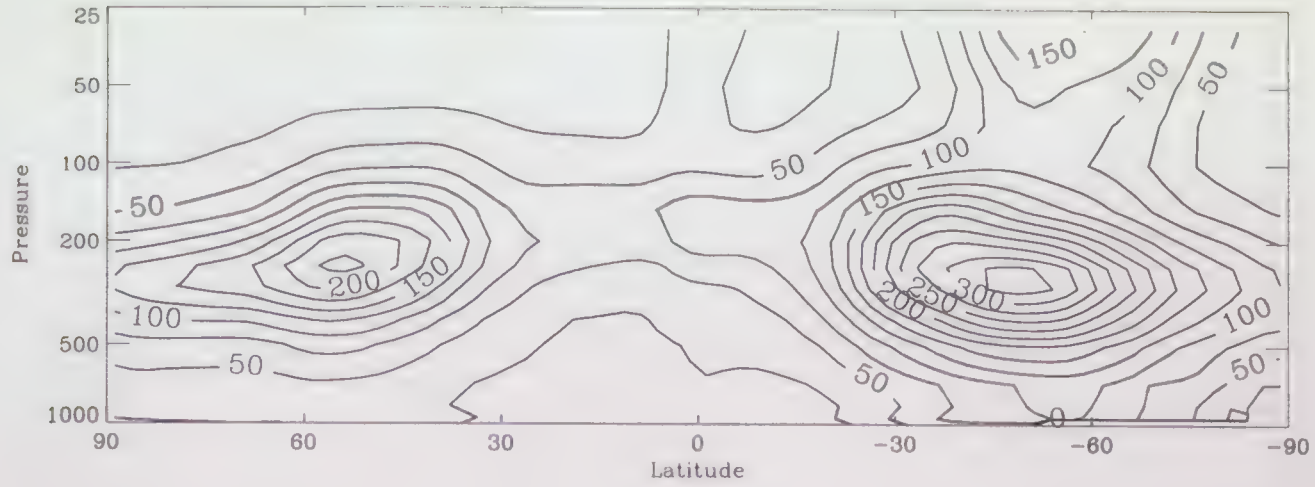

(b) Transient eddy kinetic energy for jja
standard resolution

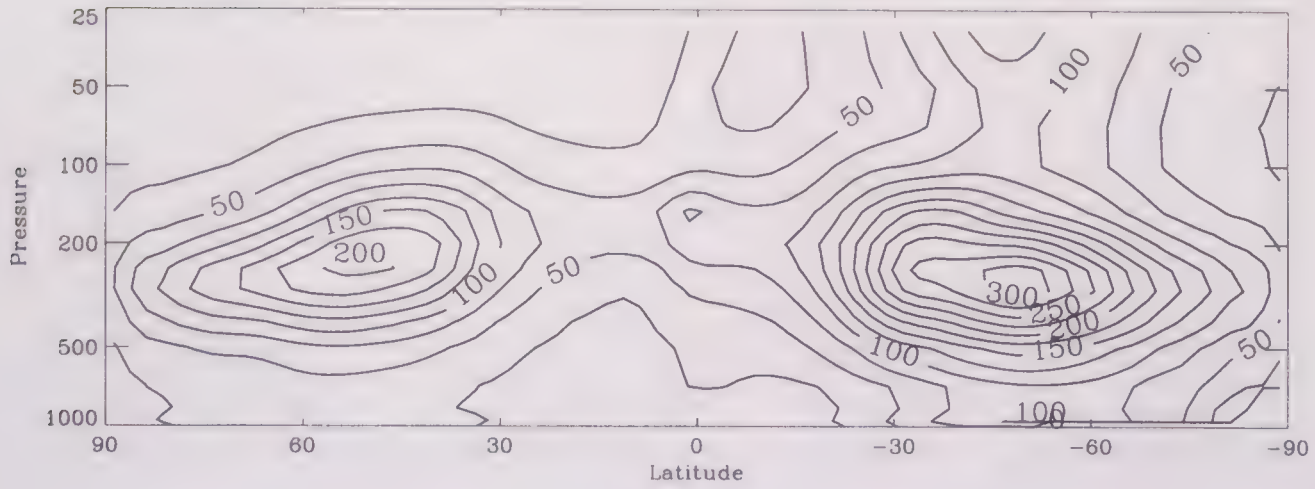

(c) Transient eddy kinetic energy for jja
ECMWF reanalysis climatology 1979–88

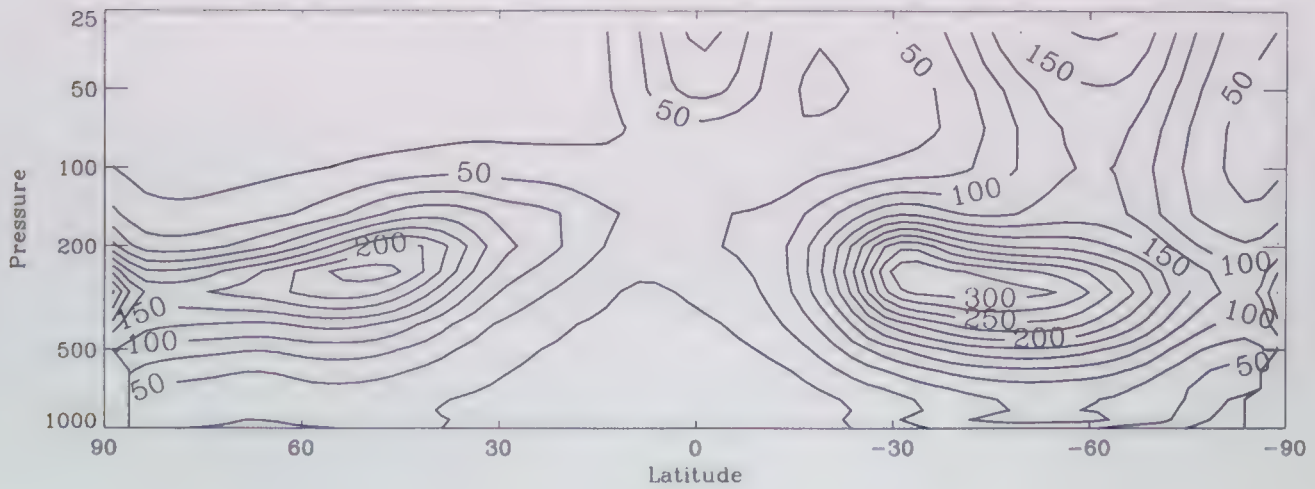

Figure 32 (a) Northward flux of transient eddy momentum for djf
high resolution

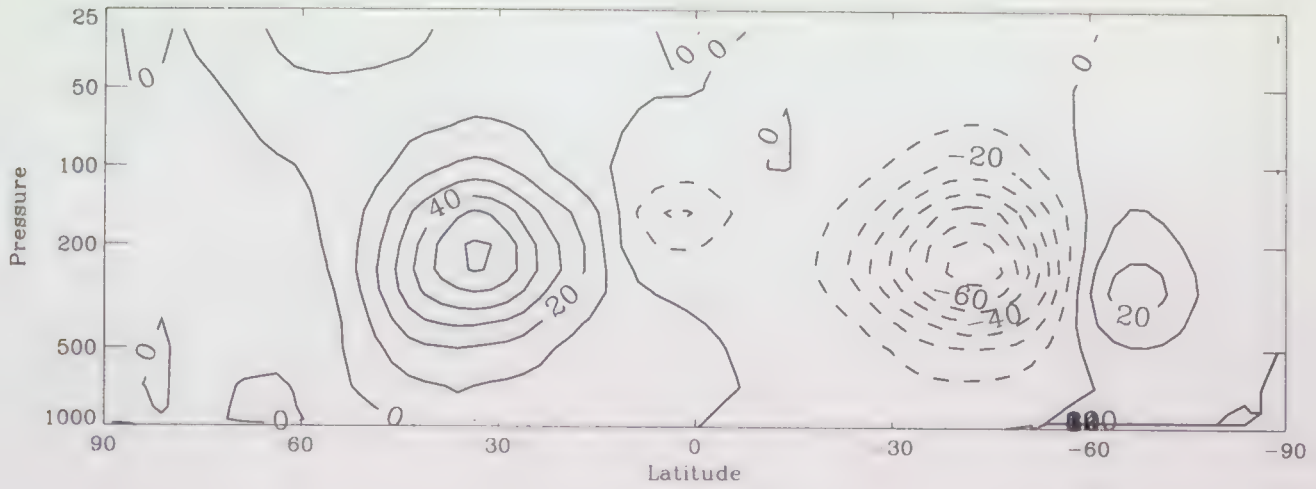

(b) Northward flux of transient eddy momentum for djf
standard resolution

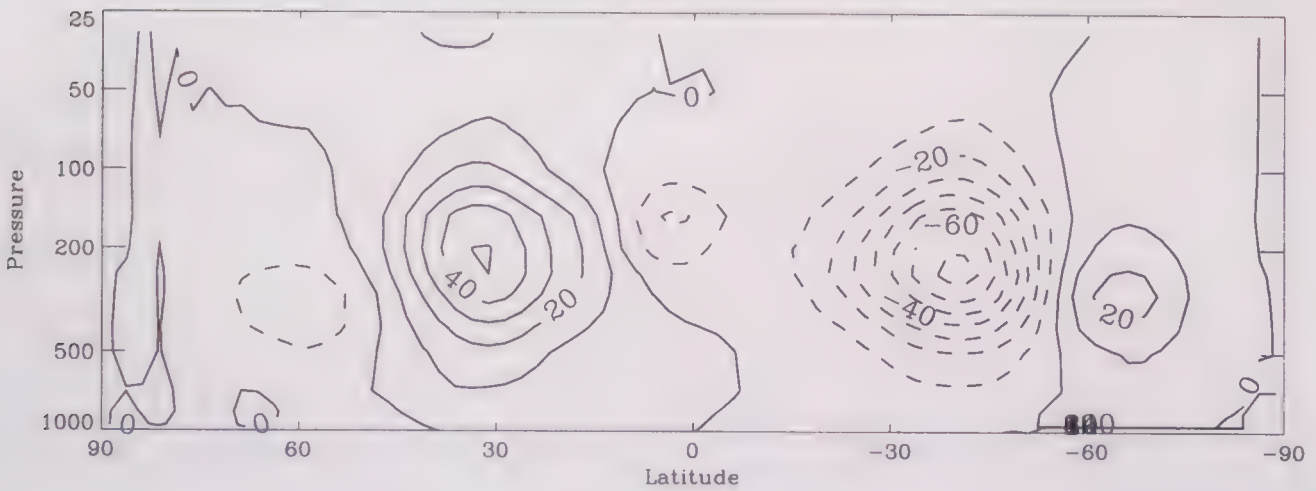

(c) Northward flux of transient eddy momentum for djf
ECMWF reanalysis climatology 1979–88

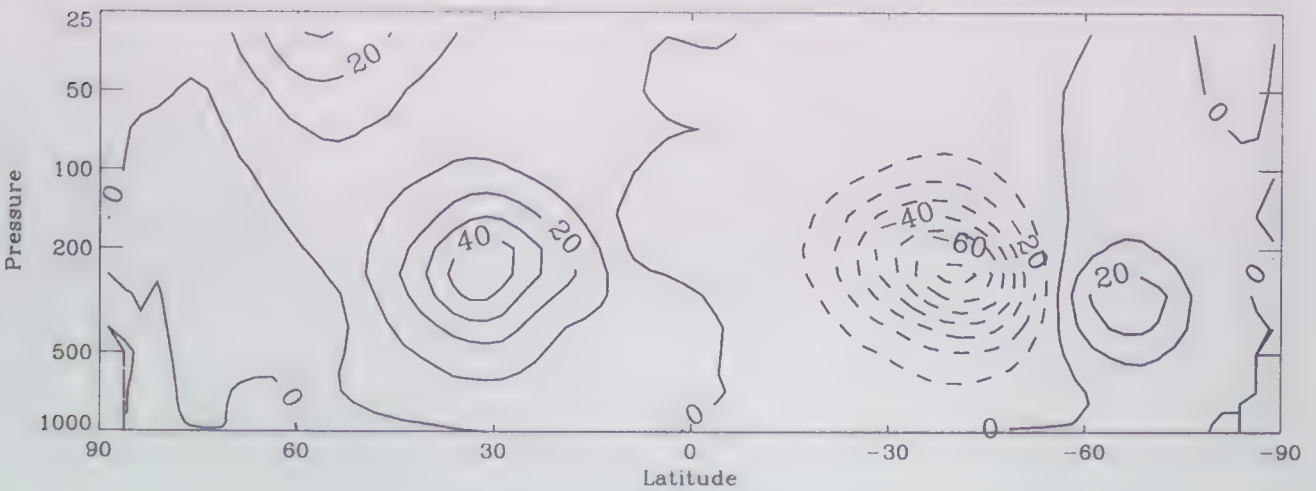

Figure 33 (a) Northward flux of transient eddy momentum for jja
high resolution

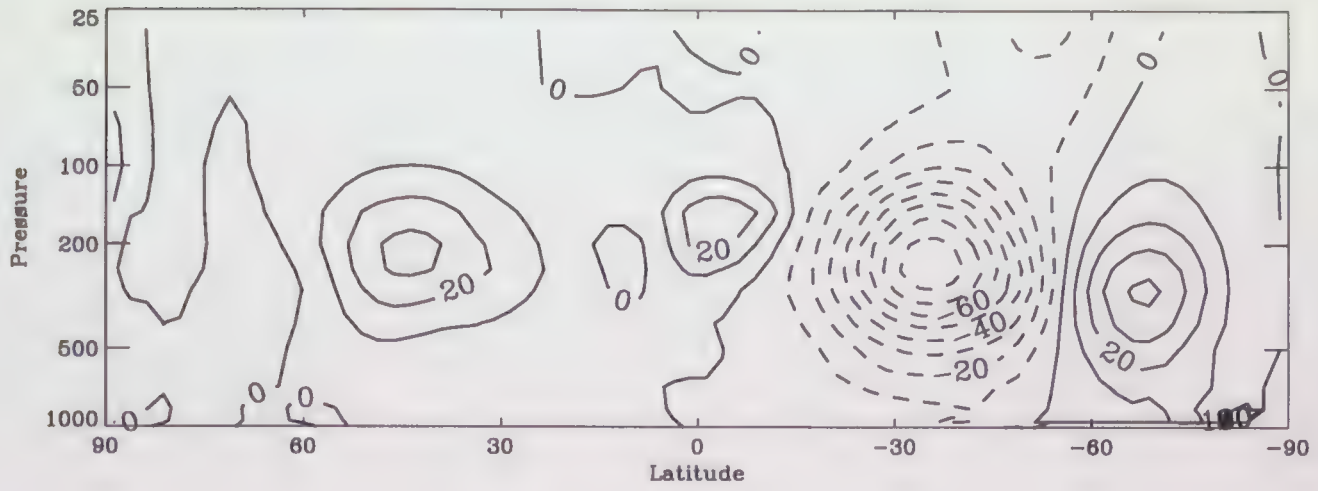

(b) Northward flux of transient eddy momentum for jja
standard resolution

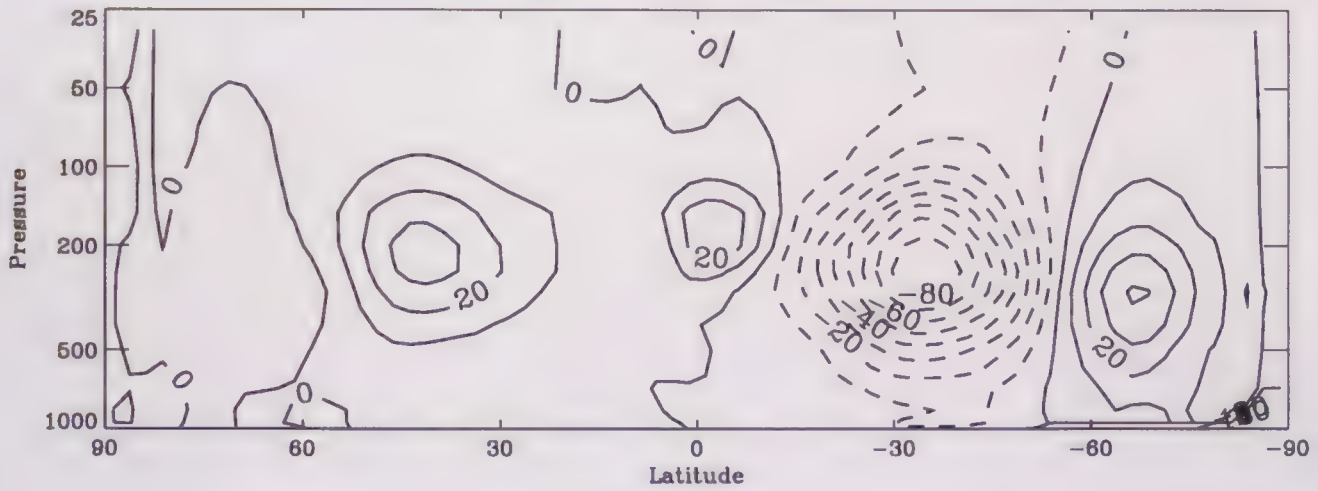

(c) Northward flux of transient eddy momentum for jja
ECMWF reanalysis climatology 1979–88

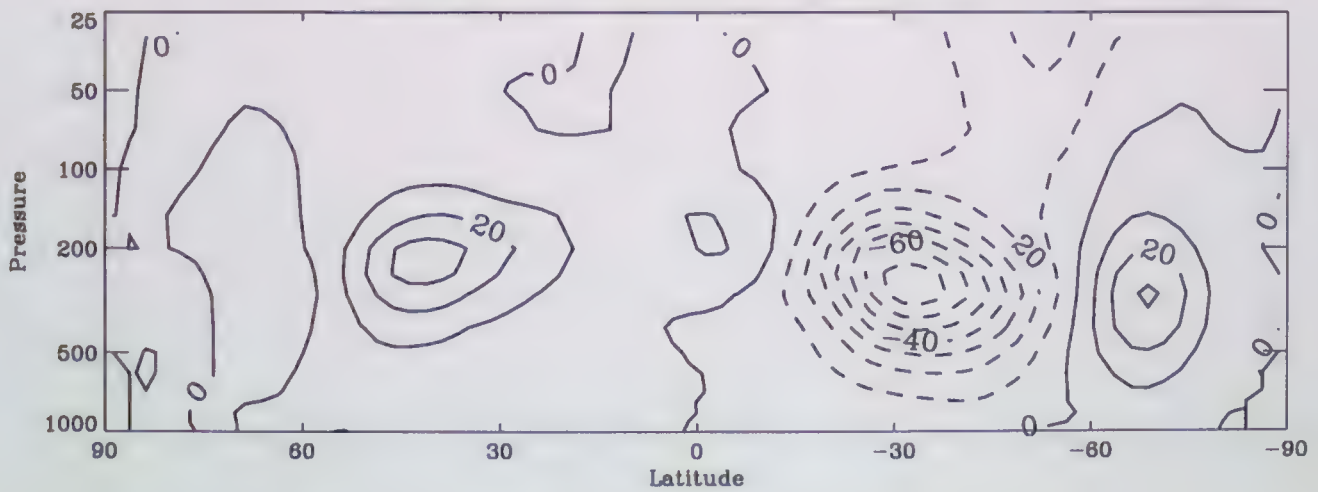

Figure 34 (a) Northward transient eddy heat for djf
high resolution

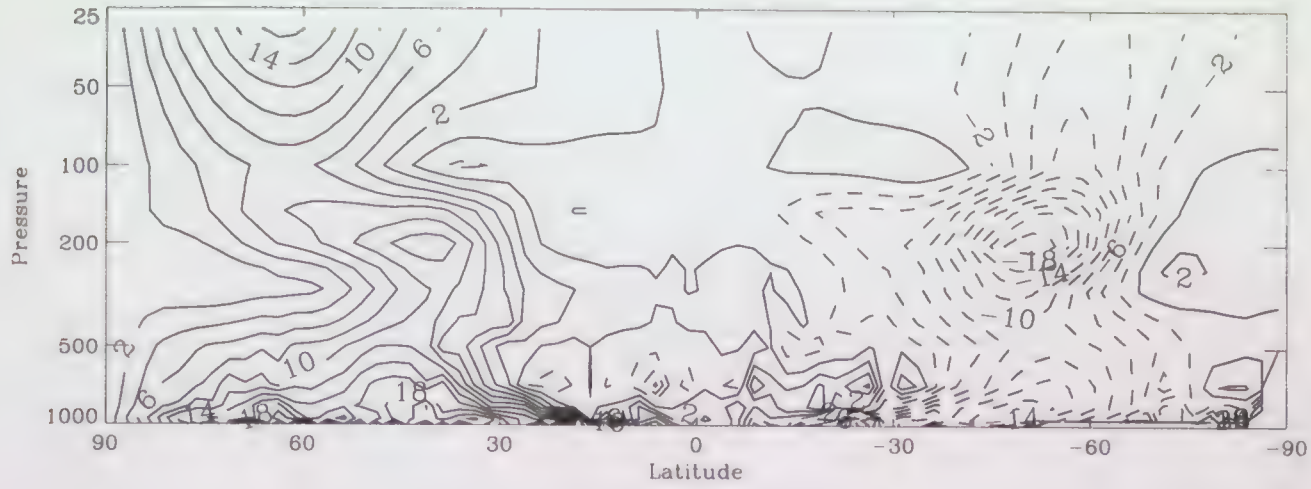

(b) Northward transient eddy heat for djf
standard resolution

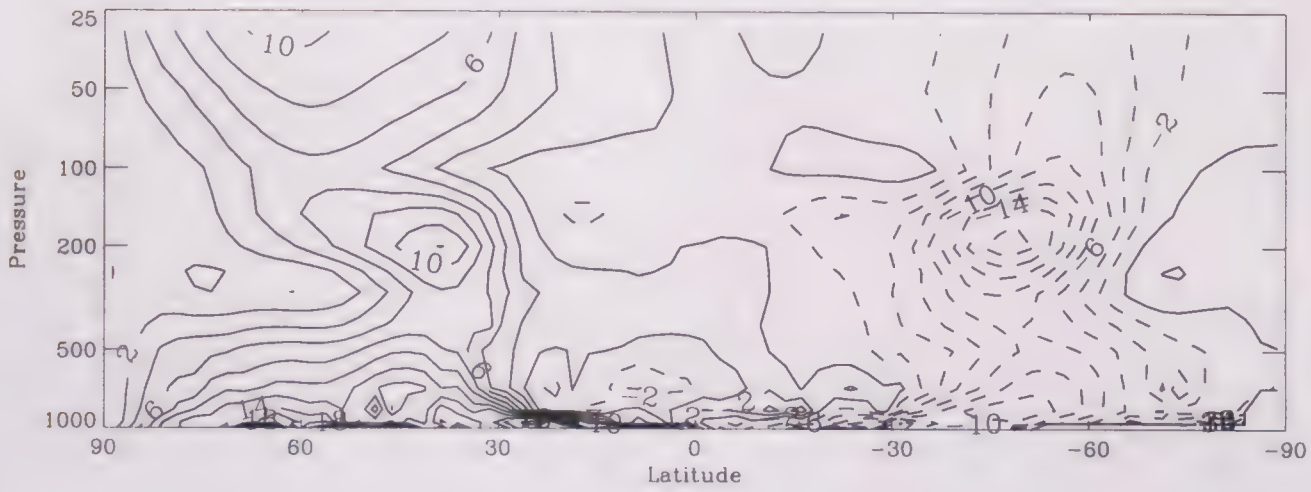

(c) Northward transient eddy heat for djf
ECMWF reanalysis climatology 1979–88

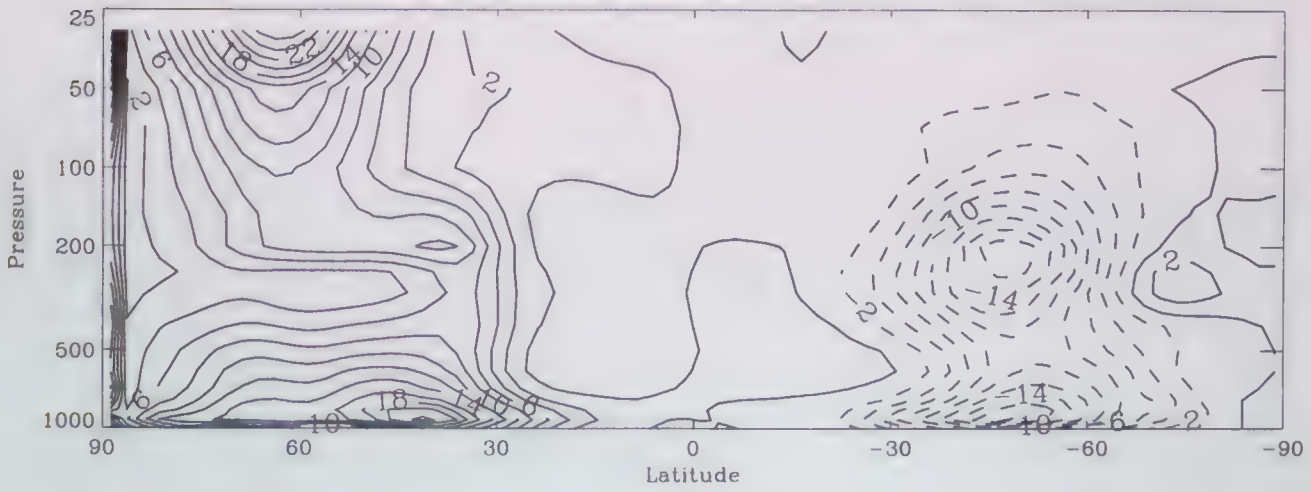

Figure 35 (a) Northward transient eddy heat for jja
high resolution

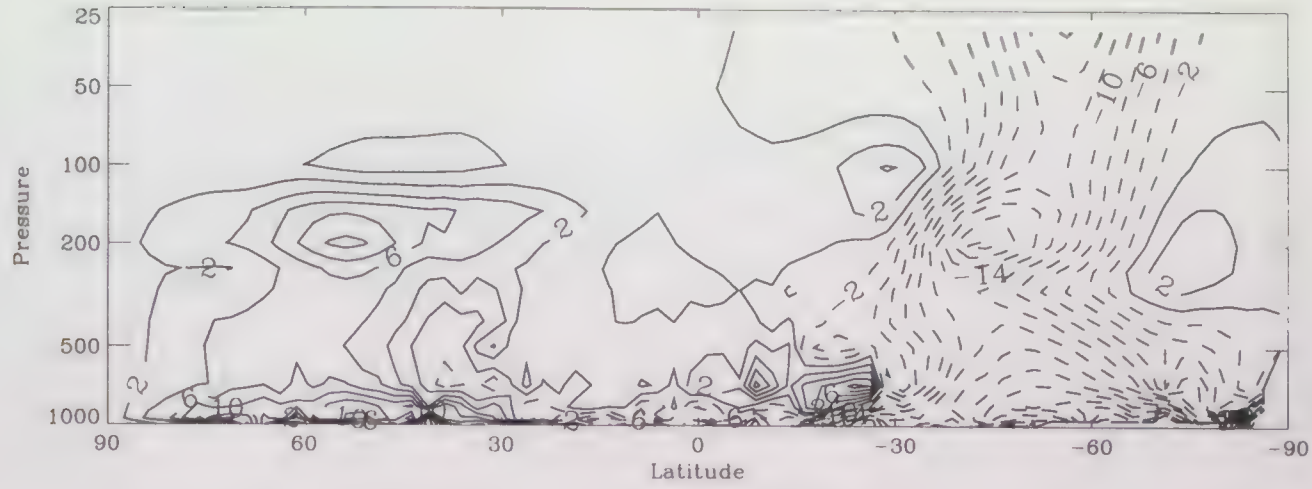

(b) Northward transient eddy heat for jja
standard resolution

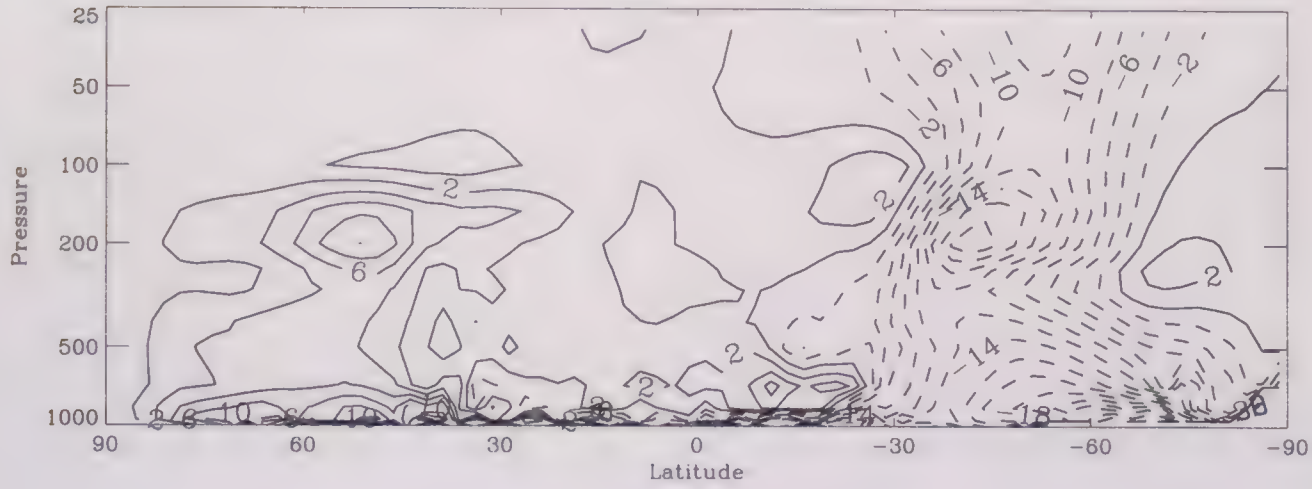

(c) Northward transient eddy heat for jja
ECMWF reanalysis climatology 1979-88

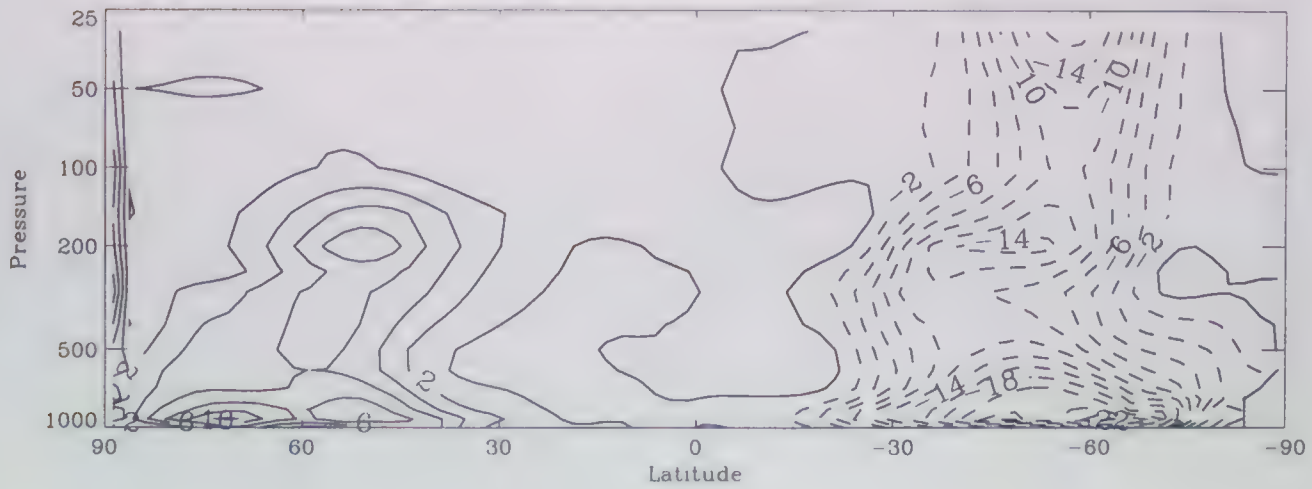

Figure 36(a) High resolution. Dec/Jan/Feb
s.d. of band pass filtered 500mb height.

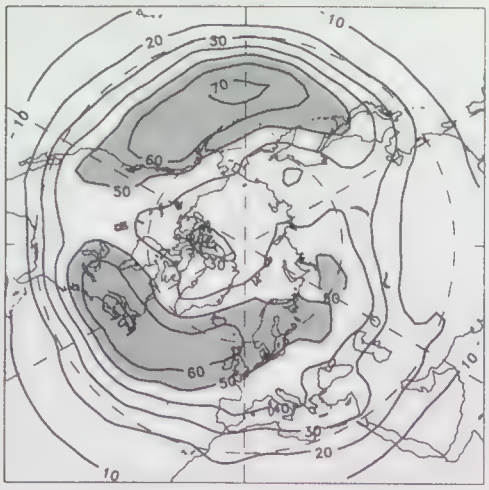

Contours every 10.m

(b) High resolution. Dec/Jan/Feb
s.d. of band pass filtered 500mb height.

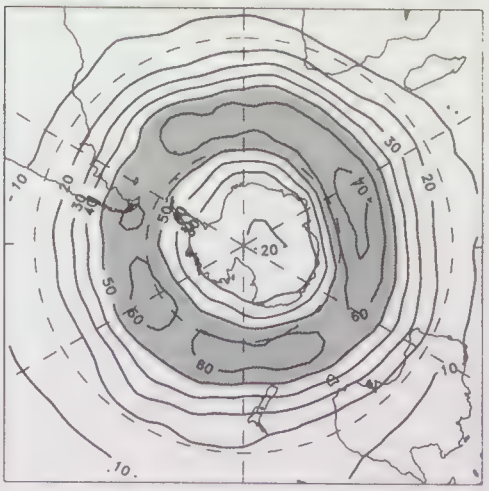

Contours every 10.m

(c) Standard resolution. Dec/Jan/Feb
s.d. of band pass filtered 500mb height.

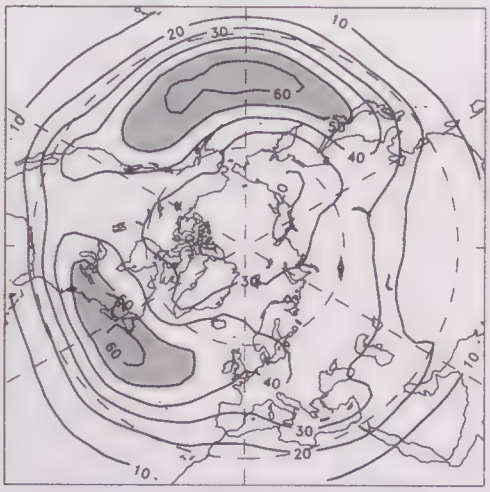

Contours every 10.m

(d) Standard resolution. Dec/Jan/Feb
s.d. of band pass filtered 500mb height.

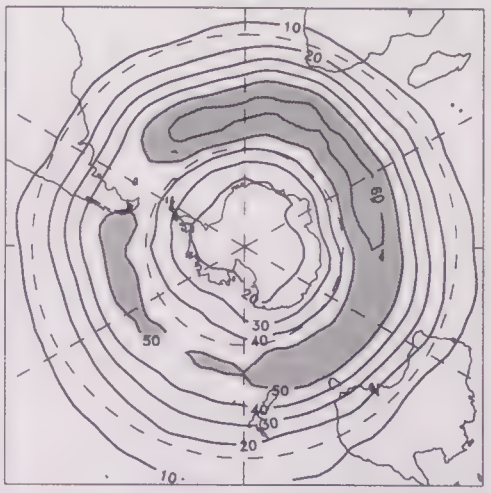

Contours every 10.m

(e) ECMWF climatology 1979-88. Dec/Jan/Feb
s.d. of band pass filtered 500mb height.

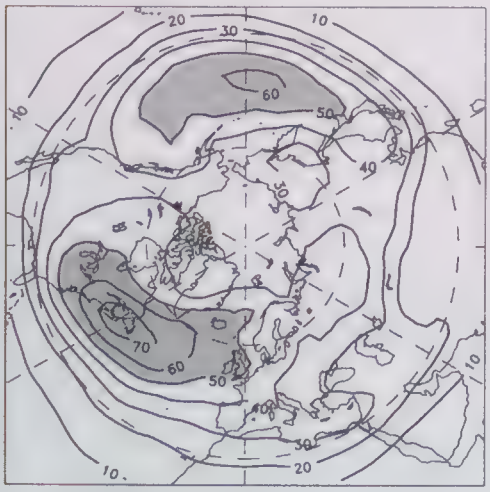

Contours every 10.m

(f) ECMWF climatology 1979-88 Dec/Jan/Feb
s.d. of band pass filtered 500mb height.

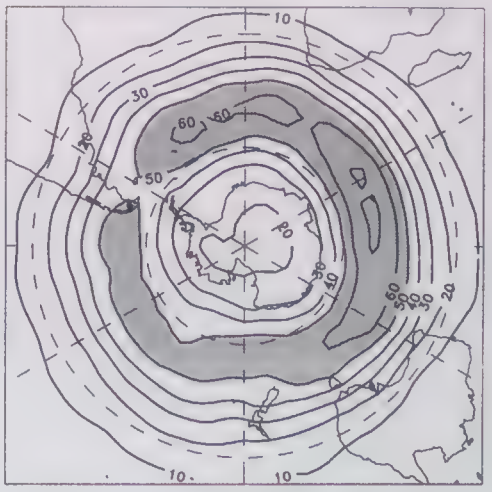

Contours every 10.m

Figure 37(a) High resolution. Jun/Jul/Aug
s.d. of band pass filtered 500mb height.

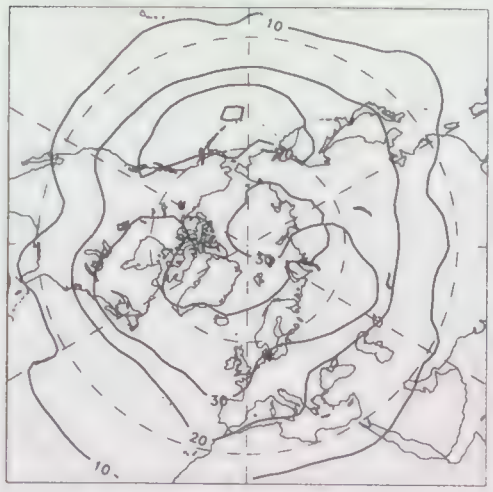

Contours every 10.m

(b) High resolution. Jun/Jul/Aug
s.d. of band pass filtered 500mb height.

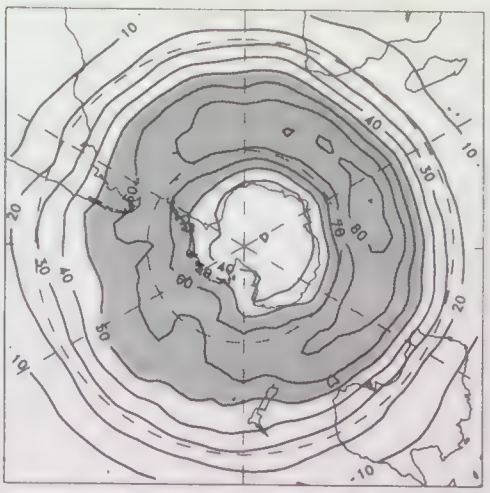

Contours every 10.m

(c) Standard resolution. Jun/Jul/Aug
s.d. of band pass filtered 500mb height.

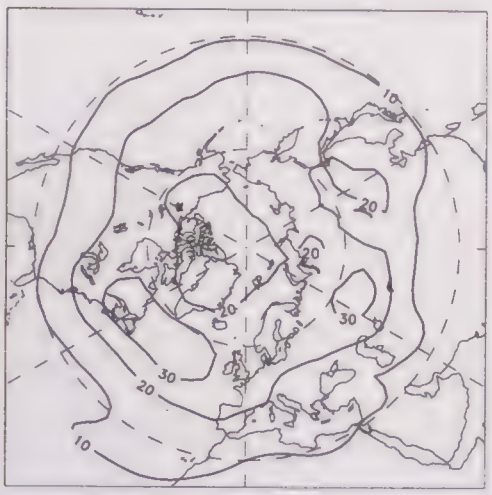

Contours every 10.m

(d) Standard resolution. Jun/Jul/Aug
s.d. of band pass filtered 500mb height.

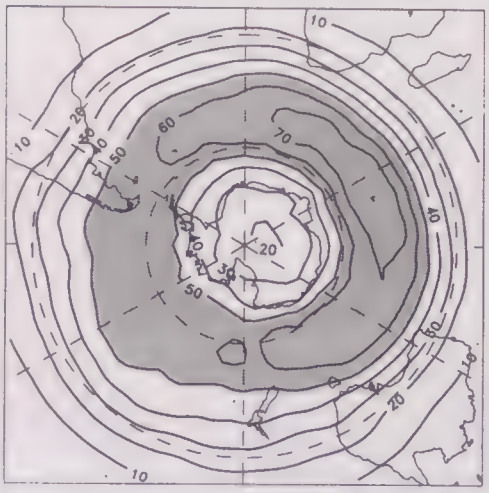

Contours every 10.m

(e) ECMWF climatology 1979-88. Jun/Jul/Aug
s.d. of band pass filtered 500mb height.

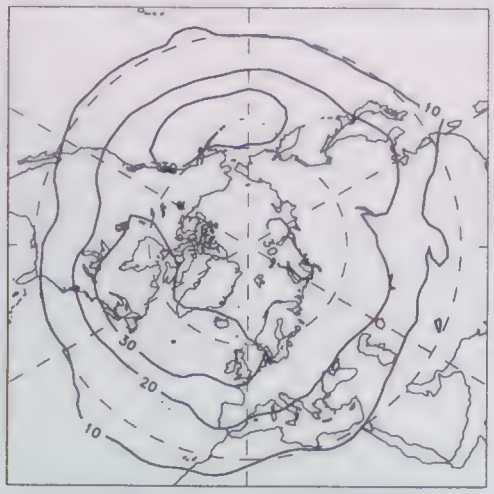

Contours every 10.m

(f) ECMWF climatology 1979-88. Jun/Jul/Aug
s.d. of band pass filtered 500mb height.

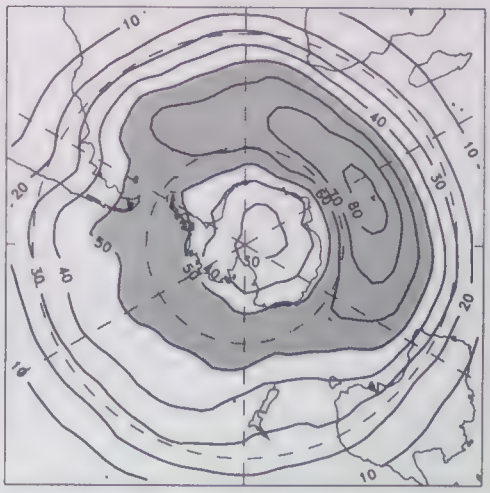

Contours every 10.m

Figure 38(a) High resolution. Dec/Jan/Feb
s.d. of low pass filtered 500mb height.

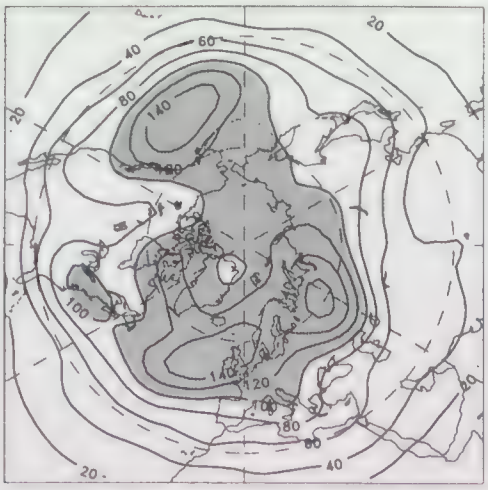

Contours every 20.m

(b) High resolution. Dec/Jan/Feb
s.d. of low pass filtered 500mb height.

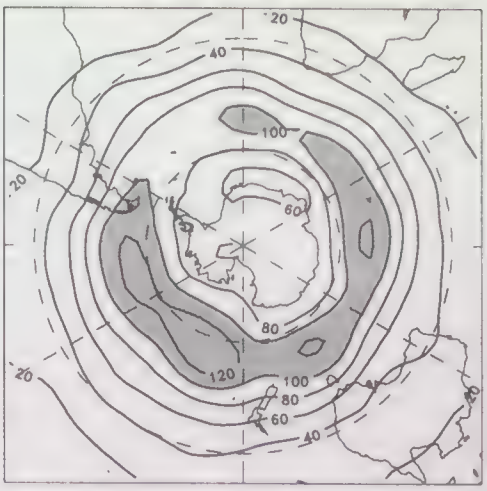

Contours every 20.m

(c) Standard resolution. Dec/Jan/Feb
s.d. of low pass filtered 500mb height.

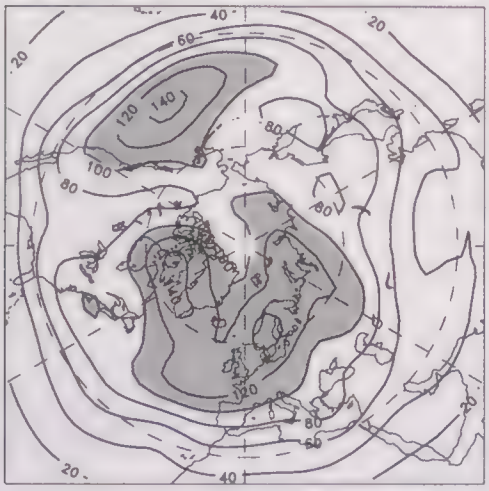

Contours every 20.m

(d) Standard resolution. Dec/Jan/Feb
s.d. of low pass filtered 500mb height.

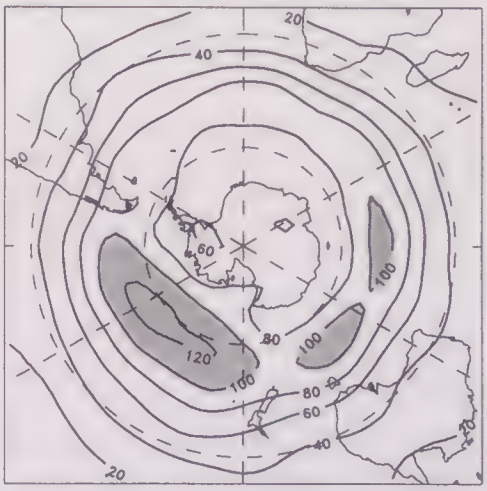

Contours every 20.m

(e) ECMWF climatology 1979–88. Dec/Jan/Feb
s.d. of low pass filtered 500mb height.

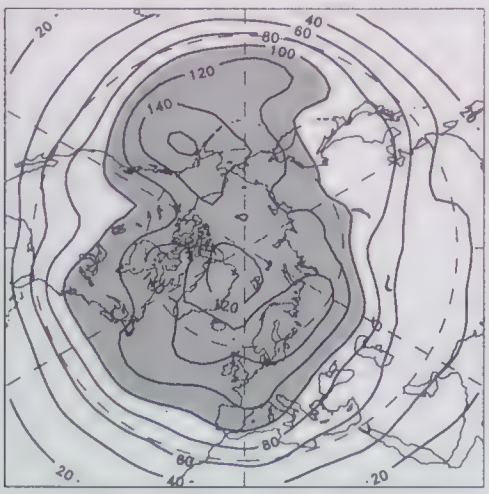

Contours every 20.m

(f) ECMWF climatology 1979–88. Dec/Jan/Feb
s.d. of low pass filtered 500mb height.

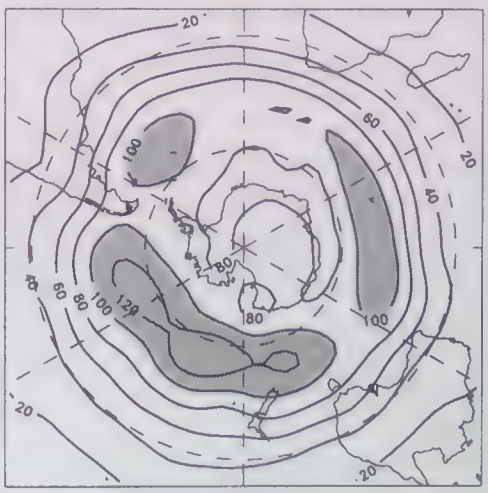

Contours every 20.m

Figure 39(a) High resolution. Jun/Jul/Aug
s.d. of low pass filtered 500mb height.

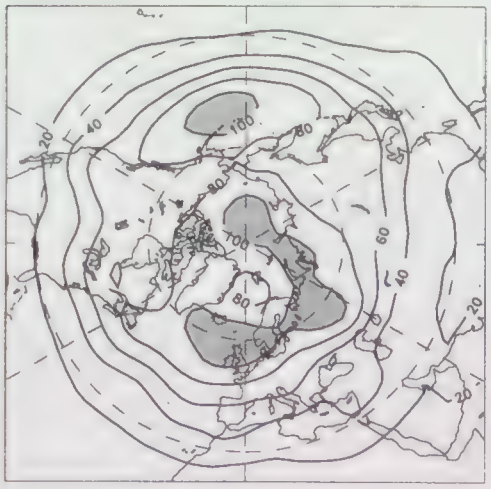

Contours every 20.m

(b) High resolution. Jun/Jul/Aug
s.d. of low pass filtered 500mb height

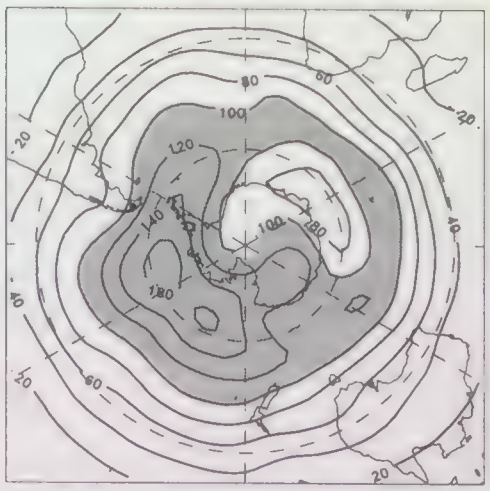

Contours every 20.m

(c) Standard resolution. Jun/Jul/Aug
s.d. of low pass filtered 500mb height.

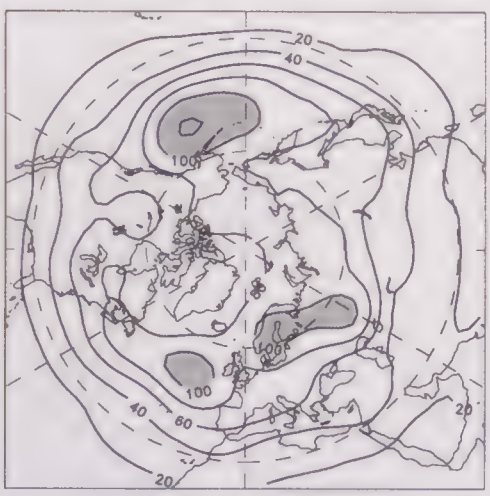

Contours every 20.m

(d) Standard resolution. Jun/Jul/Aug
s.d. of low pass filtered 500mb height.

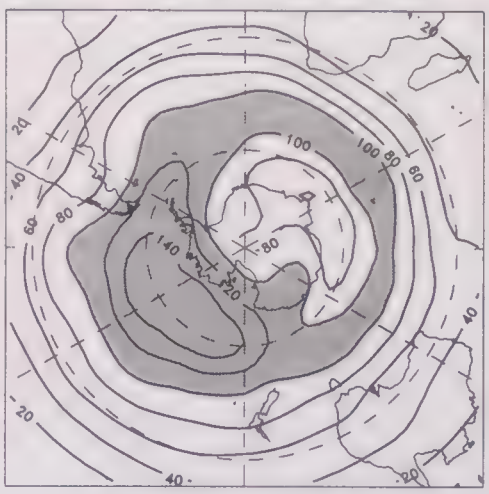

Contours every 20.m

(e) ECMWF climatology 1979–88. Jun/Jul/Aug
s.d. of low pass filtered 500mb height.

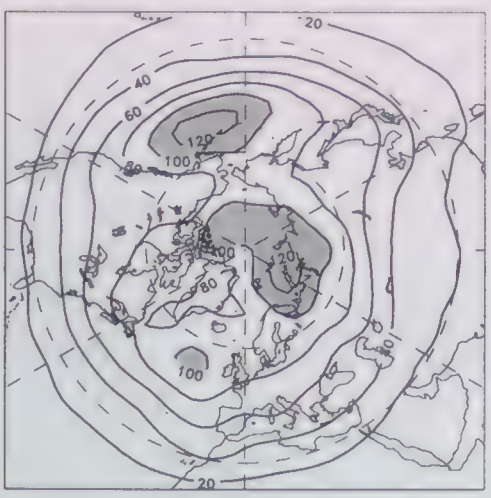

Contours every 20.m

(f) ECMWF climatology 1979–88. Jun/Jul/Aug
s.d. of low pass filtered 500mb height.

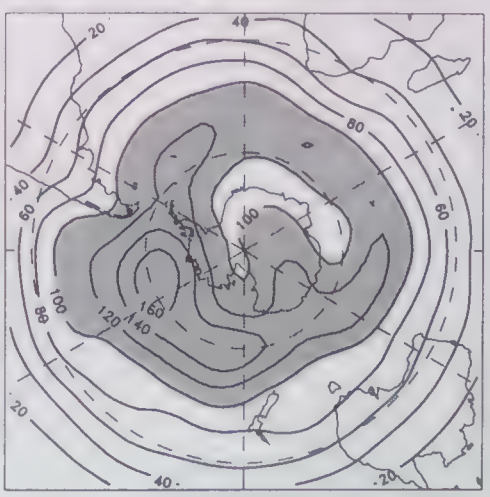

Contours every 20.m

Figure 40(a) Blocking index northern hemisphere - Dec/Jan/feb

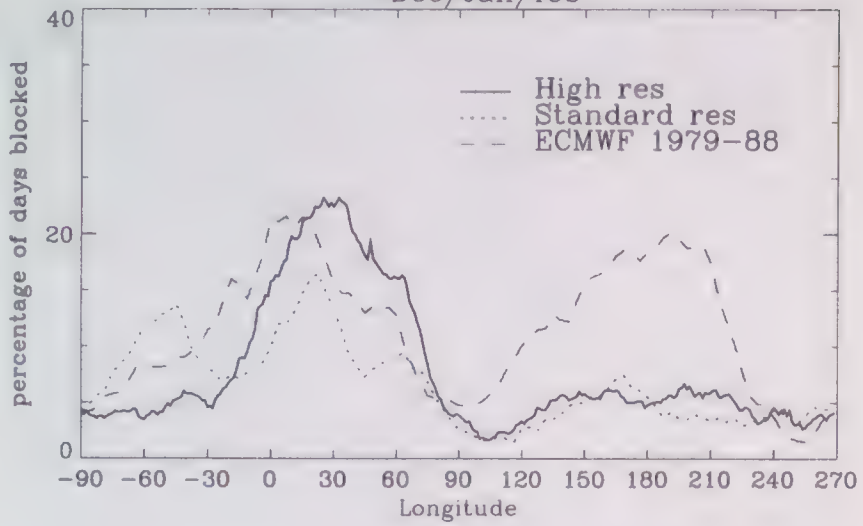

(b) Blocking index northern hemisphere - Mar/Apr/May

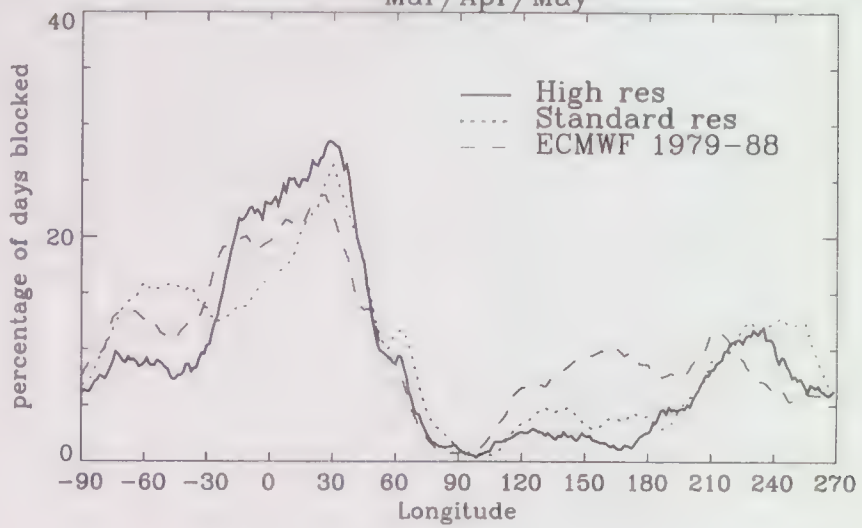

(c) Blocking index northern hemisphere - Jun/Jul/Aug

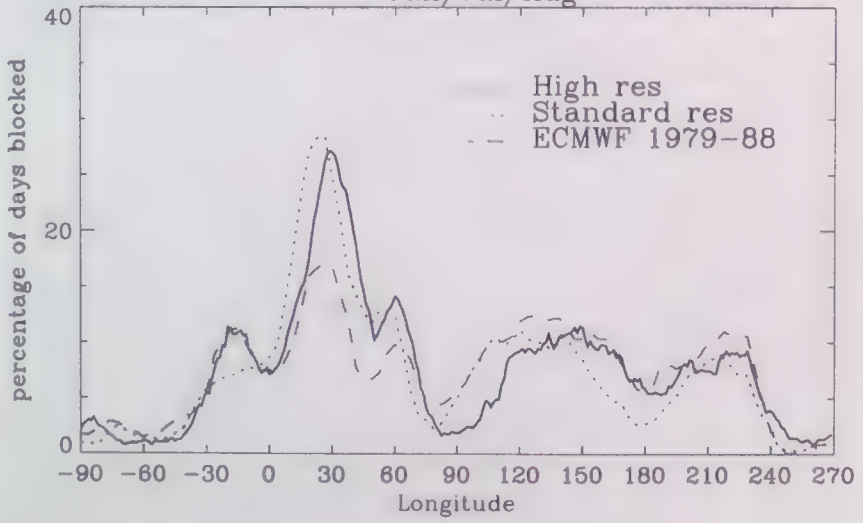

(d) Blocking index northern hemisphere - Sep/Oct/Nov

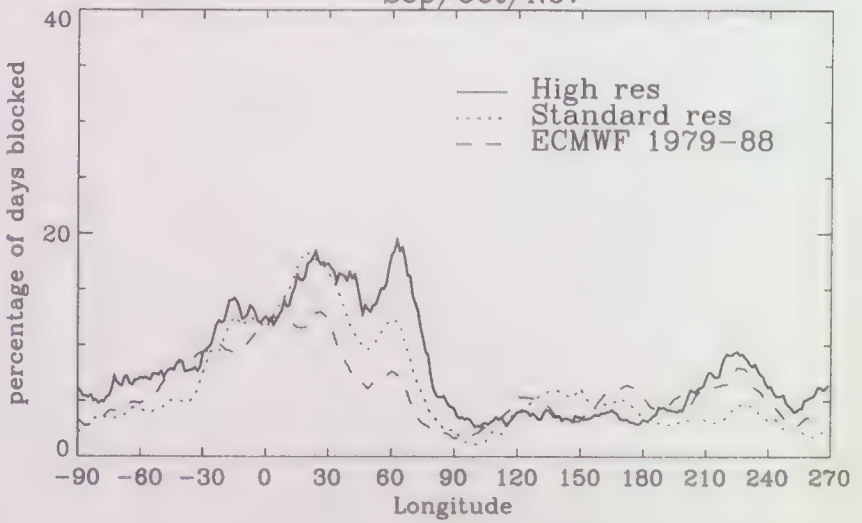

CLIMATE RESEARCH TECHNICAL NOTES

CRTN 1	Oct 1990	Estimates of the sensitivity of climate to vegetation changes using the Penman-Monteith equation. P R Rowntree
CRTN 2	Oct 1990	An ocean general circulation model of the Indian Ocean for hindcasting studies. D J Carrington
CRTN 3	Oct 1990	Simulation of the tropical diurnal cycle in a climate model. D P Rowell
CRTN 4	Oct 1990	Low frequency variability of the oceans. C K Folland, A Colman, D E Parker and A Bevan
CRTN 5	Dec 1990	A comparison of 11-level General Circulation Model Simulations with observations in the East Sahel. K Maskell
CRTN 6	Dec 1990	Climate Change Prediction. J F B Mitchell and Qing-cun Zeng
CRTN 7	Jan 1991	Deforestation of Amazonia - modelling the effects of albedo change. M F Mylne and P R Rowntree
CRTN 8	Jan 1991	The role of observations in climate prediction and research. D J Carson
CRTN 9	Mar 1991	The greenhouse effect and its likely consequences for climate change. D J Carson
CRTN 10	Apr 1991	Use of wind stresses from operational N.W.P. models to force an O.G.C.M. of the Indian Ocean. D J Carrington
CRTN 11	Jun 1991	A new daily Central England Temperature series, 1772-1991. D E Parker, T P Legg and C K Folland
CRTN 12	Jul 1991	Causes and predictability of Sahel rainfall variability. D P Rowell, C K Folland, K Maskell, J A Owen, M N Ward

CLIMATE RESEARCH TECHNICAL NOTES

CRTN 13	Jul 1991	Modelling changes in climate due to enhanced CO2, the role of atmospheric dynamics, cloud and moisture. C A Senior, J F B Mitchell, H Le Treut and Z-X Li
CRTN 14	Sep 1991	Sea temperature bucket models used to correct historical SST data in the Meteorological Office. C K Folland
CRTN 15	Aug 1991	Modelling climate change, and some potential effects on agriculture in the U.K. P R Rowntree, B A Callander and J Cochrane
CRTN 16	Aug 1991	The Boreal Forests and Climate G Thomas and P R Rowntree
CRTN 17	Aug 1991	Development of a Stratosphere-Troposphere Data Assimilation System. R Swinbank.
CRTN 18	Sep 1991	A study of asynchronous coupling using a simple climate model. M K Davey.
CRTN 19	Sep 1991	The Oceanic Carbon Cycle. N K Taylor
CRTN 20	Nov 1991	Worldwide ocean-atmosphere surface fields in Sahel wet and dry years using provisionally corrected surface wind data. M N Ward
CRTN 21	Dec 1991	Coupled tropical ocean global atmosphere models at the UKMO. M K Davey, C Gordon, S Ineson and S Lawrence
CRTN 22	Dec 1991	Empirical parameterisation of tropical ocean-atmosphere coupling. M Allen, M K Davey, D L T Anderson and P D Killworth
CRTN 23	Feb 1992	The temporal evolution of Equatorial Currents in the Indian Ocean D L T Anderson, D J Carrington, R A Corry and C Gordon
CRTN 24	Feb 1992	Stratospheric analyses provided by the U.K. Meteorological Office M J Bailey, A O'Neill and V D Pope

CLIMATE RESEARCH TECHNICAL NOTES

CRTN 25	Feb 1992	Modelling interannual variability in the Indian Ocean using momentum fluxes from the UKMO and ECMWF operational weather analyses. D L T Anderson and D J Carrington
CRTN 26	Mar 1992	A GCM simulation of the impact of Amazonian deforestation on climate using an improved canopy representation J Lean and P R Rowntree
CRTN 27	Mar 1992	The parameterization of rainfall interception in GCMs A J Dolman and D Gregory
CRTN 28	Jun 1992	Development of worldwide marine data eigenvectors since 1985 A W Colman
CRTN 29	Jun 1992	A tropical ocean model with reduced physics M K Davey
CRTN 30	Jun 1992	International Temperature Workshop, Boulder, Colorado, USA, 16 January 1992 Edited by D E Parker
CRTN 31	Jul 1992	Simulation of clear-sky outgoing longwave radiation over the oceans using operational analyses A Slingo and M J Webb
CRTN 32	Sep 1992	A prediction of the transient response of climate J M Murphy
CRTN 33	Nov 1992	LEPS scores for assessing climate model simulations and long-range forecasts. C K Folland
CRTN 34	Jan 1993	Stratospheric Data Assimilation System Guide Editer: R Swinbank
CRTN 35	Mar 1993	A Stratosphere-Troposphere Data Assimilation System R Swinbank and A O'Neill
CRTN 36	Mar 1993	Validation of hydrological schemes for climate models against catchment data. P R Rowntree and J Lean

CLIMATE RESEARCH TECHNICAL NOTES

CRTN 37	Apr 1993	Modelling of palaeoclimates: Examples from the recent past J F B Mitchell
CRTN 38	May 1993	A simulation of seasonality in ENSO forecast skill M K Davey, D L T Anderson and S Lawrence
CRTN 39	Jul 1993	ENSO Prediction experiments using a simple ocean-atmosphere model D-H Wu, D L T Anderson and M K Davey
CRTN 40	Sep 1993	Diagnosis of dynamic sea-surface and sea-level changes from the Cox ocean model J M Gregory
CRTN 41	Sep 1993	Seasonal variations of the clear-sky greenhouse effect: the role of changes in atmospheric temperatures and humidities M J Webb, A Slingo and G L Stephens
CRTN 42	Nov 1993	Sea-level changes under increasing atmospheric CO_2 in a transient coupled ocean-atmosphere GCM experiment. J M Gregory
CRTN 43	Dec 1993	Global and regional patterns of climate change: recent predictions for the Arctic P R Rowntree
CRTN 44	Feb 1994	The effect of changing horizontal diffusion in the atmospheric version of the unified climate model C D Hall and R A Stratton
CRTN 45	Mar 1994	Simulation of El-Niño/Southern Oscillation like variability in a global AOGCM and its response to CO_2 increase. S F B Tett
CRTN 46	Apr 1994	Global data required for monitoring climate change. D E Parker and C K Folland
CRTN 47	May 1994	Seasonal uptake of anthropogenic CO_2 in an ocean general circulation model. N K Taylor

CLIMATE RESEARCH TECHNICAL NOTES

CRTN 48	Jun 1994	A tropic-wide oscillation of boreal summer rainfall and patterns of sea-surface temperature. M N Ward, K Maskell, C K Folland, D P Rowell and R Washington
CRTN 49	Jun 1994	Simulation of the tropical Pacific using a simplified ocean model M A Balmaseda, D L T Anderson and M K Davey
CRTN 50	Sep 1994	Simulation of global mean temperature using a box-diffusion climate model P R Rowntree
CRTN 51	Sep 1994	Seasonal dependence of ENSO prediction skill M A Balmaseda, M K Davey and D L T Anderson
CRTN 52	Nov 1994	Simulation of the Indian Monsoon and Tropical Intraseasonal Variability by a General Circulation Model P M Inness and D Gregory
CRTN 53	Mar 1995	A comparison of modelled surface fluxes with climatological estimates. C Gordon and D K Wright
CRTN 54	Mar 1995	The representation of moist convection in atmospheric models. D Gregory
CRTN 55	Mar 1995	A consistent treatment of the evaporation of rain and snow for use in large-scale models D Gregory
CRTN 56	Apr 1995	Workshop on simulations of the Climate of the Twentieth Century using GISST, 28-30 November 1994, Hadley Centre, Bracknell, UK Edited by C K Folland and D P Rowell
CRTN 57	May 1995	Enhanced shortwave cloud radiative forcing due to anthropogenic aerosols. S E Swartz and A Slingo
CRTN 58	May 1995	The simulation of the tropical oceans in models of different horizontal resolution. C Gordon, D K Wright and C M Roberts
CRTN 59	Sep 1995	The water budget of middle latitude continental regions - a modelling and observational study P R Rowntree
CRTN 60	Sep 1995	Intraseasonal variability of the Indian summer monsoon simulated by the Hadley Centre climate model K Ashok, D Gregory and P M Inness

CLIMATE RESEARCH TECHNICAL NOTES

CRTN 61	Sep 1995	Climate simulations with the Unified Model: AMIP runs C D Hall, R A Stratton and M L Gallani
CRTN 62	Nov 1995	Validation of surface parameters over the oceans in climate simulations with the unified model. C D Hall
CRTN 63	Dec 1995	The GISST2.2 sea surface temperature and sea-ice climatology D E Parker, M Jackson and E B Horton
CRTN 64	Dec 1995	Parametrization of momentum transport by convection. II: Tests in single column and general circulation models. D Gregory, R Kershaw and P M Inness
CRTN 65	Jan 1996	Understanding the sensitivity of a GCM simulation of Amazonian deforestation to the specification of vegetation and soil characteristics. J Lean and P R Rowntree
CRTN 66	Jan 1996	On the efficient calculation of infra-red fluxes and cooling rates using the two-stream equations. J M Edwards
CRTN 67	Jan 1996	The second Hadley Centre coupled ocean-atmosphere GCM: Model description, spinup and validation. TC Johns,RE Carnell,JF Crossley,JM Gregory, JFB Mitchell,CA Senior,SFB Tett and RA Wood
CRTN 68	Feb 1996	The sensitivity of climate simulations to the specification of mixed phase clouds D Gregory and D Morris
CRTN 69	Apr 1996	Using an ensemble of Multi-Decadal GCM simulations ro assess potential seasonal predictability D P Rowell
CRTN 70	May 1996	North Atlantic and European Seasonal Predictability using an Ensemble of Multi-Decadal AGCM Simulations J R Davies, D P Rowell and C K Folland
CRTN 71	Jun 1996	A description of the Second Hadley Centre Coupled Model (HADCM2) T C Johns
CRTN 72	Jul 1996	Palaeoclimate Modelling Intercomparison: UKMO GCM simulations for 6kBP and 21kBP C D Hewitt and J F B Mitchell

CLIMATE RESEARCH TECHNICAL NOTES

CRTN 73	Aug 1996	ENSO responses and low frequency weather variability in the North Pacific/American sector 1949-93 A C Renshaw, D P Rowell and C K Folland
CRTN 74	Sep 1996	Version 2.2 of the Global sea-Ice and Sea Surface Temperature data set, 1903-1994 N A Rayner, E B Horton, D E Parker, C K Folland and R B Hackett
CRTN 75	Sep 1996	A new gravity wave drag scheme incorporating anisotropic orography and low level wave breaking : Impact upon the climate of the UK Met Office Unified Model D Gregory, G J Shutts and J R Mitchell
CRTN 76	Nov 1996	Middle atmosphere variability in the UKMO Unified Model R Swinbank, W Lahoz, C Douglas, A Heaps, R Brugge, W Norton, A O'Neill, D Podd
CRTN 77	Dec 1996	A high resolution AMIP run using the Hadley Centre model HadAM2b R A Stratton